UNIVERSITY OF CAMBRIDGE

SIGNAL TRANSFORMATION AT THE INPUT AND OUTPUT OF THE *DROSOPHILA* VISUAL SYSTEM

by

MAI M MORIMOTO

Murray Edwards College
Department of Physiology,
Development and Neuroscience

This dissertation is submitted for the degree of
Doctor of Philosophy

September 2016

SIGNAL TRANSFORMATION AT THE INPUT AND OUTPUT OF THE *DROSOPHILA* VISUAL SYSTEM

MAI M MORIMOTO

SUMMARY

A key function of the nervous system is to sample data from the external world, generate internal signals, and transform them into meaningful information that can be used to trigger behaviour. In order to gain insight into the underlying mechanism for signal transformation, the visual system has been extensively studied: partly owing to the stimulus being reliably presentable, and the anatomy being well described. The *Drosophila* visual system is one such system, with the added advantage of genetic tractability. In this thesis, I studied the filtering property of visual neurons at two levels, biophysical and circuit levels.

The first study looks at signal transformation at the biophysical level, at the input of the visual system, in photoreceptors. The photoreceptors detect photons and create an initial voltage output signal. Voltage-gated potassium channels counteract the depolarization caused by opening of light sensitive channels, and the heterogeneous properties of their kinetics can fine-tune the photoreceptor's frequency response to fulfill the animal's ecological requirements. Shaker (Kv1) and Shab (Kv2) have been identified as fast and slow inactivating components of the photoreceptor's outward currents, however a current with intermediate kinetics (I_{Kf}) has not been molecularly identified, but had been postulated to be Shal (Kv4). I focused on characterizing this current using whole-cell patch clamp in wild type and mutants, and using antibodies for Shal. My results from whole-cell patch clamp indicated that I_{Kf} in adult R1-6 cells are not Shal, from their voltage dependence and insensitivity to a Kv4 blocker. This calls for alternative molecular basis for I_{Kf}, which is likely to be a slow inactivating component of Shaker, or a combination of its many splice variants. Results from antibody staining suggest that R7 cells express Shal, which is supported by the voltage dependence of I_{Kf} in R7/8.

The second study looks at signal transformation at the circuit level, at the output end, in the third optic neuropil, lobula. Visual projection neurons project from the lobula to the central brain, and have been proposed to carry behaviourally relevant visual features to higher brain regions. It was recently shown that optogenetic activation of individual visual projection neuron types could induce distinct behaviours such as takeoff and backward walking, linking these visual neurons to specific behavioural programs downstream. Using *in vivo* two-photon Ca^{2+} imaging, I recorded visually evoked Ca^{2+} responses from three of these cell types. Cell types that showed induced takeoff and backward walking preferentially responded to dark looming stimuli or fragmented expanding local features, suggesting their role in behaviours triggered by object approach. To explore how this visual information is transformed in the downstream circuit, we identified several candidate neurons that receive input from this cell type by anatomical overlap, and then validated their connections using optogenetic activation and Ca^{2+} imaging. One downstream cell-type that projects bilaterally had very similar response properties to its upstream partner, whereas another cell-type that projects ipsilaterally seemed to filter out some information from its upstream partner. This is one of the first studies that functionally characterizes lobula visual projection neurons and their downstream partners in *Drosophila*, and their response properties agree with the general idea that visual information becomes increasingly selective as it is sent to higher brain regions.

DECLARATION

I hereby declare that this dissertation is the result of my own work and has not been submitted for any other degree or qualification.

Except for where I explicitly indicate in the text, this dissertation is the result of my own work and includes nothing that is the outcome of work done by others or in collaboration.

This dissertation does not exceed the limit of length (60,000 words) specified by the Degree Committee for the Faculty of Biology.

Signed: 森本 舞 Date: 27. 09. 2016

Mai Morimoto
Murray Edwards College
Cambridge
September 2016

ACKNOWLEDGEMENTS

Firstly, I would like to thank my two supervisors Prof. Roger Hardie at the University of Cambridge, and Dr. Michael Reiser at Janelia, for their gentle guidance. I thank them for their critical suggestions and encouragement throughout my PhD. It was an inspiration and honor, to be able to work with these brilliant scientists.

Several people directly contributed data and/or figures to this thesis. I would like to thank Prof. Roger Hardie for two figures in Chapter 2, Dr. Aljoscha Nern and Janelia Flylight for confocal images in Chapter 3 and 4, and Dr. Ryan Willamson for one figure in Chapter 3.

Technical assistance from several people made this work possible. I would like to thank Prof. Roger Hardie for teaching me the art of dissociated ommatidia whole-cell patch clamp electrophysiology, Dr. James Strother for teaching me the fly *in vivo* two-photon imaging technique and sharing the fly holder design and image registration code, Dr. Allan Wong for training me on his rig for the functional connectivity experiments and sharing the regression analysis code, Dr. Ming Wu for generating and selecting split-GAL4 lines, Dr. Aljoscha Nern for help with understanding optic lobe anatomy and selecting fly lines in general, Janelia Flycore for fly husbandry training, and Dr. Ed Rogers for help with genetic strategies and fly crosses.

I would like to thank past and present members of the Hardie lab, Drs. Alex Randall, Simon Hughes, Che Hsiung-Liu, for discussions and being great office mates whilst my time at Cambridge. I am grateful to past and present members of the Reiser lab and other scientists at Janelia, especially Drs. James Strother, Eyal Gruntman, Kit Longden, Nathan Klapoetke, Katie von Reyn, Huai-Ti Lin, Allan Wong, Yi Sun and Aljoscha Nern for fruitful discussions. I would also like to thank my Cambridge advisor Dr. Hugh Robinson, and Janelia PhD committee members, Drs. Vivek Jayaraman and Na Ji for their helpful suggestions and advice.

I would like to thank the Cambridge-Janelia joint PhD program for providing me with this opportunity and research environment, and current and past program administrators, Drs. Katie Breneman, Elena Rivas, Maryrose Franko, Susan Jones and Ulrike Heberlein, for their continued support during my PhD.

I thank Hannah Haberkern and Yinan Wan for being great housemates and classmates. It was a pleasure and an inspiration to spend time with such smart and strong girls.

Finally, I would like to thank my family in Japan, for understanding my passion for neuroscience, and supporting me to pursue my PhD.

TABLE OF CONTENTS

CHAPTER 1

GENERAL INTRODUCTION

1.1 Overview

We have all at some point in our lives, played some version of the game "Chinese whispers". In this game, the players usually gather in a circle and a message is passed on to the neighboring player through whispers. In the end, the message comes back to the first player, and the original and the final messages are revealed. The entertainment of the game comes from how unexpected modifications can be made along the way. The perceptual filters of the players are the source of this modification, so hypothetically, if we have access to all the players' filters, we would be able to predict the final message. I think this analogy fits quite well conceptually, with how we are trying to understand how information is processed in the brain. The neurons pass on information, transforming it along the way. What we have access to, is the information each neuron has. From there, we try to deduce their filters. Our "understanding" of this filter can be at different levels. It can be at the information level, where we just describe what kind of modification was made to the information between neurons. We can also go one step further and try to understand the cellular or biophysical implementation of this filter. I am interested in both of these levels.

In this thesis, I studied the *Drosophila* visual system to understand information (signal) transformations at these two levels. The *Drosophila* visual system is well suited for this study, where anatomy is well documented, and tools for genetically manipulating the expression of molecules, or the activity of single cell-types are in place.

In the first study, I looked at the input of the visual system, in photoreceptor cells. Photoreceptors perform the initial transformation of photon number into a voltage signal that is processed in subsequent layers of the visual system. They are high-performance photon detectors that are able to adapt to the wide range of light levels encountered throughout the day. One mechanism that allows this light adaptation is the existence of voltage-gated potassium channels (Kvs). Kvs counteract the light response, and shape the voltage output of the cell. I studied the heterogeneity of Kvs in the retina, focusing on identifying the molecular identity of a Kv current that hitherto had not been characterized. The result showed that this current is actually not Shal (Kv4), which was the most likely suspect. From the biophysical properties of this current, I suggest a new hypothesis; this current arises from the late component of Shaker (Kv1), or is a combination of some of its many splice variants. This

heterogeneity amongst Kvs may additionally confer the photoreceptor layer to transmit the retinal image without spatial aliasing.

In the second study, I characterized the response property of neurons at the output of the visual system, lobula. At this stage of the visual pathway, the cells project to the central brain and the number of cell-types decreases dramatically. Therefore we can hypothesize that there must be a large compression of information happening at this stage; potentially extracting behaviorally relevant visual features that are sent to higher brain regions. I characterized the response properties of three lobula columnar cell-types, and the results show that they do respond to behaviorally relevant stimuli (i.e. looms and small object motion). I further identified downstream neuron types of one cell-type and found that two downstream neuron types may perform different transformations; one-type does not seem to transform significantly, whereas another type seems to filter out some visual features. This is consistent with the general notion that visual information becomes more refined as it is sent to higher brain regions.

1.2 General architecture of the *Drosophila* optic lobe

The *Drosophila* optic lobe is a large structure within the whole brain that specializes in processing visual information. Each optic lobe has ~60,000 neurons (Hofbauer & Campos-Ortega 1990), which is approximately 6 times the number of neurons in the half hemisphere of the central brain (M. Ito et al. 2013; Yu et al. 2013), suggesting that visual processing is very metabolically costly for the fly. The *Drosophila* optic lobe consists of 5 layers; retina, lamina, medulla, lobula, and lobula plate (Fig.1.1). The first layer, retina, consists of photoreceptor cells that detect photons and create the initial voltage signal. There are 8 photoreceptor types; R1-6 which all express the same opsin (Rh1) generating a dual UV and green spectral sensitivity, and R7 and 8 each with two subclasses (y and p) expressing 4 different opsins ranging from UV through to blue and green. Together with accessory cells, these 8 photoreceptor cells form a unit called “ommatidium”, and ~800 of them tile the visual field. The second layer, lamina consists of ~4,000 neurons (Hofbauer & Campos-Ortega 1990), and 5 feed forward cell-types, L1-5. These lamina monopolar cells (LMCs) are known to invert, filter, and amplify the photoreceptor signal (Autrum et al. 1970; Laughlin 1981; Laughlin et al. 1987). Importantly, the LMCs respond to both light increments

(ON) with a hyperpolarization, and to light decrements (OFF) with a depolarization (Freifeld et al. 2013; Clark et al. 2011; Reiff et al. 2010).

The third neuropil, medulla is largest, and consists of ~40,000 neurons (Hofbauer & Campos-Ortega 1990). An early golgi study identified ~70 cell-types (Fischbach & Dittrich 1989) (a recent EM reconstruction effort (Takemura et al. 2013) identified ~40 that have intracolumnar stratification, thus this number is probably an underestimate). In contrast to lamina monopolar cells, neurons in the medulla show selectivity for either ON or OFF, a segregation termed "ON and OFF pathways" (Strother et al. 2014; Behnia et al. 2014; Ammer et al. 2015). At the last layer of the medulla, motion selectivity is observed in T4 and T5 cells, indicating that computation for directionally selective motion detection is performed on the inputs of these cells (Takemura et al. 2013; Ammer et al. 2015; Serbe et al. 2016).

The last neuropils are lobula and lobula plate. There are ~15,000 neurons in these neuropils collectively. It has been estimated that lobula plate contains ~28 cell-types (Fischbach & Dittrich 1989), and lobula contains ~24 (Otsuna & K.Ito 2006). T4 and T5 cells provide directional motion signals to the lobula plate tangential cells (LPTCs), which respond to wide-field motion stimuli (Hausen 1984; Krapp & Hengstenberg 1996; Joesch et al. 2008; Chiappe et al. 2010). Aside from the LPTCs, the response properties of other lobula plate and lobula neurons has not been studied extensively (but see (Mauss et al. 2015; Aptekar et al. 2015)).

This numerical summary suggests that the information from the retina diverges until medulla, then converges at lobula and lobula plate. Two chiasms exist between the ganglia, horizontally inverting the retinotopic mapping (retinotopy) between lamina and medulla, then rotating again between medulla and lobula, which preserves retinotopy in the inputs to the lobula and lobula plate (Hausen 1984).

Below I outline the anatomy and function of photoreceptor cells and the lobula in more detail, as they are relevant to this thesis.

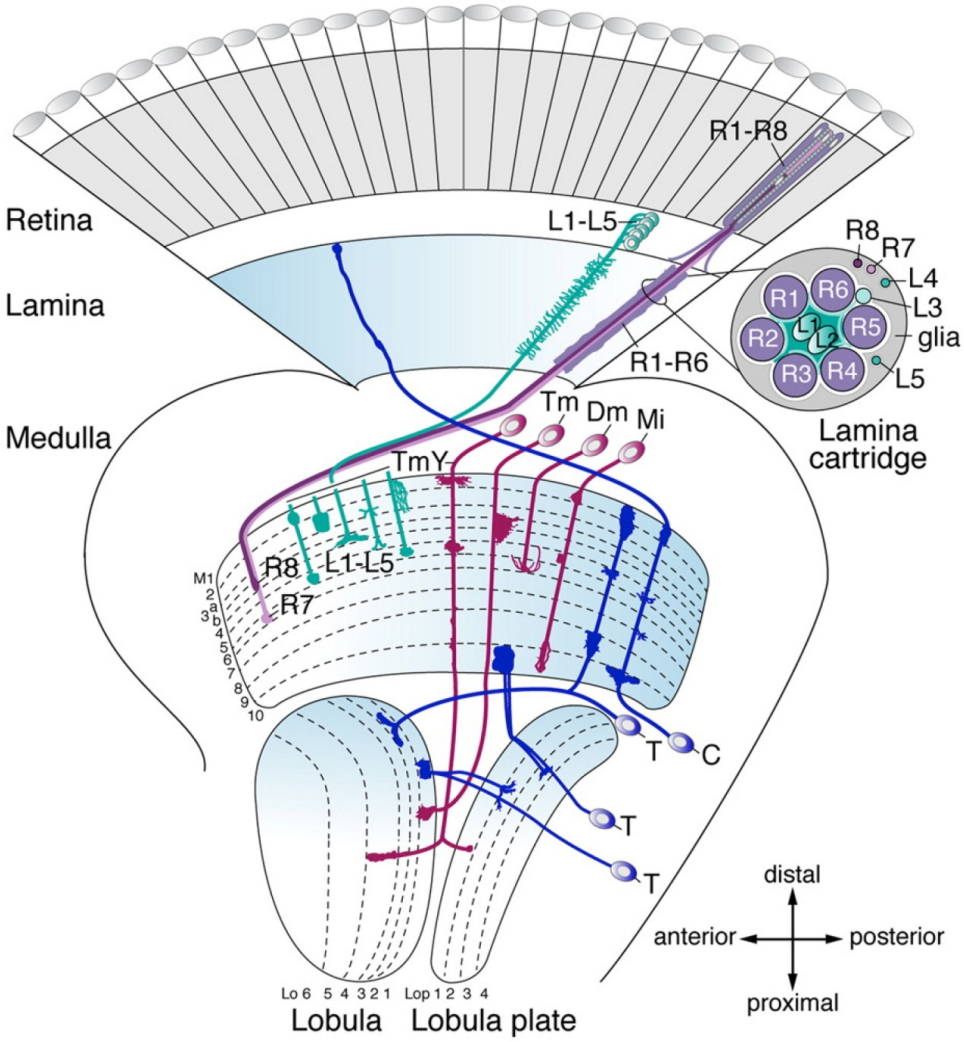

Figure 1.1 | Architecture of the *Drosophila* visual system.
The optic lobe consists of the lamina, medulla, lobula plate, and lobula. A subset of neuron subtypes and their retinotopic projections are shown. Photoreceptor R1–R6 cells extend axons from the retina into the lamina, where they connect with lamina neurons L1–L3 in cartridges. Axons of R7 and R8 cells and lamina neurons L1–L5 terminate in one or more of ten medulla neuropil layers (M1–M10). Transmedullary neurons (Tm and TmY) project from the medulla to subsets of six lobula (Lo) and four lobula plate (Lop) neuropil layers. Distal medulla (Dm) neurons innervate several columns in upper medulla layers. Medulla intrinsic (Mi) neurons connect distal and proximal layers. C neurons extend branches into the medulla and lamina. T neurons connect the lobula or lobula plate and medulla, or lobula and lobula plate. Modified from (Apitz & Salecker 2014)

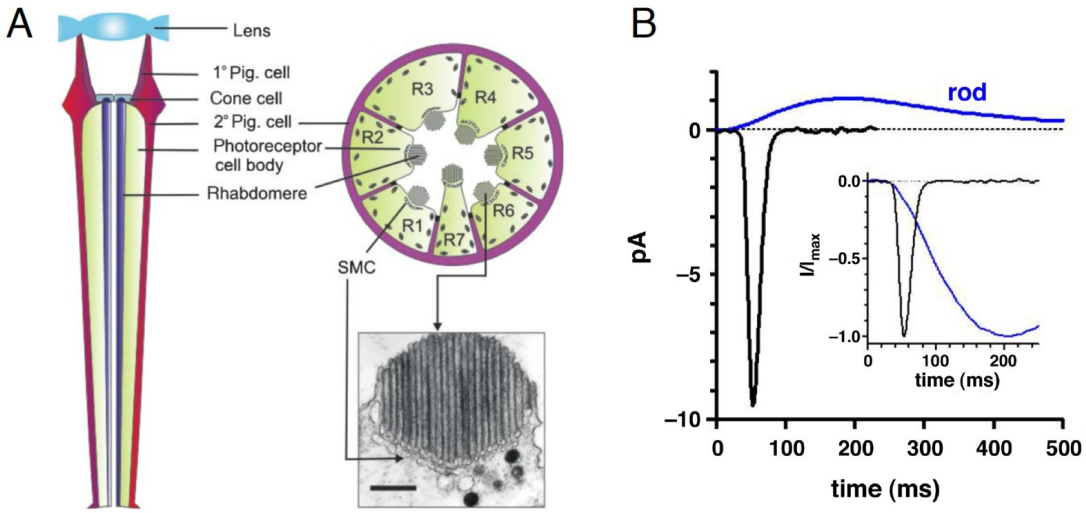

Figure 1.2 | Structure and response of the *Drosophila* photoreceptor cell
(A, Left) Section of an ommatidium showing two photoreceptors with their rhabdomeres (~80 µm long). **(Right)** in cross-section, rhabdomeres R1-R6 (λ_{max} 360 nm) surround the central R7 (UV-sensitive). R8 (blue/green sensitive) lies proximally in the ommatidium. The electron-micrograph shows one rhabdomere, with one row of its stack of ~30,000 microvilli (scale bar 0.5 µm). **(B)** Single photon responses (quantum bumps) in *Drosophila* (black) and mouse rod (blue): inset, normalised to compare kinetics. Modified from (Hardie 2011) and (Hardie & Juusola 2015)

1.3 Anatomy and function of photoreceptor cells

Photoreceptors are a specialized class of sensory neurons, which have an extremely high photon detecting performance. First of all, their structural design is unlike any other neuron in the visual system (Fig.1.2A). The *Drosophila* photoreceptor cell is composed of two compartments, the cell body and the rhabdomere. The rhabdomere is where photons are absorbed by rhodopsins, and is made of microvillar membrane, which maximizes the surface area for photon detection. Under a single facet of the compound eye, 8 of these photoreceptors are arranged radially, R1-6 cells containing the same rhodopsin (Rh1, λ_{max} = 480 nm), and R7 and R8 cells containing various rhodopsins (Rh3-6, λmax ~340, 370, 440, and 510 nm, respectively). This arrangement results in a rod-like structure with a central cavity lined with ~30,000 microvilli, acting as a light guide.

In response to light, microvillar photoreceptors depolarize, while vertebrate rods and cones hyperpolarize (Fig.1.2B). Because ~10^4 channels are open in the dark in the vertebrate rods, several hundred channels need to close in order to create enough

signal to noise, whereas in microvillar photoreceptors, only a few channels need to open for sufficient signal. This mechanism enables the single-photon resolution of *Drosophila* photoreceptors (Henderson et al. 2000).

The response to single-photons can be measured by whole-cell patch clamp recordings in dissociated ommatidia. This light-induced current, called "quantum bump", has a mean amplitude of ~10pA and has a variable latency of ~15-100ms, representing ~15 channel openings (Henderson et al. 2000). The overall time course is ~10-100 times faster than vertebrate rods (Fig.1.2B). The aspect of the photoreceptor as a mechanosensor has had renewed recognition by the recent finding that photoreceptors "twitch" in response to light, which was found to have an important role in this fast latency of the light response (Hardie & Franze 2012; Randall et al. 2015).

The rhabdomere is photosensitive and is crucial for phototransduction, which is known to be the sequential activation of rhodopsin, a heterotrimeric G-protein, phospholipase C, and two TRP channels, opening of which causes membrane depolarization (Hardie 2011). The cell body on the other hand, is enriched with Na^+/ K^+ transporter and voltage-sensitive potassium channels. The Na^+/ K^+ transporter hyperpolarizes the cell, and the voltage-sensitive potassium channels also counteract the light response preventing the response from saturation during light adaptation (Hardie 1991; Gu et al. 2005). Biophysically realistic models have been made to recapitulate the generation of the quantum bump, and explain how these underlying molecular mechanisms subserve perceptual contrast constancy, novel event enhancement, and reliable signal to noise within the naturalistic range of temporal frequencies and light levels (Song et al. 2012).

1.4 Anatomy and function of the lobula

The lobula is known to receive inputs from medulla and lobula plate (Fischbach & Dittrich 1989). The transmedullary cells (Tm and TmY) and T cells that carry signals from medulla to the lobula and/or lobula plate, are its main feedforward inputs. Some T cells and Y cells have been found to connect the lobula plate to lobula (Fischbach & Dittrich 1989), and more recently, LPLC (lobula plate lobula columnar) neurons have also been found to participate in this cross-link (Wu et al. 2016).

While medulla and lobula plate neurons of *Drosophila* have received much attention in the context of wide-field motion detection, the function of the lobula remains elusive. Since the neural substrate of many visually guided behaviors are unidentified, the lobula has become the prime candidate structure to provide visual information required for these behaviors by method of elimination. These behaviors include escape behavior or collision avoidance to expansion cues (Card & Dickinson 2008; Muijres et al. 2014), repulsive behavior to small object motion (Maimon et al. 2008), landing behavior (Tammero & Dickinson 2002), object tracking (Bahl et al. 2013), and male pursuit of females and generation of song during courtship (Cook 1979; Coen et al. 2016). *Drosophila* are also known to possess a certain capacity for object shape and color discrimination as shown by learning paradigms (Liu et al. 1999; Schnaitmann et al. 2013), and show innate preference to pursue or explore artificial objects of certain size and motion profile (Agrawal et al. 2014; Robie et al. 2010).
In larger insects however, there has been a number of electrophysiological studies showing that lobula neurons carry such ethologically relevant visual cues. I review representative studies below, categorized by the main visual features lobula neurons are found to encode.

Loom

The wide-field LGMD (lobula giant movement detector) of the locust is arguably the most well studied neuron in this category. Intracellular recordings in LGMD have shown its selectively to looming motion on a collision course (Gabbiani et al. 1999). This selectivity has led to the hypothesis that this neuron signals the time to collision, and triggers escape behavior. Indeed, through wireless telemetry recording, the downstream neuron DCMD (descending contralateral movement detector) has been shown to correlate well with the timing of leg muscle activity at the moment of escape jump (Fotowat et al. 2011).
The crab *Chasmagnathus* which have homologous optic lobe structure to insects, is also known to possesses looming sensitive tangential neurons, MLG (monostratified lobula giants) type1 and 2, and bistratified lobula giant (BLG) type1. Through intracellular recordings, it was shown that these neurons also show responses to single object motion, such as bar and small squares, but not for wide-field grating motion (Medan et al. 2007). MLG1 is a smaller tangential neuron, and was the only type that

showed directional selectivity. 16 of them tile the visual field, a configuration thought to mediate the highly directional escape behavior crabs show in response to loom (Medan et al. 2015).

In a recent account, ~3 tangential cells innervating the *Drosophila* lobula and/or lobula plate labeled by the enhancer trap line Foma-1 were shown to be loom sensitive assessed by loose-patch recordings (de Vries & Clandinin 2012). These cells possess response properties that are similar to that of LGMD, except that the timing of peak response occurs after the expected time to collision. Genetic silencing of this population reduced visually evoked escape takeoff strongly, and activation induced significantly more takeoffs. However, since this genetic line labeled several cell-types, it is difficult to interpret which neurons were mediating the escape behavior.

The moth *Manduca sexta* has been subject to exploratory intracellular cellular recordings, and some examples of looming sensitive neurons have been described (Wicklein & Strausfeld 2000). Large tangential neurons innervating both the lobula and lobula plate, and projecting to various central brain regions have been shown to be looming sensitive to differing extents. Generally, all neurons were sensitive to both loom and anti-loom (receding) and showed contrast invariant responses. One class responded to luminance change, and another to moving edges, so it was hypothesized that these two classes of neurons could collectively signal the existence of an approaching or receding disc by encoding the perimeter of the disc and the visual motion created by the edge.

This collection of neuron-types and response properties show that many different forms and mechanisms of loom detection may be taking place in the insect (arthropod) lobula.

Small targets

The dragonfly STMD (small target motion detector) is perhaps the most well documented example of small target detecting neurons in the insect lobula. STMD shows highly selective response to small moving targets (<3° angular size), and are inhibited by, or do not show responses to larger bars (>10° angular size) and wide-field grating motion. This characteristic has been compared to the “end-stopping” nature of mammalian hypercomplex neurons, which was previously thought to be a unique feature of mammalian neurons (O'Carroll 1993). A requirement for animals tracking small targets in natural environments is their ability to discriminate the

motion of the target from self-motion. STMDs show high discriminability for target motion even when the target is presented over a highly cluttered background (noise or natural scenes) that also moves, fulfilling this ethological need (Wiederman & O'Carroll 2011). Moreover, a recent study showed that a class of STMD (CSTMD1; centrifugal small-target motion detector 1) that receives input from one optic lobe and projects to the contralateral optic lobe, shows a "selective attention" like property, in which the activity of the neuron locks onto one target when two targets are simultaneously presented (Wiederman & O'Carroll 2013). The response dynamics further suggested a "competitive" mechanism underlying this selectivity. Although it has not been proven to date in freely behaving animals, CSTMDs are obvious candidates for mediating behaviors such as prey pursuit in a swarm of flies, or selecting a conspecific to chase given a number of options.

Hoverflies also possess STMDs, which have similar response properties to the dragonfly STMD. However, their sexual dimorphism may be more pronounced; the excitatory receptive field of male hoverflies' STMD is in the frontal-dorsal area whereas in females it extends to the whole frontal region (Nordström & O'Carroll 2006; Nordström et al. 2006). The male's receptive field location matches its dorsal "acute zone" which has been associated with male-specific pursuit such as courtship or territorial pursuits.

Orientation

A few studies have shown orientation selectivity in lobula neurons. The motivation for these studies were to find a neural basis for pattern or shape discrimination ability that have been shown through learning paradigms in some insects (Srinivasan et al. 1993). Orientation selective responses have been recorded extracellularly in the dragonfly lobula (O'Carroll 1993), and intracellularly in honeybee anterior optic tubercle (Maddess & Yang 1997), but the cells remain unidentified. More recently, an extensive exploration of the lobula neurons that project to central brain was conducted in the large fly *Calliphora* to find orientation selective neurons (Okamura & Strausfeld 2007). By intracellular recording and subsequent dye filling, a number of response properties and morphology of cell-types were documented. The morphology of cell-types categorized them into 1) lobula-lobula plate neurons, 2) lobula tangential neurons, 3) heterolateral protocerebral neuron, 4) optic glomerular output neuron, and 5) local spiking interneuron. The first three cell-types arborize in the lobula (and some

in lobula plate), and the last two cell-types arborize in the protocerebrum, the output region of lobula neurons, making them presumably the direct downstream targets of lobula neurons. The response properties of these neurons were generally broadly orientation tuned and only weakly sensitive to grating motion, except for the optic glomerular output neuron and local spiking interneuron that showed a narrower orientation selectivity. In all of these accounts, the link between orientation selectivity and pattern discrimination is yet to be demonstrated.

Color

There are several studies especially in bees that looked at color encoding in the lobula. The most comprehensive study might be in the bumblebee, where intracellular recording and dye filling was performed for neurons that arborize in different layers of the lobula. In brief, they found that neurons that arborize in lobula layer 1-4 responded reliably to grating motion, but those that arborize in layer 5-6 or 1-6 responded to color or color and motion. The responses in lobula layer 1-4 is reminiscent of dipteran lobula plate tangential cells, which may have their ancestral origins in the early layers of the honeybee lobula. The color responding neurons could be divided into broadband, narrowband and color opponent types in the order of selectivity, and narrower selectivity was observed in neurons innervating deeper layers of the lobula. Other studies in the honeybee have also found color opponent and non-opponent cells in the lobula (Yang et al. 2004). They found that there were more types of response patterns of color opponent cells than that of primates (8 types compared to 6 types), suggesting that honeybees may possess a more complex color encoding scheme.

One theme that arises from this brief survey of lobula neuron responses is that most neurons do not exclusively respond to one visual feature. For example, the locust LGMD is known to also respond robustly to small target motion (Rowell et al. 1977), and the crab loom sensitive neurons also respond to small object and bar motion. This may not be surprising given the convergent inputs from the medulla (and lobula plate) onto lobula. However, there are examples such as the STMD, which seem to have extremely high selectivity. These differences in the degree of selectivity among lobula neurons may indicate that they represent different stages of visual processing in different species. Alternatively, it could reflect the different ethological demands that

these species face. It is plausible that the evolutionary pressure to create a highly target selective neuron for aerial predators like dragonflies or to create many color opponent cells in the honeybee is much higher than for a fruit fly or locust.
A similar but distinct notion is that this stage of visual processing is tuned to natural images. A recent account showed that a hoverfly lobula plate projection neuron is tuned to natural image statistics (Dyakova et al. 2015), and a behavioral genetics study found that silencing some lobula tangential neurons in *Drosophila* reduced its optomotor responses to second-order motion (Zhang et al. 2013), which is apparently prevalent in naturalistic movies (Nitzany & Victor 2014). These accounts are reminiscent of the tuning found for natural image statistics in mammalian visual cortex (Field 1987), but this tuning is yet to be directly demonstrated in lobula neurons.

1.5 Aim of the thesis

The aim of this thesis is to contribute to our understanding of neural information processing by studying filtering properties of visual neurons at the biophysical and circuit level. For the biophysical level, I studied the heterogeneity of voltage-gated potassium channels (Kvs) in *Drosophila* photoreceptor cells, focusing on the molecular identity of a current that may confer the photoreceptor layer to transmit signals with more fidelity (Chapter 2). For the circuit level, I studied the response properties of *Drosophila* lobula columnar (LC) cell-types, using visual stimuli designed around features that are relevant to the behavior induced by the optogenetic activation of those neurons (Chapter 3). I then went on to identify the downstream circuit components of one LC cell-type, in order to understand the transformation between the LC cell-type and its downstream targets (Chapter 4). Each chapter contains its own methods section, since distinctly different methods were used among the chapters.

CHAPTER 2

HETEROGENEITY OF VOLTAGE-GATED POTASSIUM CURRENTS IN PHOTORECEPTOR CELLS

Data contributions:
Electrophysiology and immunohistochemistry data collection and analysis were performed by Mai Morimoto. Some additional electrophysiology data from WT adult flies (Figure 2.2 and 2.3), all pharmacology data (Fig.2.10), and data from WT pupal flies (Fig.2.11) were contributed by Roger Hardie.

2.1 Introduction

2.1.1 Voltage-gated potassium currents in photoreceptors

Voltage-dependent potassium (Kv) channels are considered to be the most highly diversified class of voltage gated ion channels, and with their wide range of gating kinetics, are known to play important roles in fine-tuning the response of neurons and sensory receptor cells (L. Y. Jan & Y. N. Jan 2012; Jensen et al. 2011; Hardie 1991). In the case of insect photoreceptor cells, inter-species differences in Kv conductance has been correlated to the animals' visual ecology, matching its required temporal frequency (Weckström & Laughlin 1995). Fast flying diptera possess "fast photoreceptors" in which delayed rectifiers are expressed predominantly, contributing to lowering the membrane resistance and reducing the membrane time constant, thereby enabling the membrane to transduce fast voltage signals. On the other hand, slow flying diptera possess "slow photoreceptors" lacking the delayed rectifier, but instead expressing fast inactivating Kvs, which contribute to the slower response properties of the cell.

Different classes of photoreceptors in the same ommatidia are also known to express different sets of Kvs, most notably the total lack of delayed rectifiers in R7/8 cells while R1-6 cells expresses a substantial amount (Anderson & Hardie 1996).

2.1.2 Modulation of voltage-gated potassium currents in photoreceptors

Modulation by neuromodulators or channel interacting proteins has been found to change the biophysical properties of voltage-dependent potassium channels. Serotonin induces a positive shift in the voltage dependence of fast and slow inactivating currents in *Drosophila* photoreceptors (Hevers & Hardie 1995), and in locusts, it creates a change similar to a switch from fast to slow dipteran photoreceptor types (Cuttle et al. 1995). In fact, photoreceptors are modulated diurnally in locusts making them "fast" during the day and "slow" during night. In *Drosophila*, calcium activated Kv channel Slowpoke binding protein Slob, known to shift the voltage operating range of the channel, has been found to be diurnally regulated in the photoreceptor, potentially contributing to changes in its sensitivity (Jaramillo et al. 2004; Zeng et al. 2005).

2.1.3 Spatial heterogeneity of voltage-gated potassium channel currents

In the fly eye, different regions of the retina respond to light with different temporal resolution, suggesting that they are tuned for different visual tasks, for example to suit the detection and tracking of small moving objects, a task required in male flies for the pursuit of females, or to match response dynamics to optic flow fields experienced during flight (Burton & Laughlin 2003; Burton et al. 2001). Such temporo-spatial tuning of photoreceptors might be reflected in differential expression of Kv currents, which could be conceptually similar to the differential expression of calcium-activated (BK) potassium channel splice variants that tunes hair cell response frequency along the cochlea's tonotopic axis (Fettiplace & Fuchs 1999). However, little is known about the differences in intrinsic properties of each photoreceptor cell throughout the retina, which contributes to shaping the response to incoming light.

2.1.4 Shal (Kv4) as candidate for molecular identity of I_{Kf}

Whole-cell voltage clamp recordings from fly photoreceptor cells offer the opportunity to quantify the Kv channels with high precision. Using this technique, it has previously been shown that these cells contain at least three sets of potassium currents, a rapidly inactivating current (I_A) encoded by the *Shaker* gene (Kv1) (Hardie et al. 1991), a slowly inactivating delayed rectifier (I_{Ks}) encoded by the *Shab* gene (Kv2) (Vähäsöyrinki et al. 2006), and a faster delayed rectifier (I_{Kf}) in varying amounts. Amongst these, I_{Kf} seemed to show the greatest variability (personal communication from Prof. Roger Hardie), but its molecular identity remains unknown (Table 1)(Hardie 1991). Judging from its kinetics, it has been postulated that this current corresponds to the Shal (Kv4) (Wei et al. 1990; Vähäsöyrinki et al. 2006).

Table 1 Major Kv currents found in *Drosophila* photoreceptors, and its molecular identity

Nomenclature of Kv currents	**Molecular identity**	**Reference**
$\boldsymbol{I_A}$	Shaker (Kv1)	(Hardie et al. 1991)
$\boldsymbol{I_{Ks}}$	Shab (Kv2)	(Vähäsöyrinki et al. 2006)
$\boldsymbol{I_{Kf}}$	Shal (Kv4)?	N/A

Thus this project hoped to attain two major goals:

- To assess the variability of Kvs (focusing on the I_{Kf}) throughout the retina, in order to provide a molecular basis for some functional phenomena such as the spatial variation in temporal resolution mentioned above.
- To characterize the molecular identity and distribution of the I_{Kf} within the retina.

2.2. Methods

2.2.1 Fly lines

Flies (*Drosophila melanogaster*) were raised in the dark at 25°C in plastic vials containing approximately 15g of a standard food recipe consisting of 1.7g dried baker's yeast, 1g agar, 9.7g cornmeal, 8.6g glucose and Nipagin to 2.9% in 100ml tap water. Both male and female flies were used. Wild type flies, Oregon-R-S (ROR) and Oregon- w^{1118} (WOR) were obtained from a stock maintained in Cambridge, UK. $Shab^{3}$ and $Shal^{495}$, Sh^{14} flies were obtained from Bloomington stock center. Sh^{14} flies were also gifted from Dr. Richard Baines after the Bloomington stock died out. Details of the mutants are outlined in Table 2. Homozygous mutants were used, except for $Shal^{495}$ which was homozygous lethal.

Table 2 Fly mutants used

Fly	Mutation	Reference
***Shab*^{3}**	Deletion leading to a frameshift; protein null	(Hegde et al. 1999)
***Shal*^{495}**	Transposon insertion; protein null	(Bergquist et al. 2010)
***Sh*^{14}**	Missense mutation in the core region; non-functional protein	(Lichtinghagen et al. 1990) (Hardie et al. 1991)

2.2.2 Solutions

The standard bath solution used to suspend dissociated ommatidia contained (in mM): 120 NaCl, 5 KCl, 10 N-Tris-(hydroxymethyl)-methyl-2-amino-ethanesulphonic acid (TES), 4 $MgCl_2$, 1.5 $CaCl_2$, 25 proline and 5 alanine. Standard intracellular solution contained (in mM): 140 KGluconate, 10 TES, 4 Adenine 5'-triphosphate magnesium salt (MgATP), 2 $MgCl_2$, 1 NAD, 0.4 Guanosine 5'-triphosohate sodium salt (NaGTP). The pH of all solutions was buffered to pH 7.15. The bath solution was made up to an osmolarity of 284mOsm, and the intracellular solution to 276mOsm.

2.2.3 Preparation of ommatidia

Individual ommatidia were obtained through a process of dissociation, after dissection from recently eclosed (<4 hr) adult flies using a procedure developed by Hardie (Hardie et al. 1991). Flies were immobilized through cooling on ice and quickly decapitated. Under red light, heads were secured under chilled working solution (composition as described above), and eyes removed with a shard of a razor. Retinas were removed (scooped-out) from the cornea using fine forceps and an insect pin flattened and slightly curled to form a scoop-like structure at the tip. Followed by an incubation of ~20 min in the dark (dark-adaptation), ommatidia were broken off from the basement membrane and isolated from surrounding pigment cells using mechanical force applied through gentle trituration of the dissected retina in bath solution supplemented with 10% Fetal Calf Serum (FCS). Trituration pipettes were made by fire-treating fibreless glass capillaries (Harvard Apparatus, GC100 -10) to form bores of 100- 200µm. Trituration pipettes were prepared manually beforehand. Briefly, one end of the glass capillary was fire-treated briefly, then taken out of the flame and instantly pulled. A diamond pen was used to scratch the surface of the thinned part of the capillary, then mechanical force was manually applied by tapping on the short side of the capillary until it was broken off. The tip of the long side of the capillary was fire-treated again until the desired diameter was achieved. Individual dissociated ommatidia were transferred to a recording chamber with a new coverslip attached to form the bottom, on the stage of an inverted Nikon microscope. Recording from the ommatidia was conducted within 30-50 mins after dissociation to ensure cell viability.

2.2.4 Patch clamp setup

After the cells had settled to the bottom of the recording chamber, they were visualized through the inverted Nikon microscope. The objective lenses used were an oil immersion objective (Nikon CF-fluor 40X, NA 1.30) and an air objective (40X, NA 0.65). The whole setup was mounted on an air-table, and a grounded aluminium-sheet Faraday cage enclosed the microscope to prevent electromagnetic interference. Lower noise recording was also achieved by covering the front opening of the cage by a copper fabric cloth during experiments. The recording electrode was manually positioned using a Piezo-micromanipulator (Burleigh). The recording and the reference electrodes were connected to an Axon Instrument's CV-4 headstage unit.

Signals were amplified using an AxoClamp-1D amplifier (Axon Instruments, Foster City, CA), filtered below 2 kHz. Scaled output signal was monitored via a digital oscilloscope. Data were acquired using Clampex 9 (Axon Instrument) on a PC interfaced with Digidata 1322A (Axon Instruments).

2.2.5 Electrode preparation

Electrodes were made using borosilicate glass capillaries (Harvard Apparatus, GC100 F-10) pulled using a vertical two-stage pipette puller (Narishige, PP-83). Both ends of the glass capillaries were fire treated briefly, then fastened into the puller. The setting for first and second pull stages was set to 13.1 and 11.2 respectively, which created electrodes of bath resistance ~ 10-20 MΩ.

2.2.6 Whole cell recordings

Whole-cell patch-clamp recording were performed on individual photoreceptors at room temperature (21°C). The recording electrode was lowered into the bath solution with constant positive air pressure applied via a mouthpiece connected to the electrode holder by flexible tubing, in order to minimize mixing of intracellular and bath solutions. Cells for patching were selected based on the perceived viability of the cell (cells with smooth surface with good tension of the membrane were considered healthy, whereas bumpy surfaced and shriveled cells were considered unhealthy) and ease of access. Electrodes were positioned at the dent below the soma using coarse control, and contact was made through a quick motion controlled by a fine micro-manipulator (Fig. 2.1A). If the somata at the distal end of the ommatidia were selected for patching, they were always R1-6 cells, whereas when somata halfway down the ommatidia were selected, it was either an R7 or 8 cells. The class of cells could also be confirmed by cell capacitance; R1-6 photoreceptors have a capacitance of 40-80pF, whereas R7 and 8 cells have a capacitance of roughly half. Using moderate suction, a seal (>GΩ) was formed between the pore of the pipette and the membrane resulting in the "cell-attached" configuration. Brief bursts of additional suction or a high amplitude voltage pulse ("ZAP" feature in AxoPatch amplifier) were applied to rupture the cell membrane so that the electrode and intracellular solution became continuous with the cytoplasm of the cell resulting in the "whole-cell" configuration. Experiments were performed with cells clamped near physiological resting potential at -70mV (after correction for a junction potential of -10mV). For pharmacology,

solutions containing phrixotoxin-2 (Alomone labs) and 4-amino-pyridine (250 µM Sigma) were made up on the day of use from aqueous stock solutions kept at -20^{o}C.

2.2.7 Clamp quality

Membrane capacitance, membrane resistance and series (access) resistance were estimated by running membrane tests on the Clampex software. Series resistance (R_S) is the electrical resistance between the pipette and the cell membrane, which generates a voltage error (voltage error =R_S*total current, from Ohm's law) and creates a series resistance error between actual membrane voltage and the voltage protocol and also limits the clamp time constanct (R_S x Cm). Thus the R_S values during experiments were routinely compensated electronically to ~70-80% using the amplifier resulting in R_S < 5 MΩ. Moreover, the membrane capacitance (Cm), which is proportional to the large surface area of microvillar membrane (~60 pF in recently eclosed adult WT flies), was also compensated for. Finally, capacitative transient currents resulting from the pipette wall (stray capacitance) were also corrected.

2.2.8 Protocols

Using voltage clamp mode, different protocols were ran to experimentally control the membrane potential in order to characterize the voltage dependence of membrane currents. All recorded photoreceptors were initially held at -70 mV unless otherwise stated. Since voltage-gated channels enter a stable non-conducting state (inactivated state) after a certain period of depolarization, a "removal of inactivation" protocol, which consisted of prepulse voltage steps of 10mV from -100 to -10 mV and a subsequent step to a more positive voltage, was used. In most cases, a step of +20 or 30 mV was used after the prepulse, which activated all outward currents. In some cases, a protocol stepping to -20 or -30 mV was used so that Shab currents would not be activated.

2.2.9 Data Analysis

Boltzmann distribution ($I/I_{max}= 1/\{1 + \exp((V_{50} - V)/s)\}$) was used to fit I-V curves, where s is the slope factor. Pearson's correlation coefficient (r) was used to assess degree of correlation. Data are presented as mean ±SEM; *p<0.05, **p<0.01, *** p<0.001 (student's t test). In boxplots, the red line denotes the mean, light red area is the 95% confidence interval, and the blue line is 1 SD.

2.2.10 Western Blot

A 9% running gel was prepared consisting of: 4.4ml ddH_2O, 2.5ml 1.5M Tris-HCl pH8.8, 3ml Acrylamide (30%), 100 µl SDS (10%), 50 µl Ammonium Persulphate (10%) and 5 µl TEMED. A stacking gel was prepared consisting of: 1.9ml ddH_2O, 1ml Tris-HCl pH6.8, 0.67ml Acrylamide (30%), 40 µl SDS (10%), 30 µl Ammonium Persulphate (10%), 5 µl TEMED. Samples were prepared using 10 whole heads for one batch. 2-3 day old flies were decapitated and homogenized at 80°C in a lysis buffer consisting of: 50mM Tris-HCl pH6.8, 25mM KCl, 2mM EDTA, 0.3M sucrose and 2% SDS. Samples were incubated for an additional 5mins at 80°C. Sample loading buffer (x5) consisting of: 250mM Tris-HCl pH6.8, 10% SDS, 30% Glycerol, and 0.02% bromophenol blue, 5% beta-mercaptoethanol, were added to make x1 concentration. Samples of 15 µl (≈ 1.7 heads) were loaded and run at 100mV constant for fractionation. The samples were then transferred onto Amersham Hybond-P transfer membranes (GE Healthcare) in Tris–glycine buffer at 400mA constant for 1hr. The blots were probed with primary rabbit antibodies: either 1/3000 dilution anti-α-tubulin (Abcam, ab15246) or 1/1000 dilution anti- Shal (a gift from Dr. Baro and Dr. Tsunoda) and then subsequently with 1/5000 dilution anti-rabbit IgG peroxidase conjugate (Promega, w401B). The signals were detected using ECL reagents (GE Healthcare).

2.2.11 Immunohistochemistry

Retinae from 0–2 days old white eyed flies (WOR) were dissected as described above under red light in chilled 4% formaldehyde (Polysciences Inc.) diluted in 1× phosphate buffered saline (PBS). The cornea was removed from the retinae for better penetration of the antibodies. They were then incubated in 4% formaldehyde for another 15 minutes at room temperature and washed three times with 1× PBS+0.3% Triton X-100 for 10–15 minutes. The tissues were then incubated in blocking solution containing: 5% fetal calf serum (FCS) in 1× PBS+0.3% Triton X-100, for 1 hour at room temperature, after which the tissues were incubated with primary anti-*Shal* antibody (gift from Dr.Baro, antibody made against lobster shal) or anti-*Shal* antibody (gift from Dr.Tsunoda, antibody made against rabbit shal) diluted in blocking solution at 1:25, overnight (≈ 16 hours) at room temperature. Secondary antibodies conjugated with a fluorophore were used at 1:1000 dilutions anti-rabbit IgG–Alexa-Fluor-488

(Molecular Probes) and incubated 2.5 hours at room temperature. During the incubation with secondary antibody Rhodamine–phalloidin (Invitrogen) was also added to the tissues to stain the F-actin (1 unit in 200 µl of blocking solution). After three washes in 1× PBS+0.3% Triton X-100 the tissues were quickly washed in 1× PBS, mounted in mounting medium (0.25% n-propyl gallate in 50% glycerol in 1× PBS). The whole-mounted preparations were viewed under a Leica TCS (SP2) confocal microscope using 488 nm and 561nm wavelength lasers.

2.3 Results

2.3.1 Measurement of Kv currents in WT fly photoreceptors

Whole cell patch clamp recordings were made from WT (ROR or WOR) photoreceptor cells as described above. By applying the removal of inactivation protocol wherein the cell is held with prepulses (1 sec duration) of negative voltages (-10mV to -100mV in decrements of 10mV) and subsequently stepped to a positive voltage (+20 or +30mV), a mixture of at least three outward currents were observed. The delayed rectifier Shab current could be observed throughout the protocol, whereas the two fast inactivating currents Shaker and I_{Kf} were observed with prepulses below ~ -40 mV (Fig. 2.1B).

In order to quantify these three Kv currents, measurements of current amplitude were taken from different regions of the recorded trace. Because of the different kinetics of the three Kvs, the first peak can be largely attributed to Shaker, and the amplitude at 100ms (when all the other fast inactivating currents have already inactivated) can be almost wholly attributed to Shab, although it had also inactivated to some extent by then (Fig. 2.1B inset). However, I_{Kf} cannot be directly measured, as its temporal range overlaps with that of Shaker and Shab (Hardie 1991). Thus the measurement of I_{Kf} was obtained by subtracting the Shab current amplitude from the amplitude 30ms after stepping to +30mV, a time point in which the Shaker current should have already inactivated (Fig. 2.1B inset). All measurements were taken at the maximum amplitude within the protocol, which was usually with the prepulse of -100mV, but in some rare cases it was with prepulses of -80 or -90mV.

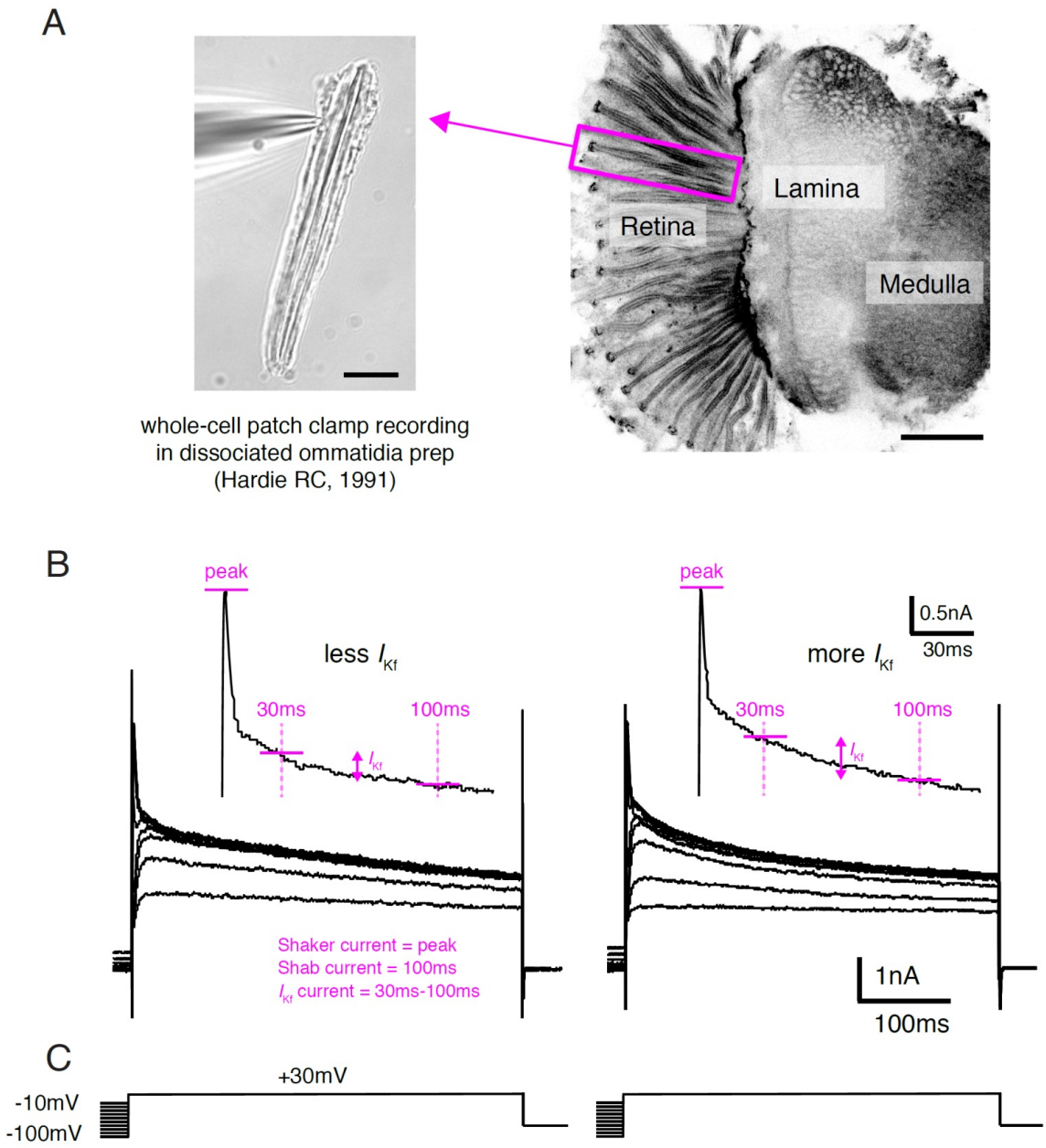

Figure 2.1 | Whole-cell patch clamp recording of three Kv currents in WT (ROR) flies

(A) Whole-cell patch clamp recordings were made in dissociated ommatidia preparation. Left image shows an electrode making contact to a patch of membrane below the soma (Image courtesy Hardie RC). Right is a confocal image of the whole optic lobe. Estimated scale bars 10 and 50mm respectively. **(B)** Example traces from two different cells. The right trace contained more I_{kf} compared to the left trace. Inset trace is the region containing the first 100ms of the most top trace (-100mV prepulse protocol) on expanded scale. Absolute current amplitudes were measured and calculated as described in magenta font. **(C)** Removal of inactivation protocol used. Prepulse ramp from -100mV to -10mV is followed by a positive step to +30mV.

2.3.2 Variability of voltage-gated potassium currents in WT photoreceptor cells

In order to assess the variability in Kv currents, the amplitude of I_{Kf} was plotted against Shaker and Shab current amplitudes, where no apparent correlation was observed (correlation coefficient r^2 ≈ 0.17, 0.09 respectively, Fig. 2.2A). The variability of current amplitude amongst cells was measured via the coefficient of variation (CV): 0.16 for Shaker, 0.18 for Shab, and 0.29 for I_{Kf}. Although CV for I_{Kf} appeared somewhat larger , given the difficulty of accurate estimation of I_{Kf}, this could be attributed to experimental variation (Fig. 2.2B). If channel density were constant, the size of the cell would be proportional to the size of the currents recorded. To test whether the cell-size variability is the source of the current amplitude variability, membrane capacitance was plotted against the Kv current amplitudes (Fig. 2.3). Membrane capacitance is proportional to the membrane area (of which typically 85-90% is microvillar membrane). The correlation between membrane capacitance and current amplitude was positive in each case, but weak, also considering the group size of ≈ 30 cells (correlation coefficient r^2 ≈ 0.1 to 0.35, Fig. 2.3 inset). Taken together, the amplitude of Shaker, Shab and I_{Kf} seems to vary independently of each other, and the amount of variation is rather similar across currents. The current amplitude and the size of the cell does not seem to correlate strongly, thus other sources such as varying expression levels of the channels, and/or experimental variation (i.e. varying voltage clamp quality, viability of the cell, etc.) could possibly account for the variation.

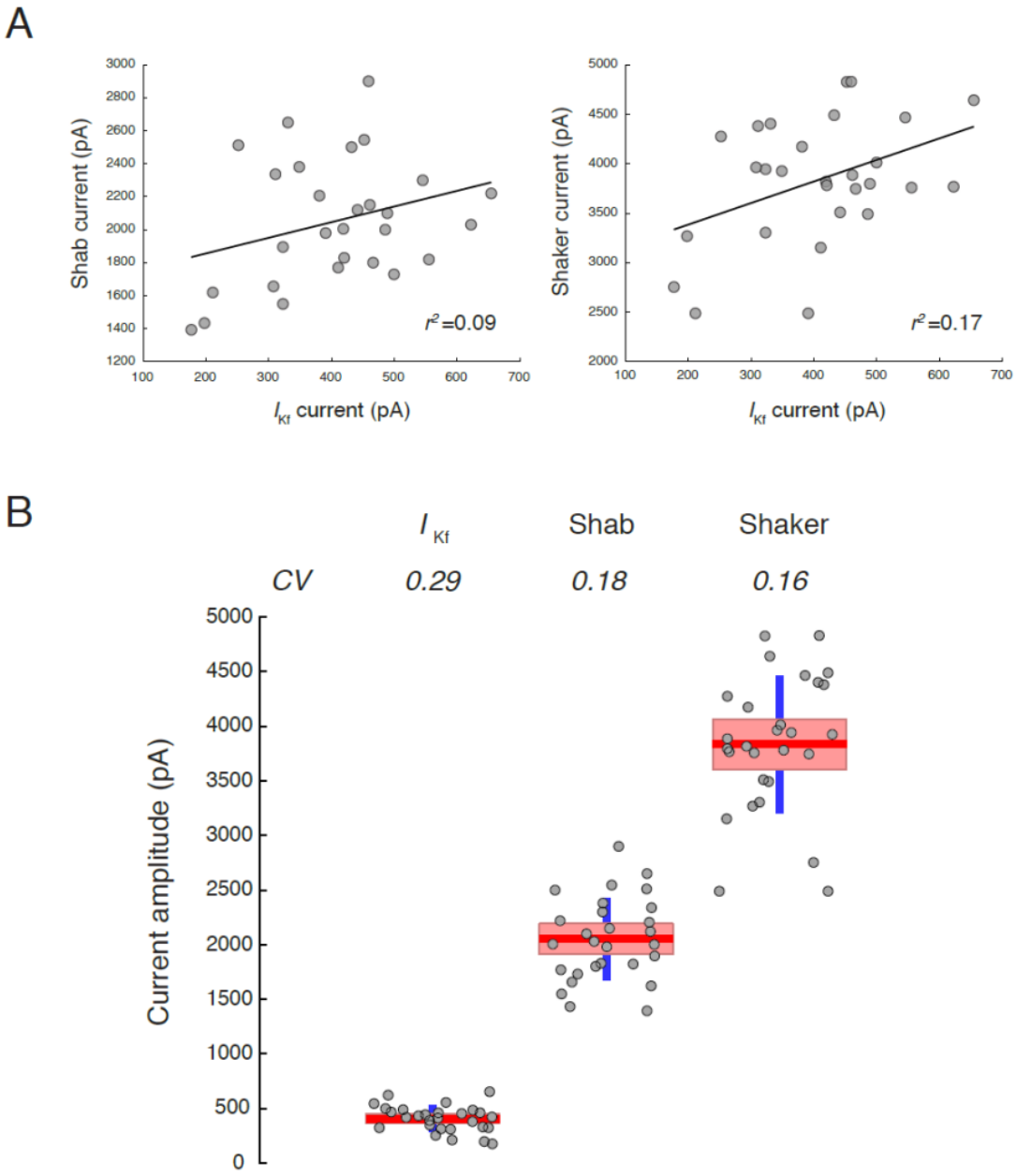

Figure 2.2 | Variation of Kvs in WT (ROR) flies
(A) Plot of I_{Kf} amplitude against Shaker and Shab current amplitudes. r is Pearson's correlation coefficient. **(B)** Comparison of variation across the three currents (N=28). Coefficient of variation (CV, S.D./mean) is denoted in italics.
Partial data from Hardie RC (unpublished).

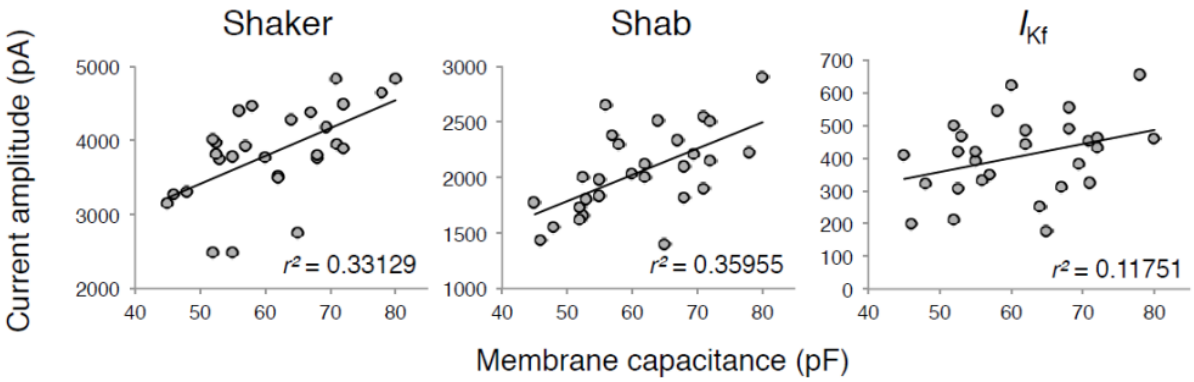

Figure 2.3 | Weak correlation between membrane capacitance and Kv currents in WT (ROR) flies

Membrane capacitance (pF) plotted against Shaker, Shab and I_{Kf} current amplitudes (N=28). Membrane capacitance correlates with the membrane area. Pearson's correlation coefficient (r) is used to assess the degree of correlation.

2.3.3 Protein detected by anti-Shal antibody is reduced in *Shal*$^{495\ +/-}$ mutant flies

Since Shal (Kv4) was thought to be the most likely candidate for the molecular identity of I_{Kf}, I analysed a *Shal*-null mutant. *Shal*^{495} mutant flies carry a P-element insertion, which hits all known transcripts of *Shal*, and have been used in other studies in larval stages (Bergquist et al. 2010). However, trials of creating homozygous adult flies in the lab were unsuccessful, presumably due to the mutation being lethal at pupal stage. Thus only Shal$^{495\ +/-}$ adult flies were used for analysis.

Whole cell patch clamp recordings were made from *Shal*$^{495\ +/-}$ fly photoreceptors, and compared to recordings from WT(ROR). The amplitude of I_{Kf} could be seen to be somewhat reduced depending on the cell (Fig. 2.4A). Quantification of the amplitude of I_{Kf} revealed significant reduction compared to WT, but the amplitudes of Shaker and Shab were also significantly reduced (Fig. 2.4B) indicating that there was no specific effect on I_{Kf}.

Western blots were performed using two antibodies from separate sources (from Dr. Baro and Dr. Tsunoda) on total protein extracted from *Shal*$^{495\ +/-}$ and WT(WOR) fly heads, in order to quantify the amount of Shal protein. With antibody from Dr.Baro, the band at the expected size for Shal (≈65kDa) had reduced signal in *Shal*$^{495\ +/-}$ compared to WT (Fig. 2.5A), whereas the other bands did not show marked signal reduction (data not shown). The *Shal*$^{495\ +/-}$ signal of this band normalized with the

tubulin band signal from the same blot showed a reduction of ≈37% compared to WT (Fig. 2.5B). However, with the antibody from Dr. Tsunoda, a band at the expected size for Shal was not observed (data not shown). Together, these results show that the *Shal*$^{495\ +/-}$ has smaller Kvs overall, and a seemingly reduced level of *Shal* protein within the head of the flies. Since a significant reduction in Shaker and Shab currents were observed in *Shal*$^{495\ +/-}$ (Fig. 2.4B), in the future, it would be interesting to see whether Shaker and Shab protein levels also show consistent decrease in these flies.

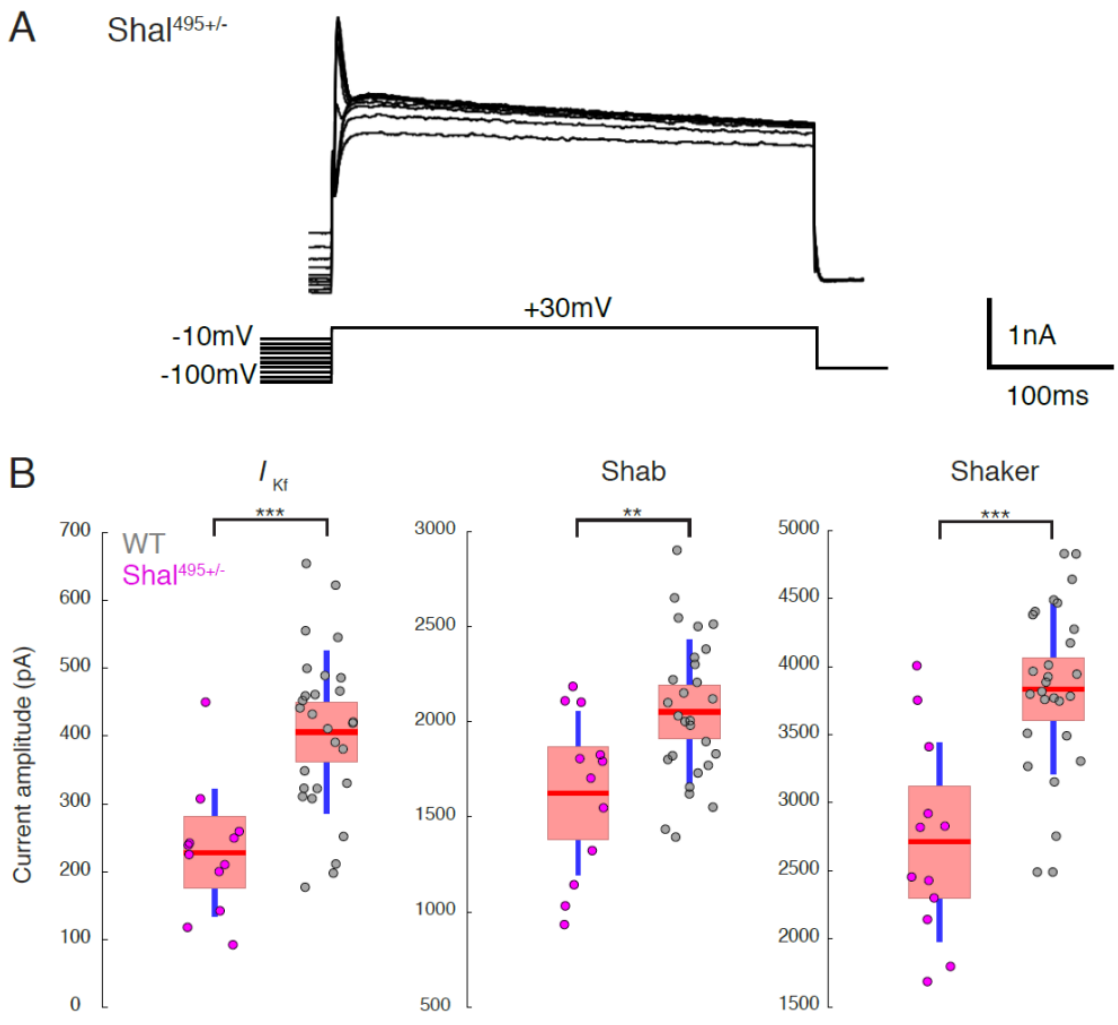

Figure 2.4 | Quantification of Kv currents in *Shal*$^{495\ +/-}$ flies

(A) (Top) Representative trace of *Shal*$^{495\ +/-}$. (Bottom) Removal of inactivation protocol used. **(B)** Comparison of Shaker, Shab and I_{Kf} current in WT and *Shal*$^{495\ +/-}$ flies (WT: N=28, *Shal*$^{495\ +/-}$: N=12). ** p<0.01, *** p<0.001 (student's t test).

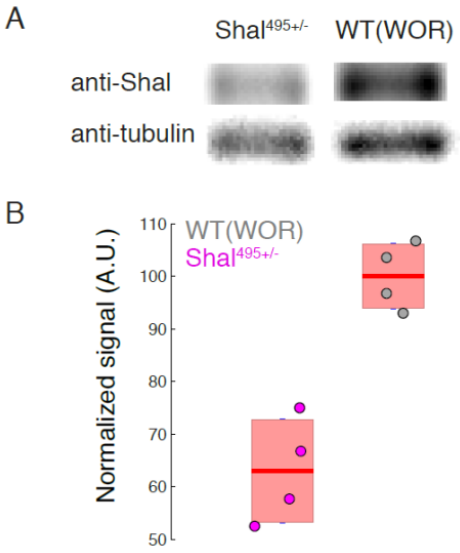

Figure 2.5 | Western Blot of Shal protein in WT (WOR) and *Shal*$^{495\ +/-}$ flies

(A) Western blots of Shal and tubulin (~1.7 heads per lane) for *Shal*$^{495\ +/-}$ (left column) and WT (right column) flies. **(B)** Signal quantification of above blots, Shal signal normalized with tubulin signal. The signal is decreased by ≈37% in *Shal*$^{495\ +/-}$ flies.

2.3.4 One Shal antibody shows localization to R7 photoreceptors, while another antibody shows localization to all cell membranes

Both Dr. Baro's and Dr. Tsunoda's antibodies were used to investigate the localization of Shal at the level of the whole retina and photoreceptor cells. Using fixed whole mount retina preparations, the distribution of the Shal signal throughout the retina was examined using confocal microscopy in order to see whether, for example, there was a gradient of expression across different eye regions. However, the distribution of the signal seemed to have no clear pattern, or seemed more or less random across cells (data not shown). The subcellular localization in photoreceptor cells was also examined using higher magnification. With Dr. Tsunoda's antibody, the R7 cells seemed to be preferentially labeled (Fig. 2.6 top row); however, with Dr. Baro's antibody, the signal was seen around the outer membrane of photoreceptors, leaving out the rhabdomeres labeled by phalloidin (Fig. 2.6 bottom row). This discrepancy is perplexing, especially since a Shal-size band could not be detected using Dr. Tsunoda's antibody. The differences in the antibodies could perhaps be explained by the antibody recognition site difference and/or non-specific labelling, but it remains unclear whether these staining patterns show a faithful localization of the Shal protein.

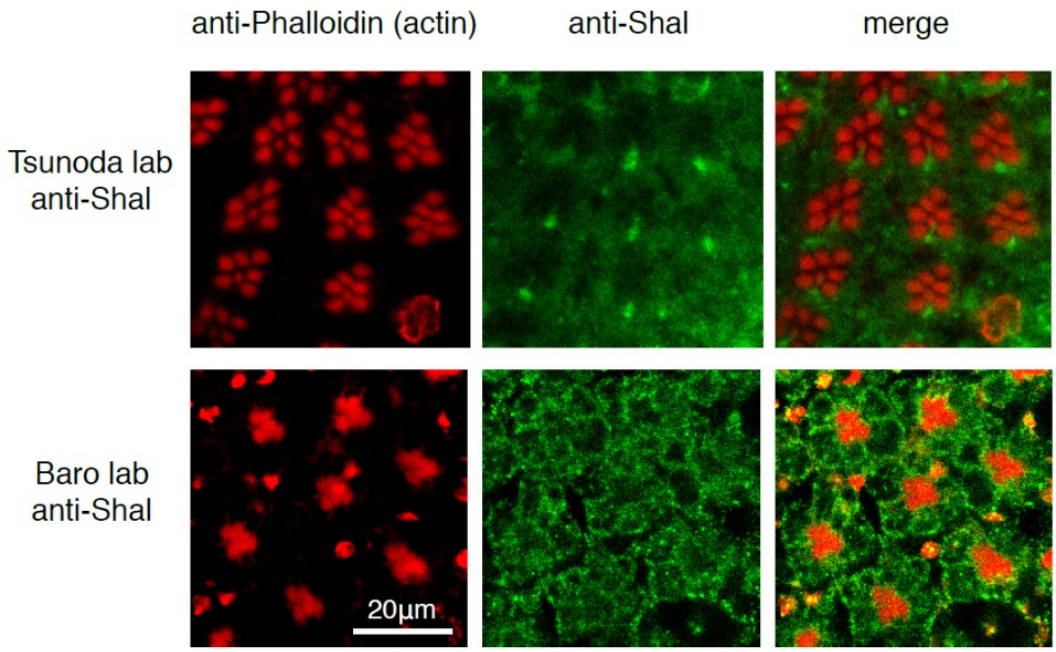

Figure 2.6 | Immunohistochemistry of Shal in WT (WOR) flies

Top row: anti-Shal antibody from Tsunoda lab showed localization to R7 cells. Bottom row: anti-Shal antibody from Baro lab showed localization to all cell membranes.

2.3.5 Voltage dependence of I_{Kf} in WT, *Shab*^{3} mutant is similar to that of Shaker

Although the biophysical properties of I_{Kf} have been reported in photoreceptors from young pupae, (Hardie 1991) they have not been investigated in adult photoreceptors in any detail, except for a brief mention in a couple of studies (Anderson & Hardie 1996; Hardie 1991) (Hevers & Hardie 1995). Yet acquiring the precise biophysical parameters is necessary for understanding the functional role of I_{Kf} in the photoreceptor.

In an attempt to obtain the biophysical parameters of the I_{Kf}, I-V relationships were plotted from WT removal of inactivation data (Fig. 2.7). V_{50} and s (slope factor) (which are characteristic parameters for a given channel class) were obtained by fitting with a Boltzmann distribution. While the parameters for Shaker (V_{50}= -56.9 ± 4.3, s = 4.5 ± 0.8) and Shab (V_{50}= -24.4 ± 2.4, s = 7.1 ± 0.8) were in line with previous studies, those for I_{Kf} (V_{50}= -49.7 ± 1.8, s = 8.3 ± 1.6) were more positive than what had been observed before in photoreceptors or other cell types (≈V_{50}= -71.6, s = 4.0, R7 photoreceptor cell (Anderson & Hardie 1996), V_{50} = -81 s =4.7 pupal R1-6 (Hardie 1991), V_{50}= -55.95 ± 5.95, s = 7.09 ± 1.12, Shal expressed in Sf9 cells (Diao et al. 2009)).

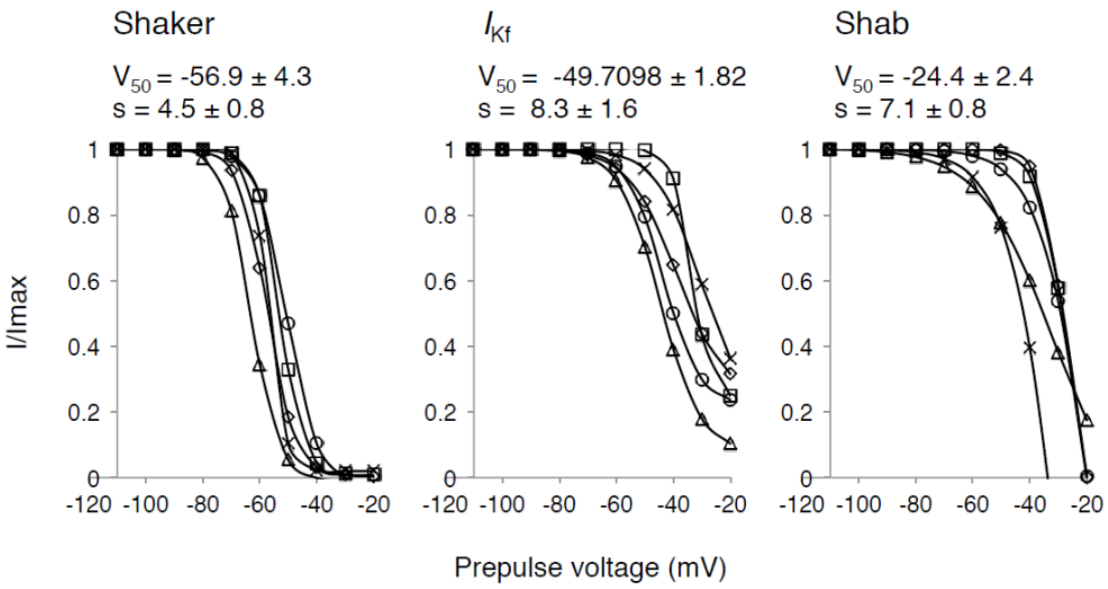

Figure 2.7 | Voltage dependence of Kvs in WT (ROR) flies

Peak normalized currents plotted against prepulse voltages in the removal of inactivation protocol. V_{50} and s (slope factor) were obtained by fitting with a single Boltzmann distribution. Each trace is from an individual fly (N=5 each). Mean ± SEM of is V_{50} and s shown in inset.

One possible explanation for this discrepancy might be contamination of the measured I_{Kf} current by the Shab current with its more positive operating range. I therefore repeated the measurements in *Shab*[3], which is a null mutant of Shab (Fig. 2.8A). The resulting parameters for Shaker (V_{50}= -55.1 ± 6.7, s = 5.8 ± 0.35) were in line with the WT data and previous studies, but those for I_{Kf} (V_{50}= -53.3 ± 6.2, s = 5.3 ± 0.7) were still more positive compared to reports in photoreceptor cells, and almost the same as those of Shaker. This might indicate contamination by the Shaker current; however an alternative possibility is that I_{Kf} is in fact nothing more than a late component of Shaker. To test whether this is the case, measurements were made from Shaker mutant *Sh*[14].

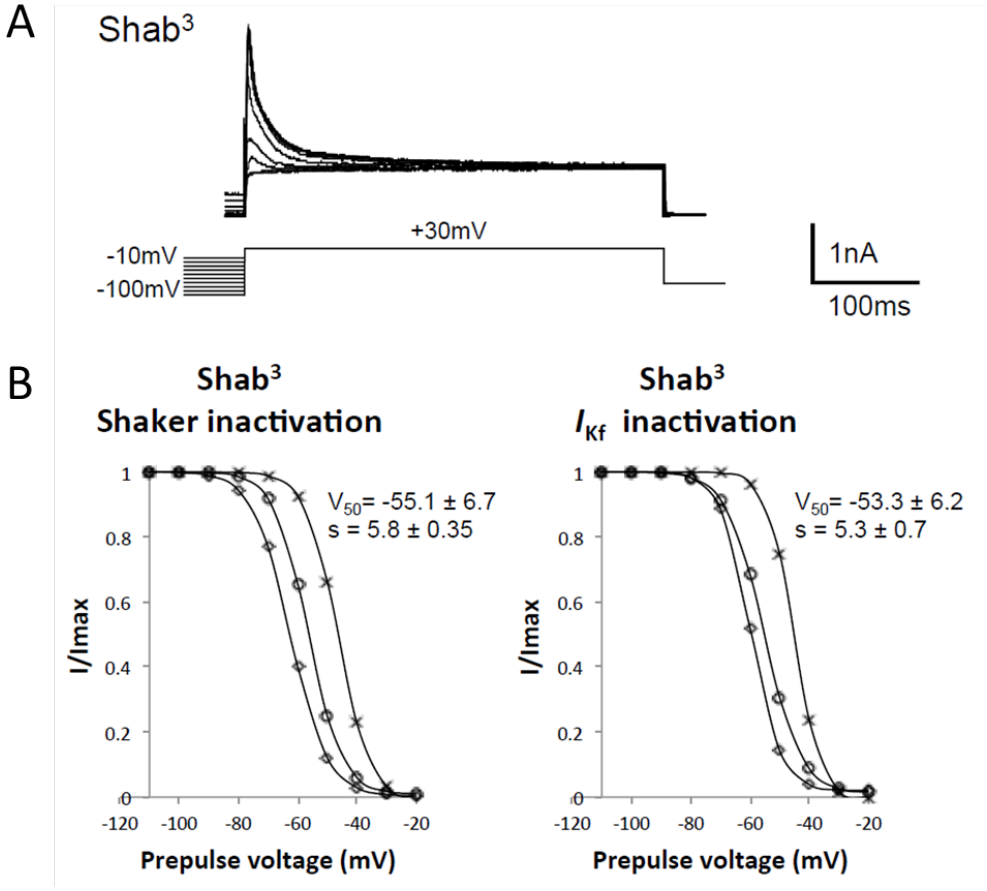

Figure 2.8 | Voltage dependence of Shaker and I_{Kf} in *Shab*^{3} flies

(A) (Top) Representative trace for *Shab*^{3}. (Bottom) Removal of inactivation protocol used. **(B)** Peak normalized currents plotted against prepulse voltages in the removal of inactivation protocol. V_{50} and s (slope factor) were obtained by fitting with a single Boltzmann distribution. Each trace is from an individual fly (N=3 each). Mean ± SEM of is V_{50} and s shown in inset.

2.3.6 Voltage dependence of I_{Kf} in *Sh*^{14} mutant pupae is consistent with Shal

The *Sh*^{14} flies carry a mutation in the core region of the Shaker gene, which results in production of non-functional Shaker channels. This mutant therefore shows no Shaker current (Hardie et al. 1991). The majority of photoreceptors in adult *Sh*^{14} flies showed almost no I_{Kf} , but when it was observed, it had a V_{50} close to that of Shal in previous reports (Fig. 2.9, V_{50} = -77.5 ± 2.4, s = 5.1 ± 1.2 N=3/12). Pupae were also used to characterize voltage dependence of I_{Kf}, since at this stage, the photoreceptors have not started to express the Shaker channel, and thus serve the same purpose as Shaker mutants. In young pupae, WT flies only rarely showed Shal-like I_{Kf} (p8/9 pupae=3/20

cells, p11/12 pupae=0/8 cells, p14/15 pupae=0/5 cells), however, surprisingly, Sh^{14} pupae showed a clear Shal-like I_{Kf} in the majority of photoreceptors (p9-11 pupae=12/13 cells), suggesting that Shal had been upregulated in the absence of the Shaker current (but see discussion).

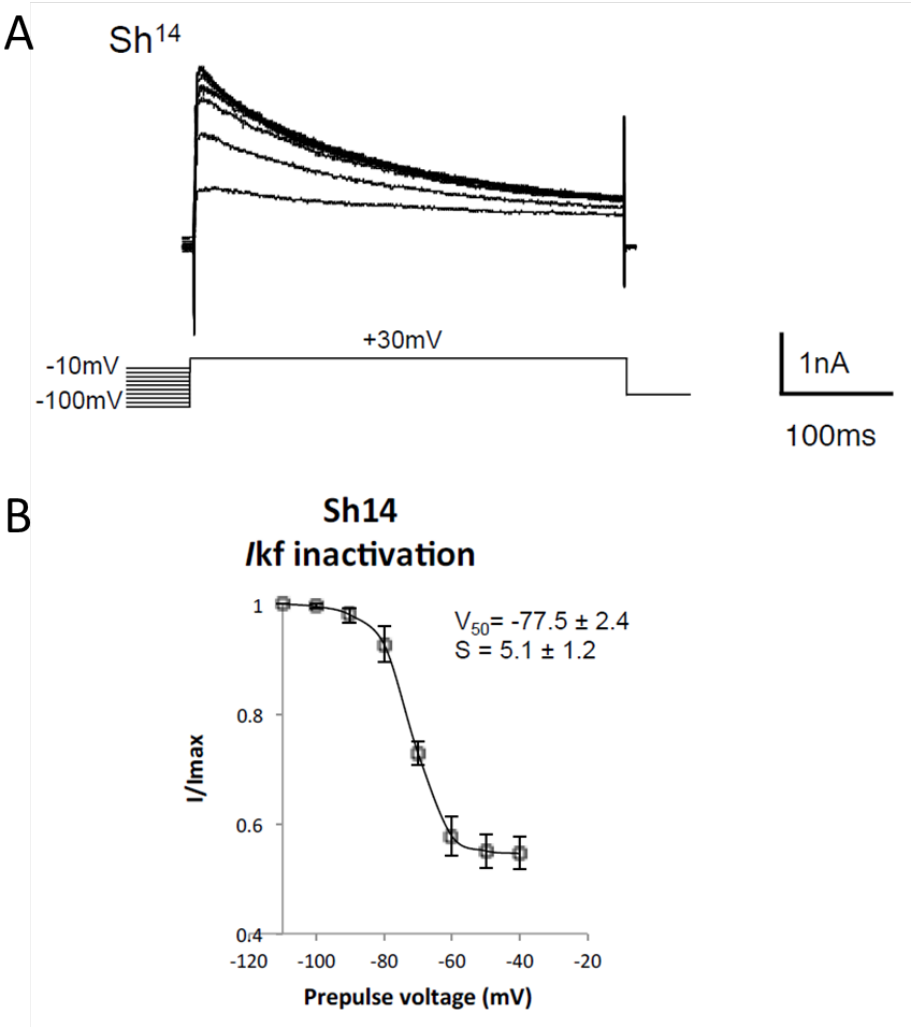

Figure 2.9 | Voltage dependence of I_{Kf} in Sh^{14} flies

(A) (Top) I_{Kf} was found occasionally (≈3/12 cells). The trace is from a Sh^{14} fly with I_{Kf}. (Bottom) Removal of inactivation protocol used. **(B)** Peak normalized currents plotted against prepulse voltages in the removal of inactivation protocol. V_{50} and s (slope factor) were obtained by fitting with a single Boltzmann distribution. Trace is the mean across flies (N=3). Mean ± SEM of is V_{50} and s shown in inset.

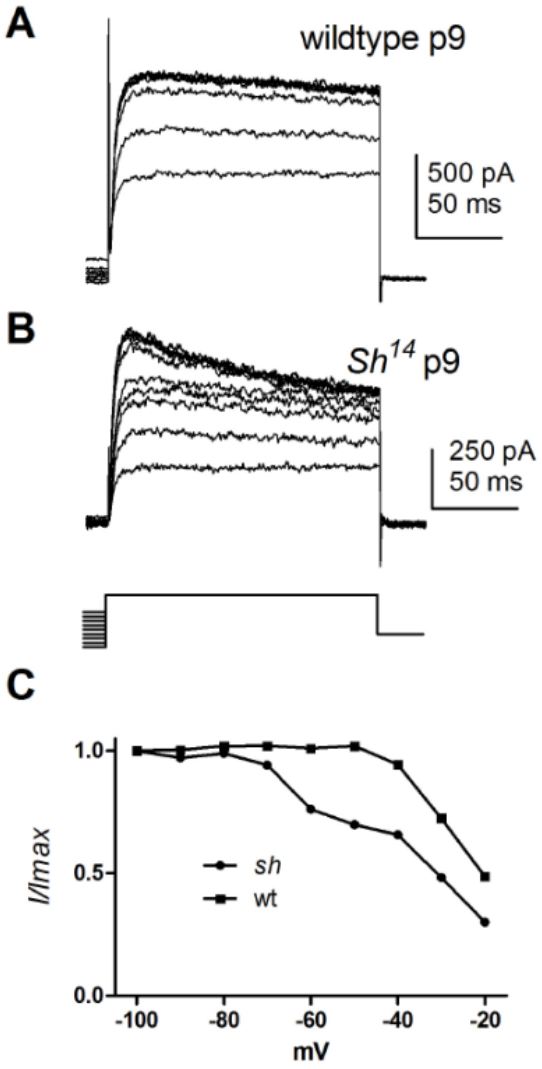

Figure 2.10 | Measurement of Kvs in wildtype and *Sh*^{14} pupae.

(A) Example of wildtype pupa Kv currents. Most showed no I_{Kf} . **(B)** Example of *Sh*^{14} pupa Kv currents. All but one had a clear Shal-like I_{Kf} (V50= -65mV). **(C)** I-V curves of *Sh*^{14} and WT pupa. Two components are clearly seen in *Sh*^{14}.
Data and analysis from Hardie RC (unpublished).

2.3.7 Pharmacology in WT and *Sh*^{14} mutant pupae confirms existence of Shal in *Sh*^{14} pupae, but not in WT R1-6 cells

In order to confirm the molecular identity of I_{Kf} in WT and *Sh*^{14} mutants, Phrixotoxin (Shal blocker) and 4-AP (Shaker blocker) were used. Phrixotoxin treatment did not affect WT adult currents (Fig. 2.11A left panels), but in the few (3/20) WT p9 pupae which showed a Shal-like I_{Kf}, a slight block was observed (Fig. 2.11A top right panel). In *Sh*^{14} pupae however, a ~50% block was observed (52 ± 6%, N= 11), which supports their clear Shal-like voltage dependence. On the other hand, 4-AP treatment blocked all the Kvs to some extent in WT (Fig. 2.11B). The extent and time course of the block seemed very similar for Shaker and I_{Kf} supporting the possibility that the wild-type adult I_{Kf} arises from a late component of a Shaker dependent channel.

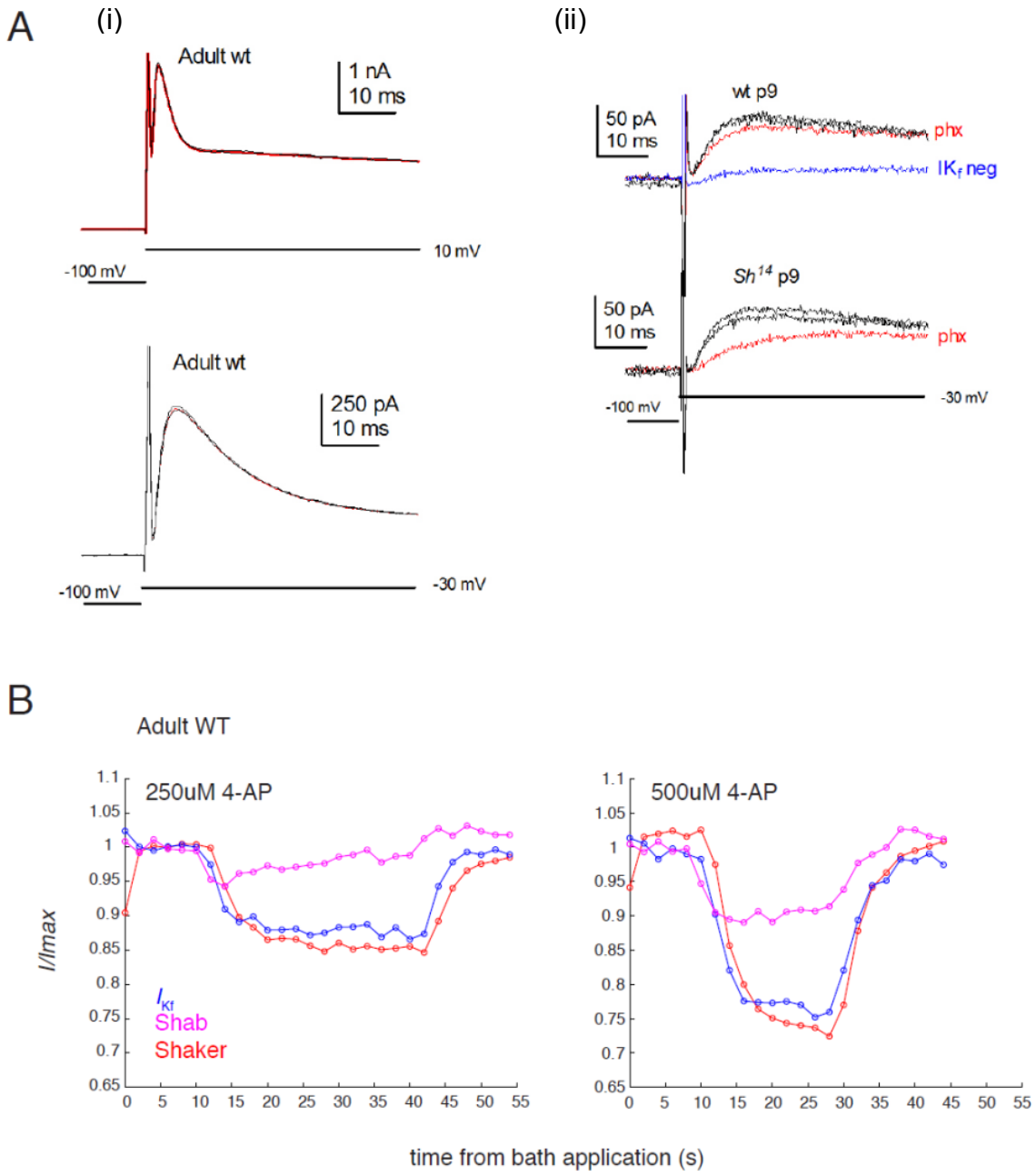

Figure 2.1| Pharmacology in WT adult and pupae

(A) Phrixotoxin (phx; 2µM) treatment (red traces) did not block I_{Kf} in WT adults and pupae. (i) No phx block in WT adults. Three superimposed traces: before (black), during phx application (red) and after washout (black). Protocols shown below traces. Note that protocol stepping from -100mV to -30mV protocol (bottom trace) activates only Shaker (and Shal if present). (ii) Top: In rare WT p9 pupae with small I_{Kf}, phx induced a slight block: majority of wt pupae had no I_{Kf} and showed virtually no current with this protocol (e.g shown from different cell shown in blue). Bottom: In Sh^{14} pupae, phx reliably suppressed I_{Kf} (=Shal), recovering within a few seconds after washout. Both traces used protocol stepping from -100mV to -30mV(shown below trace). **(B)** 4-AP treatment blocked I_{Kf} and Shaker components to a similar degree and with similar timecourse. Shab was hardly blocked with 250µM, but was clearly blocked with 500µM. Voltage steps from -70 to +30mV was repeated every two seconds. Data and analysis from Hardie RC (unpublished).

2.4 Discussion

2.4.1 Heterogeneity of voltage-gated potassium currents is not only attributed to I_{Kf}

The initial aim was to assess variability of the Kvs, with a focus on the I_{Kf}, which had been noted as being especially variable compared to other Kv currents. However, the recordings made so far from WT fly photoreceptors indicate that Shaker and Shab are also variable to a nearly similar extent, and the slightly larger variation in I_{Kf} might be attributable to experimental difficulties of accurate measurement. This result needs to be further assessed with an increased number of good quality recordings, since the quality of the recording, and in particular series resistance errors, can significantly affect the current amplitudes. For example, the larger Shaker currents observed (>4500 pA) are particularly susceptible to series resistance and clamp time constant and might also be contaminated by oscillations elicited by excess series resistance compensation, which could boost signal amplitude at the start of the trace. Also with the measurement method used, contamination of I_{Kf} by Shaker and Shab currents cannot be avoided, which could interfere with measuring its variability, especially in cells with small amounts of I_{Kf}.

Putting these technical concerns aside, there are known mechanisms that may be playing a role in variability of I_{Kf}. Firstly, a Shal interacting molecule has been identified in *Drosophila* (SKIP), which slows down the inactivation rate of Shal (Diao et al. 2009). Another binding molecule SIDL, has been implicated in targeting Shal to the dendrites in neurons, which may have a role in photoreceptors for the trafficking of Shal as well (Diao et al. 2010). These molecules could contribute to changing the amount of Shal current found amongst photoreceptor cells. Secondly, homeostatic mechanisms of expression amongst Kvs has been reported, namely, transcriptional coupling of Shaker and Shal in drosophila motoneuron (Bergquist et al. 2010). Thus it would be interesting to see whether there exists some compensatory up/down regulation coupled amongst Kvs in photoreceptor cells as well.

2.4.2 Molecular identity of I_{Kf} in Sh^{14} pupae and adult R7/8 cells is most likely Shal

It had previously been observed that WT R7/8 cells showed a component that is Shal-like, from its voltage dependence of inactivation (Anderson & Hardie 1996). Moreover, a similar current was also found in some wild-type pupal photoreceptors (Hardie 1991). Here, we confirmed the occasional presence of a Shal-like current in young (p9) wild type pupae, but only in a small minority (3/20) of cells. By contrast, we found a clear Shal-like component in the majority of Sh^{14} p9-p11 pupae, based on both voltage dependence (Fig. 2.10) and phrixotoxin sensitivity (Fig. 2.11). At face value this seems to be a clear example of homeostatic up-regulation as has been shown reciprocally for Shaker and Shal in *Drosophila* motoneurons (Bergquist et al. 2010). However, it is interesting to note that at the pupal stage where this apparent up-regulation of Shal was observed (p9-p11), Shaker is actually not functionally expressed at all (Hardie 1991). Furthermore, the up-regulation seems largely restricted to these early pupal stages, as the majority of adult Sh^{14} photoreceptors again showed no Shal-like currents. Given that photoreceptors have presumably no functional roles in pupae beyond developmental ones, the significance of these unusual findings remains unclear.

2.4.3 Speculation of subcellular localization of Shal in photoreceptors

The western blot initially did not yield a band near the expected size for Shal when a standard lab protocol was used. Thus the protocol used for the Shaker channel in a previous study (Rogero & Tejedor 1995), which required lysis and extraction at 80°C as opposed to room temperature in standard protocols, was employed in the next trial. The fact that this protocol yielded a band near Shal size, may perhaps indicate that the subcellular localization of Shaker and Shal are similar. Indeed, Shaker signals have been observed in the outer membrane of photoreceptor cells (Rogero et al. 1997), which is comparable to the pattern observed in this study with a Shal antibody (from Dr. Baro). However, another antibody (from Dr. Tsunoda) showed signals in R7/8 cells, which is supported by previous electrophysiological studies (Anderson & Hardie 1996).

2.4.4 Candidate molecular identity of I_{Kf} in WT adults – Shaker slow inactivating component or splice variant?

Apart from the Shal-like currents discussed above, I observed that the wild-type I_{Kf} had a more positive voltage dependence than previously reported, with a V_{50} essentially indistinguishable from that of Shaker. Together with the findings that I_{Kf} in adults was phrixotoxin insensitive and absent in most recordings from adult Sh^{14} mutants, this leads us to think that I_{Kf} in adult WT photoreceptors is in fact a component of the Shaker current, rather than arising from Shal or some other distinct class of channel. The underlying mechanism could be a splice variant of Shaker having a slower activating time course, or a late component of Shaker, as the channel is known to have more than one inactivating state (Hoshi et al. 1991). If I_{Kf} were indeed the slow inactivating tail of Shaker, one would expect to see that they covary. However, we did not see a clear correlation between their amplitudes within the cell (Fig. 2.2A), although the correlation could have been foiled by the fact that the extent of inactivation is correlated to the current amplitude (because of more depolarization), which is related to the quality of the voltage-clamp.

It has been proposed that the *Shaker* gene could produce as many as 10 different transcripts by alternative splicing. Most of these transcripts could be detected collectively in the head and body, and four have been detected in the retina (*Sh*A1, *Sh*A2, *Sh*G1, *Sh*G2; Hardie 1991). Each transcript is assumed to encode a single subunit, and since Shaker is known to be composed of four subunits, these four transcripts could generate 4 distinct homomultimers, or >50 heteromultimers. At least one class of subunits seems to be involved in the I_A current, since Sh^{E62} mutants with mutation in the class1 region of the *Shaker* gene (lacking *Sh*A1 and *Sh*G1), has altered I_A current, inactivating slower than WT (Hardie et al. 1991). This lack of class1 subunits could be a mechanism for I_{Kf} to have a slower inactivation, but there are many other potential combinations of subunits as discussed above, which may confer the slower kinetics of I_{Kf}.

In order to test this hypothesis of involvement of differential Shaker subunit composition to the I_{Kf}, it would be desirable to obtain and analyse mutants for each subunit expressed in photoreceptors. An orthogonal approach may be to conduct a

transcriptome analysis of R1-6 cells and compare to R7/8 cells, since I_{Kf} is rarely found in R1-6 cells but almost always seen in R7/8 cells.

Using voltage dependence of inactivation and pharmacological block as criteria, we have so far not found convincing evidence for the contribution of Shal to I_{Kf} in wildtype adult flies. However, we have been unfortunate that the *Shal*^{495} mutant was homozygous lethal. Thus in the future, one could create a homozygous mutation of *Shal* only in the eye (using techniques such as genetic mosaic), and perhaps explore mutants of different transcripts, since *Shal* also has two alternative splice variants (Wei et al. 1990).

CHAPTER 3

PROBING THE RESPONSE PROPERTIES OF LOBULA COLUMNAR CELLS

Data contributions:

All Ca^{2+} imaging data collection and analysis were performed by Mai Morimoto.

Confocal images (Fig.3.3, Fig.3.5A, Fig.3.7A) were contributed by Aljoscha Nern.

Behavioral data (Fig.3.2) were contributed by Ryan Williamson and Ming Wu.

3.1 Introduction

3.1.1 Lobula Columnar (LC) neurons anatomy

Lobula columnar (LC) neurons are a class of cells that project from the lobula to the central brain, and are a prominent group of so-called visual projection neurons (Otsuna & Ito 2006)(VPNs; Fig.3.1). The name "columnar" describes the fact that their dendritic arborizations are smaller as compared to the "wide field" cell-types, which have dendrites often spanning the whole visual field (Fig.3.1, Fig.3.3 *d.*=dendrites). As a population, LC neuron dendrites 'tile' the visual field. Another characteristic of LC neurons is the convergence of their axon terminal to a specific target region in the central brain forming a dense neuropil structure (Fig3.1, Fig.3.3 *a.*=axons). These structures are referred to as "glomeruli" in analogy to the olfactory glomeruli of the antenna lobe. The majority of glomeruli are enervated by the axons of a single LC type, so that information from each LC-type is spatially segregated into these glomeruli, which has been proposed to be anatomically and functionally similar to the organization of the olfactory glomeruli (Mu et al. 2012). In *Drosophila*, 22 LC types have been observed to date, each estimated to contain ~50-100 cells per hemisphere (Wu et al. 2016). Columnar cells in the lobula has been found widely in other arthropods such as larger flies (*Calliphora*) (Strausfeld & Okamura 2007), hoverflies (Nordström et al. 2006), crabs (Medan et al. 2015) and bumblebees (Paulk et al. 2008).

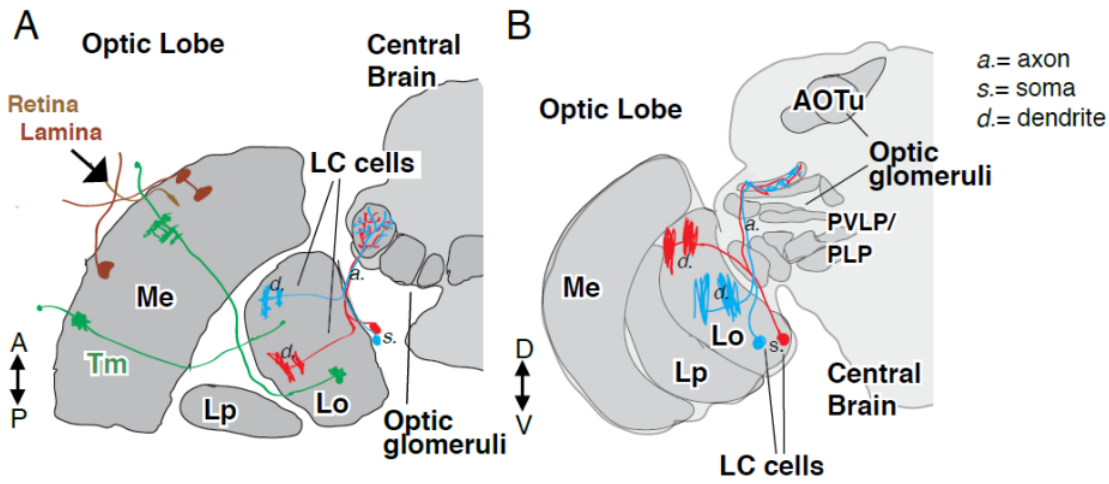

Fig.3.1 | Anatomical position of lobula columnar (LC) neurons.

Schematics of the lobula and adjacent parts of the visual system. (A) Horizontal sections and (B) anterior views of the lobula. Some subregions of the optic lobe (Me, Medulla; Lp, Lobula plate; Lo, Lobula) and central brain (AOTu, Anterior Optic Tubercle; PVLP, Posterior Ventrolateral Protocerebrum; PLP, Posterior Lateral Protocerebrum) are indicated. Dendrites of individual LC neurons (red and blue cells) span only part of the visual field. As populations, the neurons of a LC cell type cover most or all of the lobula. LC neurons receive feed forward visual inputs from photoreceptors in the retina via a series of optic lobe interneurons (a few lamina neurons, in brown, and transmedullary neurons [Tm], in green are illustrated as examples in (A)), and also lateral inputs from the Lobula Plate. This places LC at least 2-3 synapses downstream of the photoreceptors. The majority of LC neurons projects to distinct target regions in the central brain called optic glomeruli; some of these are illustrated in (A) and (B). Most optic glomeruli are located in the PVLP and the adjacent more posterior PLP. The more dorsal AOTu [illustrated in (B)] is considered a specialized optic glomerulus. Figure modified from Wu et al. 2016, contributed by Aljoscha Nern.

3.1.2 Lobula Columnar (LC) neurons function: hypotheses

Based on their anatomical position, LC neurons have been assumed to represent one of the last processing steps in the visual system. Since there are ~20 LC types in *Drosophila*, it has been proposed that LC neurons collectively serve as an information bottleneck, reducing the complex visual scene into ~20 behaviorally relevant visual features. While the visual processing of wide-field motion required during flight control has been well studied (Borst et al. 2010; Krapp et al. 1998), the neural substrates for many other visual behaviors seen in *Drosophila* remain unidentified. *Drosophila* have been known to be able to discriminate object shape and color (Liu et al. 1999; Schnaitmann et al. 2013; Gao et al. 2008), and show avoidance or attractive

behavior towards objects based on their size and motion profile (Card & Dickinson 2008; Agrawal et al. 2014; Coen et al. 2016; Maimon et al. 2008). It has been hypothesized that LC neurons may mediate some of these behaviors, partly owing to their small dendritic fields making them ideally suited to detect visual features required in such behaviors. This hypothesis for feature encoding of LCs has also been postulated from an anatomical point of view, which states that the convergence of axons to the glomerulus reduces the LC neurons' capability to carry retinotopic information, and therefore it should represent a "feature" that is invariant of its position in space (Strausfeld & Okamura 2007).

In order to test this, Janelia colleagues first developed a collection of driver lines to target individual cell types (using the split-GAL4 method (Luan et al. 2006; Pfeiffer et al. 2010)). An activation screen was carried out for most of these identified LC neuron types, where individual LC neuron types were optogenetically activated, and the resulting behavior observed (Wu et al. 2016).

3.1.3 Optogenetic activation of LC6 and 16 induce avoidance-like behaviors

Amongst the ~20 cell-types tested in behavioral assays (single fly assay and an open field assay) measuring the response of the flies to the Chrimson activation (Klapoetke et al. 2014), LC6 and LC16 showed strong and consistent jumping, or backward walking behavior, respectively (Fig.3.2). The results of these activation screens were confirmed to not be attributed to the optogenetic light response, differences in genetic background, or non-specific labeling in the split-GAL4 pattern with the following controls; a blind (norpA) fly line to control for optogenetic light evoked response (Fig.3.2 A, B yellow), an "enhancerless" split to control for background of this fly line (Fig.3.2 A,B green), flies that were fed a "no retinal" normal diet (Fig.3.2 A,B blue) and flies carrying only one half of the split-GAL4 (Fig.3.2 A,B red), which all showed significantly lower jumping or backward walking compared to the split-GAL4 lines with targeted expression in LC6 or 16 (Fig.3.2 A,B gray, multiple split-GAL4 lines pooled, to ensure that other labeled neurons are not playing a part in the behavior). High-speed videography revealed that their activation phenotypes also closely resembled those of behaviors elicited by a visual looming stimulus, as measured by the takeoff sequence duration for LC6 (Fig.3.2 C, D) and their backward displacement for LC16 (Fig.3.2 E, F). It is known that jumping and backward walking behaviors are elicited in natural circumstances when there is an imminent threat by a

predator (Card 2012; Parigi et al. 2014), suggesting that these are typical avoidance behaviors for the fly.

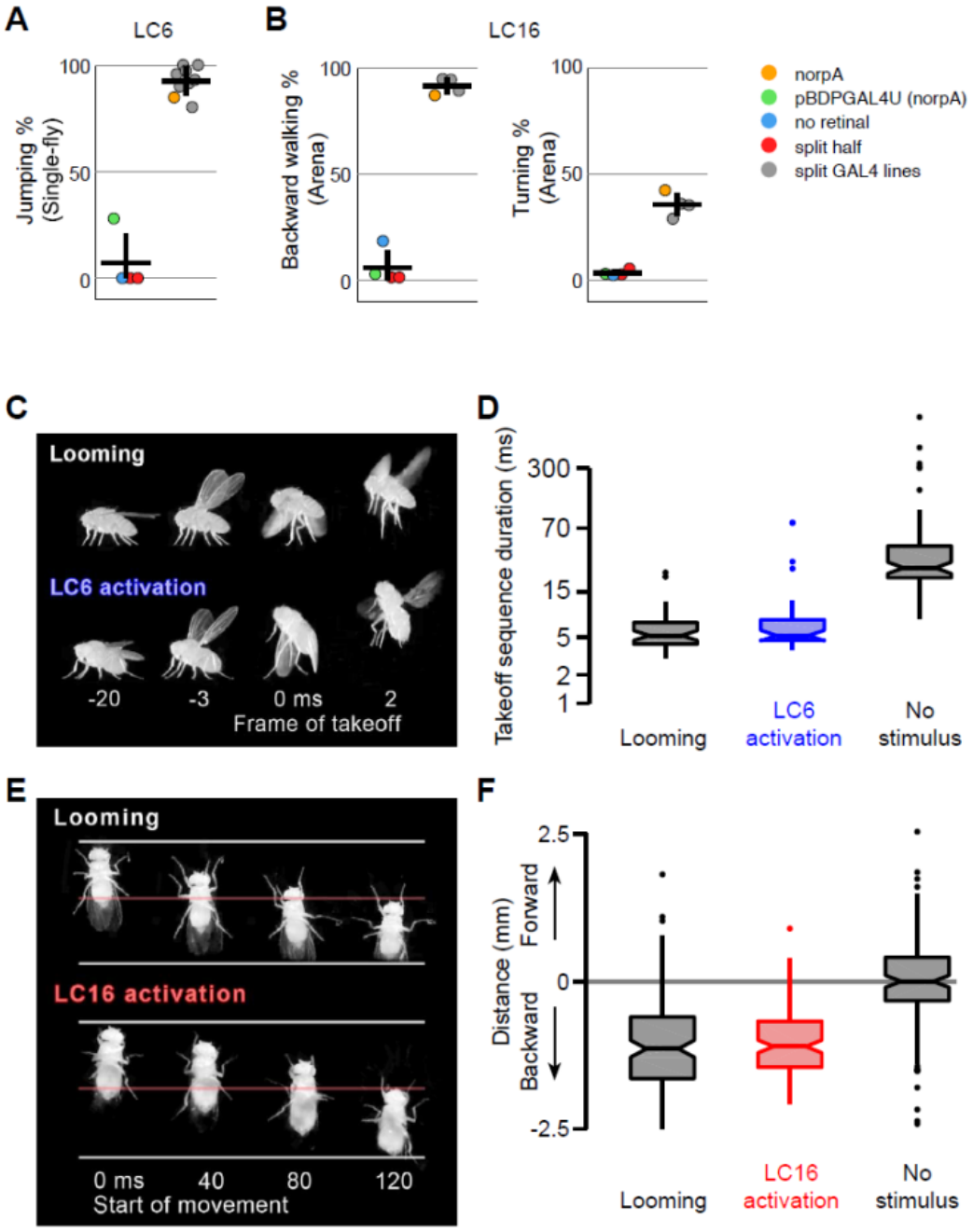

Fig.3.2 | LC6 and LC16 activation behaviors resemble avoidance responses evoked by visual looming.

(A,B) Behavioral penetrance for different controls and multiple split-GAL4 driver lines for (A) jumping (flies that jumped within 200ms of stimulation onset) with LC6 controls based on the OL0077B driver line and (B) backward walking and turning with LC16 controls based on the OL0046B driver line. Each dot represents an experiment done with a different genotype: orange, LC neuron activation in blind norpA flies that also carry an LC6 (A) or LC16 (B) split-GAL4 line; green, pBDPGAL4U control in blind norpA flies; blue, flies reared on food without supplemental retinal; red, split-GAL4 DBD or AD halves; grey, genetically distinct split-GAL4 driver lines with targeted expression in LC6 (A) or LC16 (B). Horizontal and vertical lines indicate mean and standard deviation, respectively, for the control group and split-GAL4 group. Single-fly assay was used for jumping behavior, and arena assay was used for backward walking and turning behavior.

(C) Representative video images from the single-fly assay showing that a looming stimulus and LC6 activation evoke very similar coordinated behavioral sequences, which include wing elevation, middle leg extension and initiation of flight. Time stamp is set at 0 ms for the frame of takeoff. Negative and positive values are for frames before and after takeoff, respectively. (D) Notched box plots showing the duration of the takeoff sequence measured as the time from the first moment of wing movement to the last moment of tarsal contact with the ground after the stimulus (Kruskal–Wallis test, $p = 0.29$ between looming and LC6 activation, and $p < 0.001$ between LC6 activation and no stimulus). (E) Representative video images from the single-fly assay showing that a looming stimulus and LC16 activation evoke very similar backward walking behaviors. Time stamp is set at 0 ms for the start of backward walking. (F) Total distance flies walked on the platform of the single-fly assay. Positive and negative values are for forward and backward walking, respectively (Kruskal–Wallis test, $p = 0.71$ between looming and LC16 activation, and $p < 0.001$ between LC16 activation and no stimulus). Scale bars represent 50 μm (A) or 20 μm (B).

Figure from Wu M et al. 2016, contributed by Williamson R. Single fly assay carried out by Williamson R and an open field assay carried out by Wu M.

3.1.4 LC6 & 16 share similar input layer patterns and project to nearby target regions

Since cell-types of the medulla and lobula plate, presynaptic to the lobula, innervate the layers of the lobula in a stereotypic manner, the input layer of LCs in the lobula provide some constraints on the identity of their presynaptic partners. In addition to their projection target in the central brain, the stereotypic layer patterns of the dendrites within the lobula are a key detail in the description of each LC type. These characteristics further validate the use of the term 'cell type' in reference to each group of LC neurons with common morphological features. The LC6 and LC16 cells were observed to have similar lobula innervation patterns, mainly arborizing in lobula layer Lo 4 and Lo 5 (Fig.3.3B). In contrast, for example LC11, has innervation mainly in Lo2 and Lo 3, having little overlap with those of LC6 and 16. This would suggest that the presynaptic partner for LC6 and 16 are similar, while LC11 is different.
LC6 and LC16 also project to a close but non-overlapping region in the posterior ventrolateral protocerebrum (PVLP), whereas LC11 projects to a relatively distant region (Fig.3.3A). This proximity of target region was shown to correlate with the type of activation induced behaviors (i.e. avoidance vs. attractive, Wu et al. 2016), and suggests common downstream pathways for LC types projecting to nearby target regions.

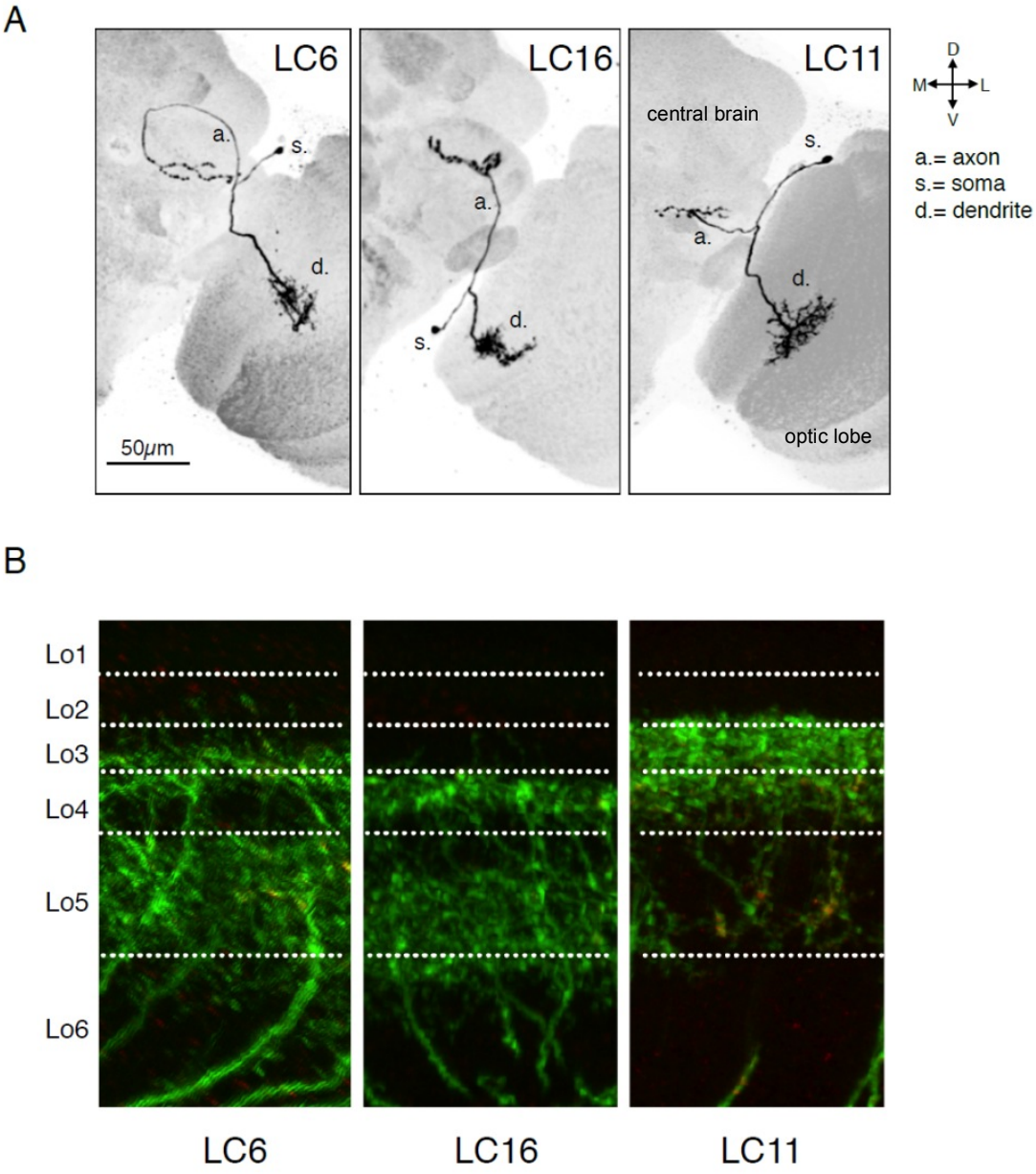

Fig.3.3 | Anatomy of LC6, LC16 and LC11

(A) LC6, 16 and 11 single cell morphology. Dendrite and axon locations are distinct. Single-cell labeling was obtained by multi-color flip out (MCFO) technique. (B) LC6 and 16 dendrites arborize mainly in lobula layer (Lo) 4 and 5 while LC11 dendrites arborize mainly in Lo3. Images from Aljoscha Nern.

Thus the above anatomical information and results from the activation assay generated the following somewhat contradicting hypotheses about the response property of LC6 and LC16:

- Since activation of LC6 and 16 evoke distinct types of avoidance behavior (jumping and backward walking), their encoding property is expected to be somewhat different.
- However, the similarity of their input layers predict that they likely have shared presynaptic inputs, and therefore may have some similarity in their encoding properties.

The aim of this project therefore was to probe the response properties of lobula columnar cells to see whether they encode behaviorally relevant visual features, as predicted by anatomical and behavioral evidence. Specifically, I wanted to measure visually evoked responses from LC6 and LC16 to see whether I can find overlapping and non-overlapping stimulus selectivity, given the above hypotheses. I also focused primarily on LC6 to explore its spatial and temporal encoding properties further.

3.2 Methods

3.2.1 Fly lines

Cell-type specific expression of the fluorescent calcium indicator GCaMP6m (Chen et al. 2013) was achieved using the Split-GAL4/UAS expression system (Luan et al. 2006; Pfeiffer et al. 2010). The GAL4 driver lines were constructed using previously described methods (Pfeiffer et al. 2010), and selected based on the imaged expression patterns (Jenett et al. 2012; Kvon et al. 2014, and personal communication from Barry Dickson).

All flies used for calcium imaging experiments were reared under standard conditions (25 °C, 60 % humidity, 12 h light/12 h dark, standard cornmeal/molasses food), and all imaging experiments were performed on females 3-6 days post-eclosion. To image from individual lobula columnar (LC) cell-types, split-GAL4 driver lines (LC6: OL0070B, LC16: 0L0046B, LC11: OL0015B) were crossed to pJFRC7-20XUAS-IVS-GCaMP6m in *VK00005* (DL background) effector line. LC cell-types split-GAL4 driver line images can be seen in high-resolution at www.janelia.org/split-GAL4.

3.2.2 In vivo 2-photon Ca^{2+} imaging: preparation

The imaging preparation was almost identical to that described in (Strother et al. 2014). Briefly, flies were cold anesthetized and tethered to a fine wire at the thorax using UV-curing adhesive. The two most anterior legs (T1) were severed and glued down along with the proboscis to prevent grooming of the eyes and to immobilize the head. Tethered flies were glued by the head capsule into the fly holder and after addition of saline (103mM NaCl, 3mM KCl, 1.5mM $CaCl_2$, 4mM $MgCl_2$, 26mM $NaHCO_3$, 1mM NaH_2PO_4, 8mM trehalose, 10mM glucose, 5mM TES, bubbled with 95% O_2 / 5% CO_2 ; final Osm=283, pH=7.3 (modified from Wilson & Laurent 2005)) to the bath, the cuticle at the back of the head was dissected away to expose the brain. Muscles 1 and 16 (Demerec et al. 1965) were severed to reduce motion of the brain within the head capsule, and the post-ocular air sac on the imaged side of the brain was removed to expose the optic glomeruli. The right side of the brain was always imaged unless otherwise stated.

3.2.3 In vivo 2-photon Ca^{2+} imaging: microscopy

The optic glomeruli were imaged using a two-photon microscope (Bruker/Prairie Ultima IV) with near-infrared excitation (930 nm, Coherent Chameleon Ultra II) and a 60× objective (Nikon CFI APO 60XW). The excitation power was never greater than 20 mW at the sample. Two-photon imaging is advantageous in this case because the long wavelength does not overlap with the fly's visible wavelength, and the small two-photon excitation volume produces minimal phototoxicity to the tissue. Imaging parameters varied slightly between experiments but were within a small range of my typical acquisition parameters: 128×90 pixel resolution, and 10 Hz frame rate (10.0-10.5 Hz). LC cell axon calcium data were collected from single planes selected to capture a consistently large slice of each glomerulus. Since only one LC-type projects to one glomerulus, imaging at the glomerulus also ensures recording from a single LC-type.

3.2.4 Visual stimulus

Flies were placed in the center of a modular LED display (Reiser & Dickinson 2008) on which visual stimuli were presented (Fig.3.4A). Since the head is fixed into the fly holder with approximately 30° upward tilt (relative to horizontal), the whole display was tilted to roughly match this angle. It is important to note that this fly holder occluded ~15-30° of the dorsolateral part of the fly's field of view. The display consists of 574 nm peak output LEDs (Betlux ultra-green 8×8 LED matrices, #BL-M12A881UG-XX) covered with a gel filter (LEE #135 Deep Golden Amber) to greatly reduce stimulus emission at wavelengths that overlap with those of GCaMP emission, resulting in emission range of 560-600nm (directly measured by Ocean Optics spectrometer). The display was configured to cover 60 % of a cylinder, with LEDs subtending 72° in elevation and 216° in azimuth (maximum pixel size of 2.25°) as seen by the fly in the center of the cylinder (flattened diagram: Fig.3.3B). Loom related stimuli were presented in a 54°×54° square region centered at 27° elevation and 0°, 27° or 45° azimuth (Fig.3.3B, magenta). Receptive field mapping stimuli were presented in a 45°×90° region centered at 27° elevation covering most of the area where looms were presented (Fig.3.3B, green). Other stimuli were presented in a 72°×126° region covering the whole right hemifield of the arena (Fig.3.3B, cyan).

The stimuli were generated using custom MATLAB (Mathworks, Natick, MA) scripts, and presented at 64 frames/sec. Schematic of loom-related stimuli are shown in Fig.3.4C. The dark loom stimulus consisted of a series of 35 disk sizes, with the edge pixel intensity interpolated to approximate a circle on the discrete LED screen. The luminance-matched stimulus was created using the dark looming disk stimulus, spatially scrambling the location of dark pixels of each frame only within the area of the final size of the disk. The edge-only loom was created by masking away the inner diameter (leaving the outer 9° diameter) of the dark disc stimulus for every frame. The quadrant loom stimuli were created by masking away three quadrants of the dark disc stimulus for every frame. The time series of looming stimuli sizes were presented based on the classic parameterization for looming stimuli assuming a constant velocity of approach. The angular size of the object (θ) increases according to the equation $\theta(t) = 2\tan^{-1}(R/Vt)$, where R is the radius of the object, V is its approach speed. Speed of the loom is represented by the ratio of these parameters (R/V time course, Fig.3.3E top) (Gabbiani et al. 1999). As a comparison, the dark disc loom stimulus was presented at constant speed, covering the speed range of the R/V time course presentations (constant speed, Fig.3.4E bottom). All looming stimuli appear as 4.5° spots and increase to a maximum diameter of 54°. The experimental protocol consisted of 3 repetitions of each stimulus type presented using a randomized block trial structure. Stimulus epochs were interleaved with at minimum 2 seconds of blank frame epochs that allowed the GCaMP6m fluorescence to decay back to baseline. Each protocol lasted 15-20mins and subsequently presented 3 times, resulting in the total experiment time of ~ 1 hour.

3.2.5 Data analysis

Data were analyzed with software written in MATLAB. Motion compensation was performed by cross-correlating each frame to a mean reference image and maximizing the correlation iteratively, using software written by James Strother (https://bitbucket.org/jastrother/neuron_image_analysis). The fluorescence signal is determined within hand-drawn regions of interest selected to tightly enclose the entire slice of each glomerulus captured within the imaging plane. $\Delta F/F$ is calculated as the ratio of $(F - F_0) / F_0$, where F is the instantaneous fluorescence signal and F_0 is calculated as the 10^{th} percentile of the fluorescence signal within a sliding 300 frame window. These parameters were determined empirically to optimally fit the actual

baseline fluorescence. For combining responses of individual flies across animals, I normalized the ΔF/F responses from each individual fly to the 98th percentile of the ΔF/F across all visual stimuli within one experiment. Instead of choosing the maximum response, which may include outliers, I chose the 98th percentile as a more robust measure of reference. All responses are the mean of the mean response (across repeated stimulus presentations) of all flies in the dataset. Error bars indicate mean ± SEM. All significance results presented for Ca^{2+} imaging were determined with the Mann-Whitney test.

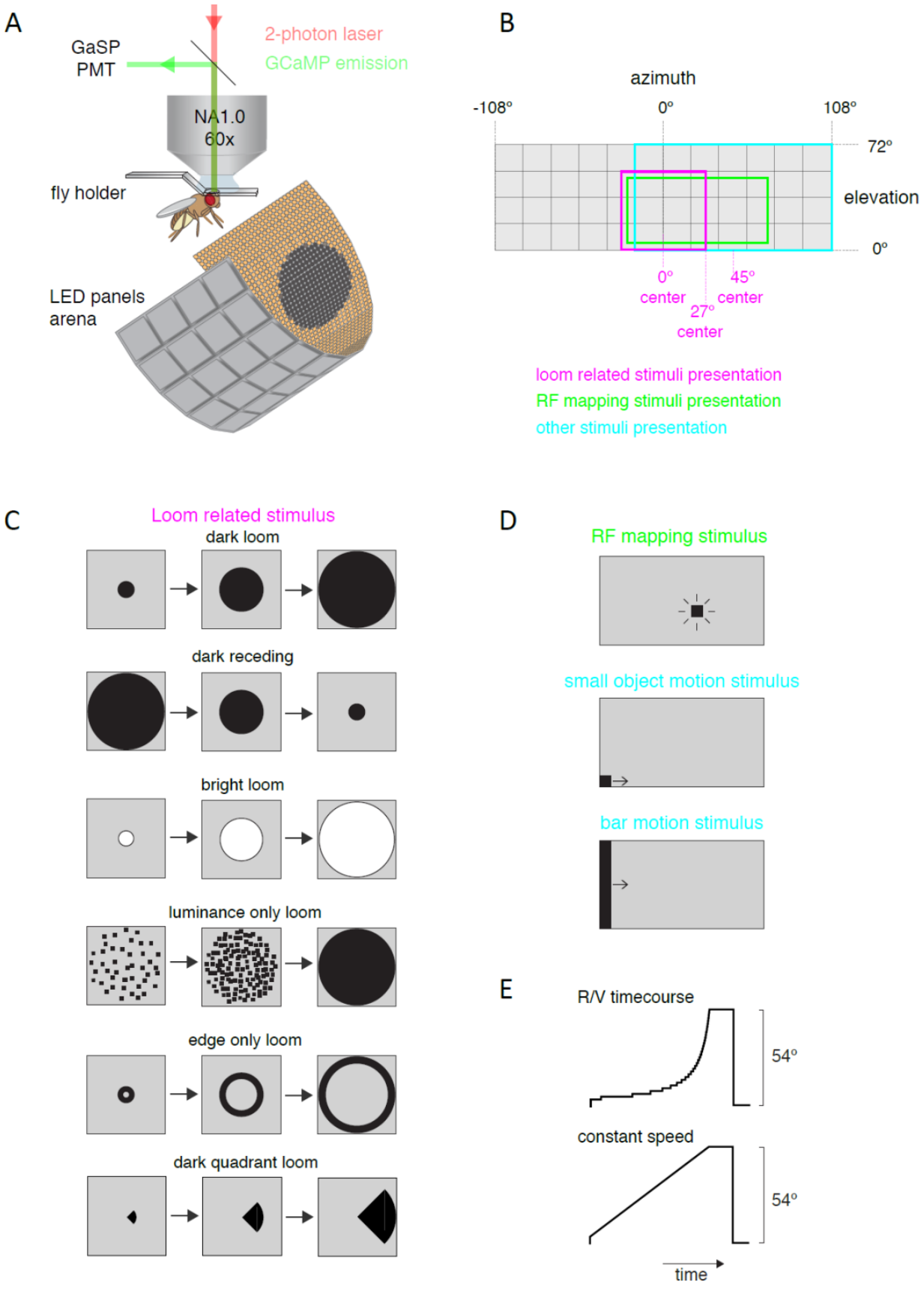
A
GaSP
PMT
2-photon laser
GCaMP emission
NA1.0
60x
fly holder
LED panels
arena
B
azimuth
-108°
0°
108°
72°
elevation
0°
0°
center
45°
center
27°
center
loom related stimuli presentation
RF mapping stimuli presentation
other stimuli presentation
C
Loom related stimulus
dark loom
dark receding
bright loom
luminance only loom
edge only loom
dark quadrant loom
D
RF mapping stimulus
small object motion stimulus
bar motion stimulus
E
R/V timecourse
54°
constant speed
54°
time

Fig.3.4 | *In vivo* two-photon imaging of evoked calcium responses to visual stimuli

(A) *In vivo* two-photon GCaMP imaging in head fixed flies. Visual stimuli were presented via an LED arena. **(B)** Position of the visual stimulus presentation relative to the whole LED arena. Magenta squares (54°×54°) centered at 0°, 30°, 45° azimuth denote the area where loom and loom related stimuli were presented. Green rectangle (45°×90°) denotes the area where receptive field mapping stimulus was presented. Other stimuli were presented in the cyan rectangle covering the right hemifield of the arena. **(C)** Schematic of loom and loom related stimuli frames. **(D)** Dark square (9°×9°) flicker stimulus was used for receptive field (RF) mapping. Small object motion stimulus consisted of a dark square (9°×9°) moving at the bottom of the arena. Bar motion consisted of a dark bar (72°×9°) moving. **(E)** Two time courses were used to present looms: R/V time course simulating an object approaching at constant velocity (top) and a looming timecourse exhibiting constant speed of edge motion (bottom).

3.3 Results

3.3.1 LC6 &16 responds preferentially to dark loom stimuli, while LC11 does not

To explore whether LC6 and LC16 encode visual features such as looming, that are sufficient to evoke jumping and backward walking (Fig.3.2), I investigated the visual responses of these cell types using *in vivo* two-photon Ca^{2+} imaging from head-fixed flies (Fig.3.4A). I measured calcium responses of single LC neuron types by imaging from the axons within each glomerulus using an imaging plane selected to obtain the largest slice through the volume of the glomerulus (Fig.3.5A). I observed that looming stimuli evoke responses in several axons that span each glomerulus (Fig.3.5B). I quantified the population response of these axons by integrating the calcium signals within the glomerulus region.

Calcium signals integrated over each of the LC6 and LC16 glomeruli both show similar increases in response to dark looming disks (Fig.3.5 C(i), top row). Both cell types appear similarly tuned, responding with larger calcium increments to the slower looming speeds presented (Fig.3.5 C(ii), row). Both cell types are selective to dark looming stimuli, as a looming disk that was brighter than the background did not elicit large responses (Fig.3.5 C (i,ii), second from top row). Looming stimuli provide compound visual cues, so to further test for the specificity of these neurons' responses to dark looming objects, I decomposed the looming stimuli into their two major components—a luminance decrement within a region of the visual display over time and the edge motion. I presented a luminance-only stimulus that darkened over time with the same temporal profile as the dark looming disk, but lacked any coherent edge motion. This stimulus elicited moderate responses in both cell types that were significantly smaller than the dark looming disk (Fig.3.5 C (i,ii), second from bottom row; Mann-Whitney test, $p < 0.01$ for both LC6 and LC16 for R/V=550). Lastly I presented the edge-only stimulus, which contained the edge motion of the original dark disk stimulus, while having minimal changes in the overall luminance. This stimulus also induced a slightly smaller response compared to the dark looming disk in both cell-types, but with a more transient response profile (Fig.3.5 C (i,ii), bottom row; Mann-Whitney test, $p < 0.05$ for LC6 and $p < 0.01$ for LC16 for R/V=550).

Taken together, the lower response to these "components" of the looming stimuli suggests that a synergistic or additive effect of the edge motion and darkening shapes the dark loom preference in these neurons.
To confirm that the similar responses of LC6 and LC16 to looming stimuli were a specific property of these cells, I performed the identical experiments on an additional LC neuron type. I measured the responses of LC11 (Fig.3.5A, B), which was selected because its dendrites arborize in lobula layers that are distinct from LC6 and LC16 (Fig.3.3B), and because LC11 was not found to have any strong activation phenotypes in behavioral assays (data not shown).

LC11 did not show significant calcium response changes to any of the looming-related stimuli (Fig.3.5C (i,ii) black trace). However, I observed large responses from LC11, when I presented simpler moving stimuli that did not contain looming motion. LC11 showed large responses to a small moving object, and more moderate responses to a moving bar spanning the visual display (Fig.3.5D). In contrast, LC6 and LC16 also showed calcium responses to the small object, but these responses were smaller than those to the loom stimuli, and much smaller than those of LC11 (Fig.3.5D, Mann-Whitney test, $p < 0.01$ for both LC6 and LC16). Taken together, these results demonstrate that LC6 and LC16 exhibit selectivity for slow, dark looming objects, while LC11 encodes a distinct set of visual features.

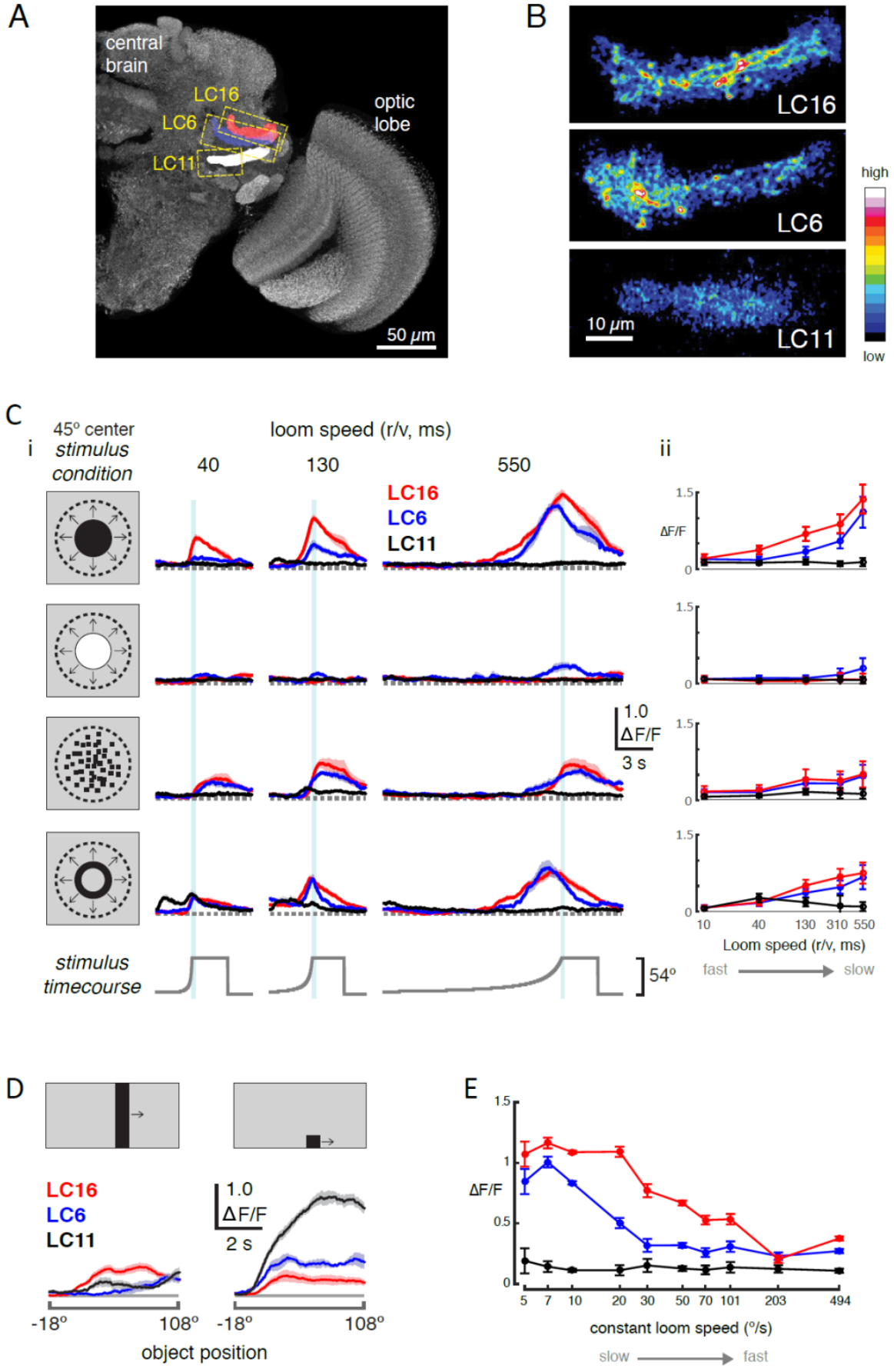
A
central brain
LC16
LC6
LC11
optic lobe
50 μm
B
LC16
LC6
LC11
10 μm
high
low
C
i
45° center
stimulus condition
loom speed (r/v, ms)
40
130
550
LC16
LC6
LC11
1.0 ΔF/F
3 s
stimulus timecourse
54°
ii
ΔF/F
1.5
0
10 40 130 310 550
Loom speed (r/v, ms)
fast
slow
D
LC16
LC6
LC11
1.0 ΔF/F
2 s
-18°
108°
-18°
108°
object position
E
ΔF/F
1.5
1
0.5
0
5 7 10 20 30 50 70 101 203 494
constant loom speed (°/s)
slow
fast

Fig.3.5 | LC16 and LC6, but not LC11, respond to dark looming stimuli and its components.
(A) The axon terminals of LC cells bundle to form cell-type specific glomeruli (subset shown in B). I imaged from a single glomerulus by using spilt-GAL4 lines labeling individual cell-types (LC16, LC6 or LC11). Representative regions for calcium imaging experiments are marked with the yellow dashed rectangles. Image from Aljoscha Nern. **(B)** Exemplary responses of LC16, LC6 and LC11 to a slow dark looming disk are shown. Single frame taken from peak response of an individual fly. Different split-GAL4 lines were used to image from each glomerulus. **(C)** (i) LC16, LC6 and LC11 responses to looming visual stimuli are shown for four variants of the stimulus (from top to bottom: dark looming disk, bright looming disk, luminance-only, edge -only) expanding at r/v= 40,130 and 550 ms (n=5 per genotype). All stimuli were centered at an azimuthal position 45°to the Right/Left of the midline. Error bars indicate mean ± SEM. (C) (ii) Tuning curve of the responses (area under the curve during ±2s from stimulus stop) are shown for the stimuli in the same row in C(i). **(D)** As a comparison to looming stimuli, I also presented moving object stimuli that contain local motion that is distinct from looming. LC11 responds strongly to the motion of the small (9°×9°) spot, but not the long bar (9°×72°) moving object. The objects moved at 22.5°/s. **(E)** Dark looming stimuli were presented with constant edge speed motion. The tuning curves of peak responses are shown for the 3 cell types. All stimuli were centered at 45° azimuth (R or L). Error bars indicate mean ± SEM.

3.3.2 What features of the dark looming stimulus do LC6 & 16 encode?

In order to understand what spatial and temporal aspect of the looming stimulus is being encoded, I first looked at a parameter that loom sensitive neurons have been known to signal, the time to collision (in pigeons, Frost & Sun 1998; in locusts, Rind & Simmons 1992; Fotowat & Gabbiani 2011). Total time to collision (t) was calculated according to equation $t = (R/V) \times \tan(\theta/2)^{-1}$ for each R/V speed, assuming $\theta = 180°$ at collision. Time of peak of the Ca^{2+} response relative to this time of collision was plotted as a function of R/V speeds (Fig.3.6). This revealed a linear relationship between the time to collision at peak and the R/V (particularly for LC6). This linear relationship is predicted by a previously established model of loom sensitive neurons, which consists of the multiplication of velocity and size signals, suggesting underlying computations (Gabbiani et al. 2002; Hatsopoulos et al. 1995). Time to collision at peak response was not significantly different for stimuli centered at 0° and 45°($p>0.05$ for all speeds, data shown for 45°center). It is important to note however, that the accuracy of the peak timing measurement is compromised due to the slow time course of Ca^{2+} indicators, and my sampling rate (~10Hz).

I wondered whether this peak timing corresponds to a specific size of the disc, and thus translated the timing into disc size according to each R/V time course. Since there exists some sensory delay and Ca^{2+} indicator rise time, we can assume a fixed delay from the time a disc size was presented, to the time the corresponding Ca^{2+} response is observed. As the exact delay is unknown, I tentatively selected reasonable fixed delays (100 and 200ms) based on estimated sensory delay (~5-25ms von Reyn et al. 2014) and Ca^{2+} indicator rise time (~100-150ms, Chen et al. 2013) to calculate the corresponding disc size. As the delay is made longer, the disc size at peak becomes more constant across the R/V speeds (Fig.3.6B). Because the faster speeds have a steep disc size change around the time of the peak, with the above mentioned issue with the time resolution of Ca^{2+} imaging it is challenging to accurately measure the disc size (Fig.3.6B (i),(iii), see error bars for fast speeds). However, measurement at the slower speeds is less sensitive to the length of the delays and more reliable, with the mean disc size at peak around 32° for LC6 and 44° for LC16 at R/V=550ms.

Since loom sensitive neurons in some organisms are known to selectively respond to looming object motion that is on a collision course (R/V time course) (Rind & Simmons 1992; Jones & Gabbiani 2010), I wanted to see whether this is the case for LC6 and 16. I designed dark looming disc stimuli with constant edge speed motion, which cover the range of instantaneous/average speeds that my R/V speeds cover (5°/s ~ 494°/s). Both LC6 and 16 showed tuning for slower speeds, which is expected based on the preference for the slower speeds from the R/V speed tuning (Fig.3.5E), but also, the response amplitude at the slower speed was comparable to that for R/V speeds ($\Delta F/F \sim 1.0$). This suggests that LC6 and 16 are generally tuned to slow speeds, and that they do not show obvious preference for object motion on a collision course. I also analyzed the time to collision at peak and disc size at peak for responses to the constant speed looms. The time to collision at peak also increases as a function speed, but does not show a linear relationship; rather, it has an exponential profile (Fig.3.6B (ii)). The mean disc size at peak was around 31° for LC6 and 35° for LC16 at 5°/s, which is similar to the size obtained with the slowest R/V loom stimuli (Fig.3.6B (iv)).

In many insects, it has been proposed that there is an absolute angular threshold that triggers aversive behaviors such as escape or collision-avoidance (Gabbiani et al. 2001; Wicklein & Strausfeld 2000; von Reyn et al. 2014). Interestingly, the mean disc size at peak response I obtained for LC6 and LC16 (~31° and ~39° respectively), are

in the range of angular thresholds that trigger escape (~30° for long (≥7ms) mode escape, ~40° for short (<7ms) mode escape (von Reyn et al. 2014)) or aversive saccades away from an obstacle (~33°, van Breugel & Dickinson 2012) in *Drosophila*. This apparent agreement may provide hints about what kind of behaviors LC6 and LC16 may mediate in the natural setting.

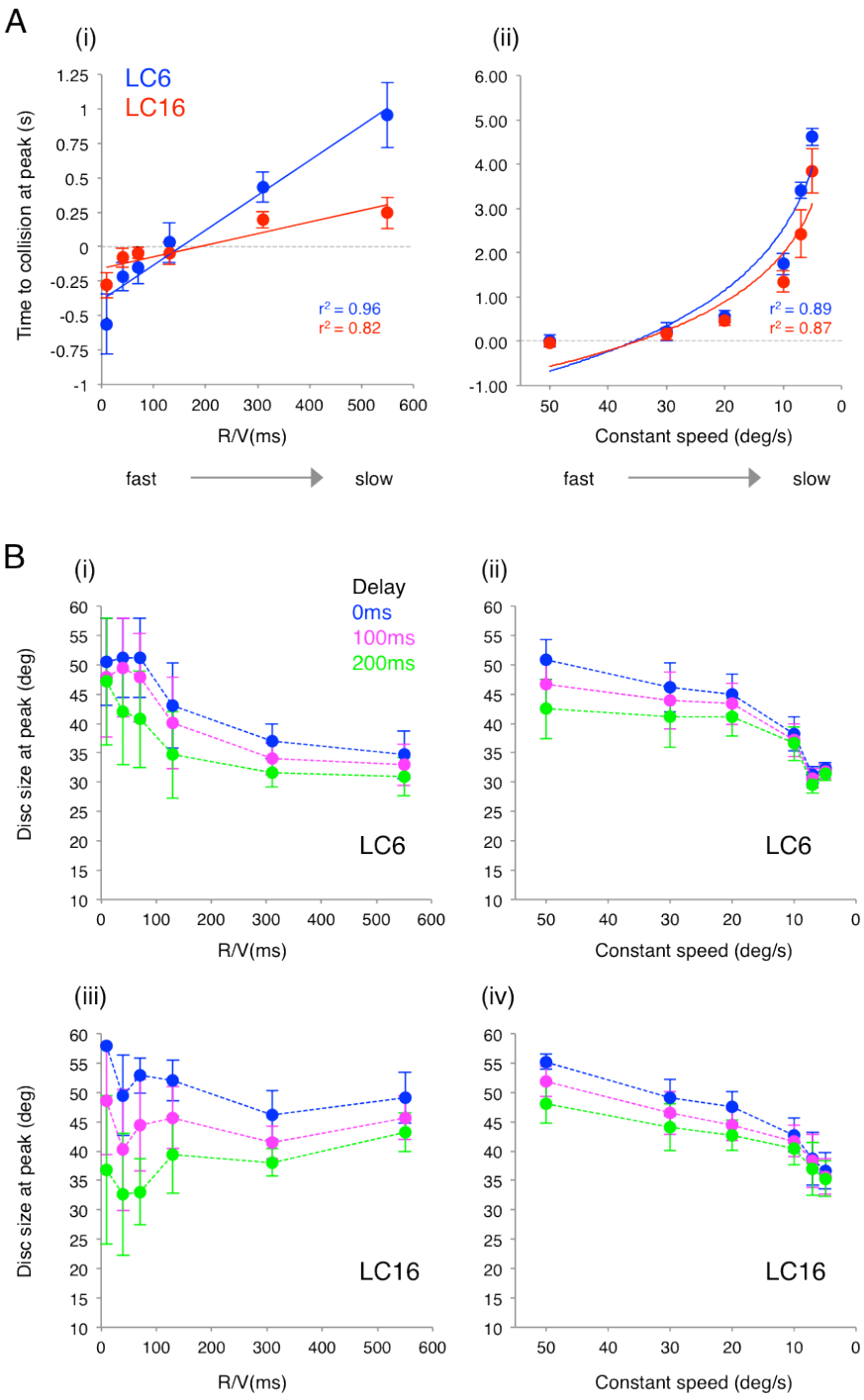

Fig.3.6 | Analysis of time to collision and disc size at response peak

(A) (i) Time to collision at peak response as a function of R/V speeds. r^2 values for the linear fit are shown in inset. (ii) Time to collision at peak response as a function of constant speeds. r^2 values for the exponential fit are shown in inset. Error bars indicate mean ± SEM. **(B)** (i),(iii) Disc size at peak response as a function of R/V speeds. (ii),(iv) Disc size at peak response as a function of constant speeds. Different colors denote the assumed time delay (sensory delay + GCaMP rise time) between time of disc size presentation and the time of Ca^{2+} response detection. Error bars indicate mean ± SEM.

3.3.3 Receptive field mapping of LC6

LC6 receptive field size can be predicted to be around 10~20° angular size, from the anatomical size of the cross section of a single cell dendritic field relative to the whole lobula (Fig.3.7A(i)). Receptive field mapping was performed using a small 9°×9° dark flashing square appearing in pseudorandom order on a non-overlapping grid subtending 45°×90° (Fig.3.7B). Sparse activity pattern was seen throughout the imaging plane for some but not all positions (Fig.3.7C). The Ca^{2+} response pattern suggests the activation of one or two cells, given the anatomical profile of these axon terminals (Fig.3.7A (ii), axon terminal of each cell branches 1-2 times, extending across the glomerulus). This indicates that the size of the functional receptive field is not much larger than 9°×9°, also given that I am probably sampling below the nyquist sampling criterion. This functional receptive field size is in line with the anatomical prediction of receptive field size.

Positions for which intermediate to strong response was frequently observed, had the tendency to cluster around the medial-ventral part of the visual display (Fig.3.7B Position 1-3), with less strong responses at more peripheral areas (Position 4-7). It would be interesting if this were a genuine bias of the spatial representation of this cell-type. However, it is currently unclear if this is the case, since my measurement is spatially limited by the single-plane 2-photon imaging method, which does not encompass the depth of the whole glomerulus (Fig.3.7A (iii), glomerulus A-P axis ≈10μm > 2-photon Z-resolution ≈3μm), and also possibly the GCaMP labeling strategy, which does not label the whole LC6 population (~70% labeling, with slight ventral skew).

I also observed that response patterns evoked by adjacent stimulus positions are more similar compared to activity patterns evoked by positions spaced apart (Fig.3.7D; more overlap in top row (Pos.1, 2, 3) for both flies, compared to bottom row for Fly1 (Pos.6, 2, 4) and Fly2 (Pos.5, 2, 7)). Because of the spatial bias of the response pattern to the medial-ventral area, I could not test whether this adjacent position pattern overlap holds true for other parts of the visual field, but this should be tested in the future using a more complete measurement method. Given the anatomical arrangement of the axon terminal of single cells, which often branches out to the whole width and length of the glomerulus (Fig.3.7A(ii)), it would be hard to imagine an accurate retinotopic "map" along the D-V or M-L axis of the glomerulus. Instead, this observation may hint at a very low-resolution map, perhaps with the dorsal and ventral halves of the glomerulus corresponding to the dorsal and ventral visual fields.

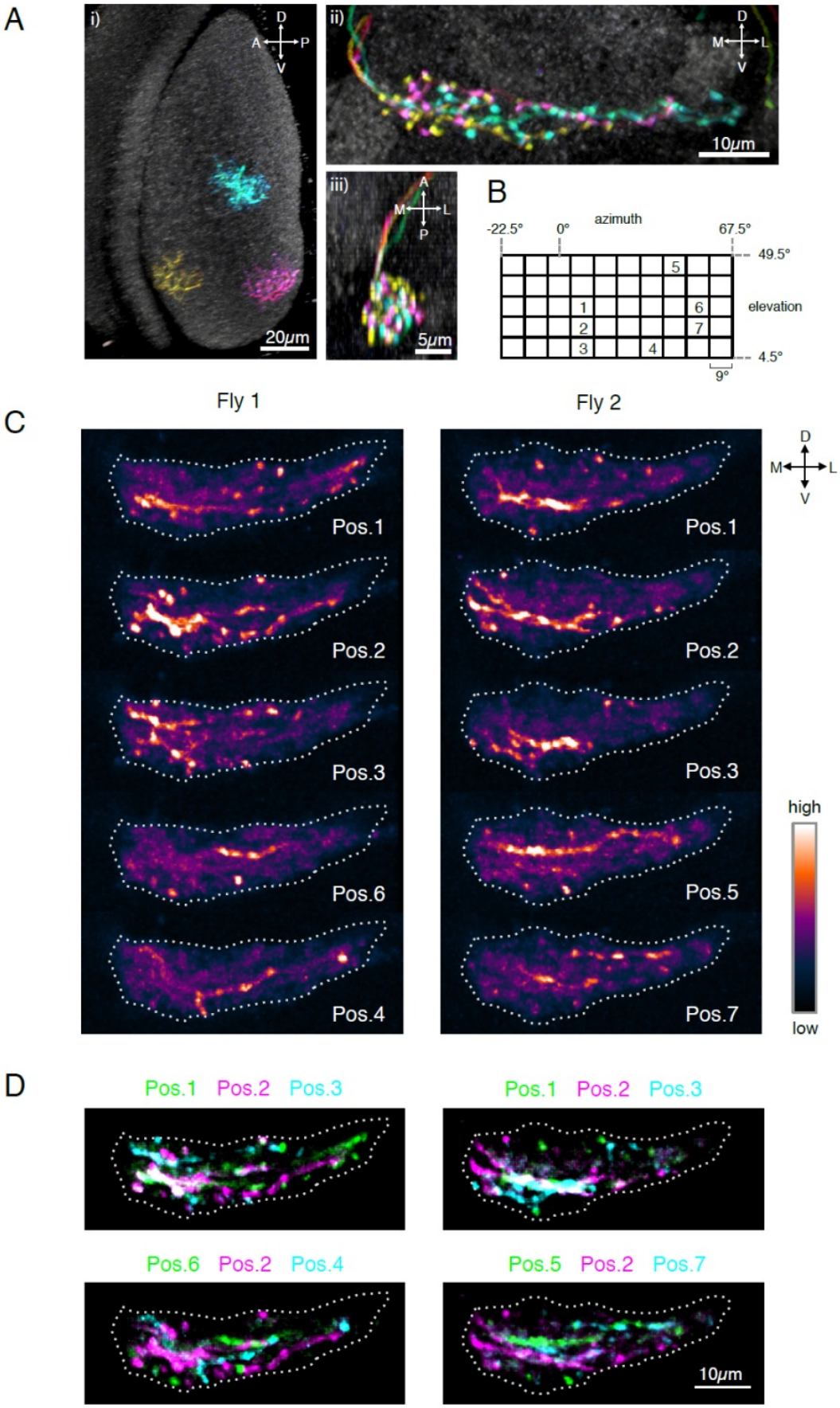
A
i)
D
A
P
V
20μm
ii)
D
M
L
V
10μm
iii)
A
M
L
P
5μm
B
azimuth
-22.5°
0°
67.5°
49.5°
elevation
4.5°
9°
1
2
3
4
5
6
7
C
Fly 1
Fly 2
D
M
L
V
Pos.1
Pos.2
Pos.3
Pos.6
Pos.4
Pos.1
Pos.2
Pos.3
Pos.5
Pos.7
high
low
D
Pos.1 Pos.2 Pos.3
Pos.1 Pos.2 Pos.3
Pos.6 Pos.2 Pos.4
Pos.5 Pos.2 Pos.7
10μm

Fig.3.7 | Anatomy and receptive field mapping of LC6 at the axon terminal show no obvious retinotopy.

(A) (i) Position of the dendrites of three LC6 cells in the lobula in a layer cross-section view. Each cell occupies a distinct retinotopic position along the long (DV) and short (AP) axes of the lobula. By contrast, within the target glomerulus (two roughly orthogonal views are shown in ii and iii) the axons terminals of the same cells are intermingled without an obvious correlation to the retinotopic pattern in the lobula. Scale bars represent 20μm (i), 10μm (ii) and 5μm (iii). Single-cell labeling was obtained by multi-color flip out (MCFO) technique. Images are from Aljoscha Nern. **(B)** Receptive field mapping was conducted in a 45°×90° area covering the midline area and extending to the right visual field of the fly (green rectangle, Fig. 3.4B). Dark 9°×9° flashing squares were shown in pseudorandom order on this grid. Grid positions with numbers (1-7) denote examples of positions where intermediate to strong responses were often observed. **(C)** Example Ca^{2+} responses to receptive field mapping stimuli measured at the glomerulus for two different flies. The images are maximum intensity projections from a single trial for stimulus positions denoted in white (Pos.#), which corresponds to the grid numbers in (B). The responses are sparse, and could probably be attributed to 1-2 cells based on the arborization pattern of a single cell at the glomerulus in the MCFO images in A(ii). **(D)** Overlays of axons responsive for different positions. The adjacent positions (position 1,2,3, both flies) show more overlap compared to positions spaced apart (position 6,2,4 for Fly1, position 5,2,7 for Fly2).
White dotted lines outline the glomerulus. Scale bar represents 10μm. All images in (C) and (D) are on the same scale.

3.3.4 Spatial and directional dissection of the LC6 loom response

Since the receptive field size of LC6 is smaller than the extent of the full looming stimulus, I wondered whether some portion of the spatial and/or directional feature of the loom is critical for responses that I observed. A simple way to test this is to mask out all but quadrants of the full loom, and present them separately, so that it would contain only a quarter of the area and one cardinal net motion direction of the full loom.

On presenting a single quadrant, to my surprise, the ventral and medial quadrant of the looming disc evoked a larger response than with the full looming disc, while the dorsal and lateral quadrants evoked similar or smaller responses (Fig.3.8.A, B). This indicates that the response to the full loom is less than the sum of the response to its parts, suggesting that some neurons are inhibited when the dark area and/or the

direction of motion are increased. By simultaneously presenting another quadrant, I could observe this effect directly. The most dramatic inhibitory effect was observed when the lateral quadrant was simultaneously presented with the ventral quadrant, where there was a significant dampening of the response (Fig.3.8.B, compare Ventral to V+L). Similar inhibitory effects (but to a lesser extent) were observed with other combinations that contained the dorsal or lateral quadrants (Fig.3.6.B, D+M, D+L, D+V and L+M).

This stimulus design proved useful because all quadrant loom responses are directly comparable to each other, and to the full loom response. However, I cannot determine whether the observed effects are spatial or directional, because these parameters are coupled for all quadrants. Nevertheless, given the result of the receptive field mapping, the large responses I saw with the ventral and medial quadrant looms is likely due to a spatial effect, and not directional. It is also possible (and is suggested by anatomical data) that the dendrites of LC6 are more elliptical than circular, which would confer an apparent bias for different directions of motion, even if the cells themselves are not directionally selective. We need to investigate this more directly in the future with stimuli that would test all directions for each location. Single cell recording would be necessary for this purpose, because if directional tuning existed, it would likely get averaged out in the population response.

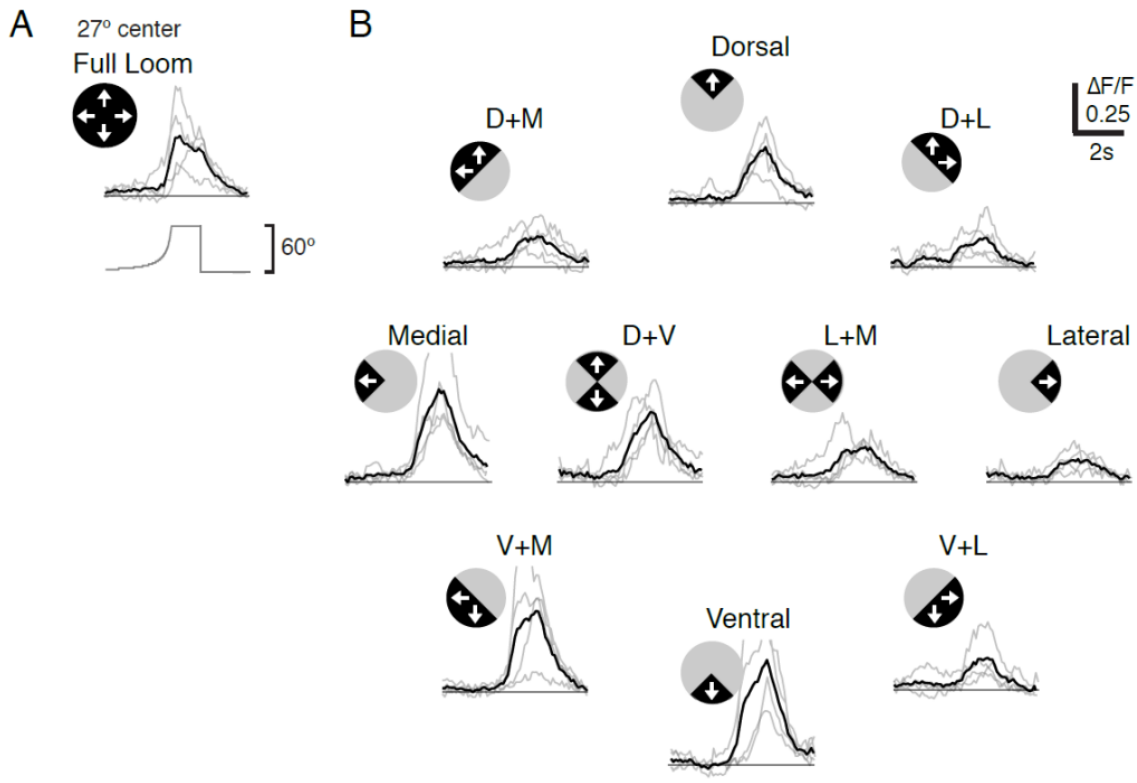

Fig.3.8 | Combinatorial quadrant loom stimuli reveal inhibitory effects in the LC6 population.

(A) Ca^{2+} responses to a full dark looming disc stimulus centered at an azimuthal position 27° to the right of the visual midline. Individual flies in gray, mean of all flies in black (N=4). **(B)** Ca^{2+} responses to single or pairs of quadrants of the dark looming disc centered at 27°. The ventral quadrant evoked the largest response, whereas the lateral quadrant evoked the smallest. Note that these single quadrant responses are larger than the full loom. On combining these two quadrants (V+L) a diminished response is observed, indicating an inhibitory effect of the lateral quadrant on the ventral quadrant response. Similar inhibitory effects (but to a lesser extent) are observed for other combinations containing the dorsal and lateral quadrants (D+M, D+L, D+V and L+M).

3.4 Discussion

3.4.1 The link between visual features encoded by LC neurons and behavior

The three LC neuron types examined, preferentially responded to distinct stimuli, to either a dark looming stimulus (LC6 and LC16) or a small moving object (LC11). LC6 and LC16 showed stronger responses to a dark expanding disc than to related stimuli such as an expanding bright disk or a darkening stimulus that lacks the expanding motion (luminance-only stimulus). However, there were also notable differences in the LC6 and LC16 responses to the small field motion stimuli, where LC16 responded more strongly to the bar motion, whereas LC6 responded more strongly to the small object motion. These dissimilarities along with the differences in time to collision and disc size at peak response, may hint at differential visual feature parameters that elicit either jumping or backward walking.

Nevertheless, making such a direct one-to-one link between visual features encoded by LC neurons and the optogenetically triggered behaviors could also misguide us. While the activation screen suggests a command-like role for LC neurons in triggering behavior, the single cell-type activation is an artificial situation that flies would almost never experience in nature. Given the similarity observed here for LC6 and LC16 responses, what is likely to occur given an actual visual stimulus is the co-activation of several LC cell-types with similar selectivity. This would result in and a patterned sequence of temporal and spatial activation of LC cell-types, which could be interpreted by the downstream circuits as a population code to “select” a behavior to trigger. Therefore we can hypothesize, that in natural conditions, the overlap or difference between the encoding of several LC neuron types is readout by downstream neurons to trigger behavior.

Another reason to expect integration and comparison of LC neuron responses in downstream circuits is their rather broad selectivity. As far as I have observed with my visual stimuli, at least LC6 and LC16 responded with comparable strength not only to one type of stimulus, but a few (LC6: dark loom and small object motion, LC16: dark loom and bar motion). Thus a further refinement of stimulus selectivity seems to be required downstream to disambiguate between categories of visual features that these LC neurons convey.

3.4.2 Are LC6 and LC16 "loom detector" neurons?

Behavioral studies in houseflies have shown that darkening contrast combined with edge motion is the most effective stimulus for triggering takeoffs (Holmqvist & Srinivasan 1991). LC6 and LC16 responses had an increased response to the full dark loom compared to either only its darkening, or edge motion components, fulfilling this requirement for extracting features of loom that trigger escape.

However, physiological studies on loom sensitive neurons have found additional characteristics that more narrowly define a "loom detector" neuron. There are perhaps five main features: 1) the time to collision at peak response (firing rate) is linearly related to the R/V speed, 2) the time to collision at peak response is stimulus location invariant, 3) the time to collision at peak response is stimulus contrast invariant, 4) global luminance change is not required for the neuron's response to loom, and lastly, 5) preference of R/V time course over constant speed loom (de Vries & Clandinin 2012; Jones & Gabbiani 2010).

From my Ca^{2+} imaging data so far, it seems that LC6 and LC16 have response properties broadly in line with the first two features. The third feature however, is not fulfilled, since both LC6 and LC16 respond mainly to dark contrast looms. The fourth feature has not been strictly proven with appropriate stimuli (such as random dot flow fields), but given that the neurons responded to the edge-only loom stimulus rather strongly (~70% of the dark loom response), it is inferred that global luminance change is playing a relatively small role in the loom response. Given the comparable responses I saw with constant speed looms, LC6 and 16 do not seem to exhibit the fifth feature.

Having made these comparisons, it is clear that LC6 and 16 possess only a part of the classic physiological definition of a "loom detector". Therefore, it may not be appropriate to call LC6 and LC16 a "loom detector" in this context. However, it is important to note that the above definition comes from wide-field neurons that have a very different anatomy to the LC neurons (Gabbiani et al. 1999; Rind & Simmons 1992; Simmons & Rind 1992).

In *Drosophila*, the Giant Fiber (GF) escape pathway is known to mediate a fast mode of escape behavior, that is elicited largely by fast looms (R/V< 20ms, von Reyn et al. 2014). This fast loom response is thought to be mediated by LC4, which is known to affect the GF speed tuning when genetically silenced (significant reduction in GF response for looms at R/V<20ms and constant speed>500°/s, von Reyn et al. 2017). However, since blocking the GF renders a longer escape mode intact, an alternative pathway for escape behavior is thought to exist (von Reyn et al. 2014). With the slow speed tuning of LC6 and LC16, it is possible that these neurons provide input to this alternate escape pathway, and therefore serve their roles as "loom detectors" for this behavior.

3.4.3 Possible mechanisms of loom sensitivity in LC neurons

While the wide-field loom detector neurons are able to signal the existence of a looming object in the field of view with a single neuron, LC neurons need to recruit several neurons to accomplish the same task, given their small receptive field size. Below, I discuss completely hypothetical mechanisms of how loom (expansion) sensitivity might be implemented with such configuration (Fig.3.9). The mechanisms strongly depend on the selectivity of individual neurons, and the interaction between them.

Model 1: Individual cells are loom sensitive

This hypothetical selectivity is similar to that observed in starburst amacrine cells in the mammalian retina (Briggman et al. 2011). If this is true, one neuron could detect a very small loom, within the limits of its receptive field. I currently have no evidence that individual neurons are loom sensitive, but single cell recordings could provide some insights in the future.

Model 2: Radially arranged directionally selective cells

This is a simple, but perhaps developmentally implausible way to achieve loom sensitivity amongst a population of cells. It would require very precise wiring to make these cells with different directional selectivity to be arranged in a neighboring and

radial manner. Also, this mechanism is inflexible in that the response of the population would be dependent on the loom center location.

Model 3: Facilitation between non-directionally selective cells

This seems the most simple and flexible way to achieve loom sensitivity using a population of cells. If lateral facilitatory mechanisms are in place, the first cell that is excited by a small disc would facilitate the neighboring cell, and as the disc grows in size, the surround facilitation would spread as a radial wave. At the same time, this scenario would ensure a null-response for receding loom, and also loom center location invariance. In fact, in *Calliphora*, Okamura et al. found that when a single lobula-lobula plate columnar neuron was intracellularly filled with Lucifer yellow, dye coupling was observed between 7-8 of these cells, suggesting gap junction coupling (Okamura & Strausfeld 2007). Therefore, it seems plausible that if gap junctions exist in a similar fashion between individual LC neurons, it could implement facilitatory mechanisms. However, this mechanism alone does not explain why the maximal response disc size falls off around ~30-40° diameter, and also is somewhat contradictory to inhibitory effects I observed using quadrant loom stimuli.

The mechanisms illustrated above, are all at the level of LC populations. However, if we are to understand how selectivity of individual LCs arise, we must study its inputs. The estimated number of inputs from anatomy (number of transmedullary cells projecting to lobula layers that LC6 and LC16 innervate) are >30. Understanding the role of >30 inputs presents a daunting task with the current methods we are using (manipulating or recording cell-types one by one). Perhaps an imaging method where spatially patterned activation or inhibition of multiple inputs is made possible using holography (Emiliani et al. 2015), may provide means for approaching this question.

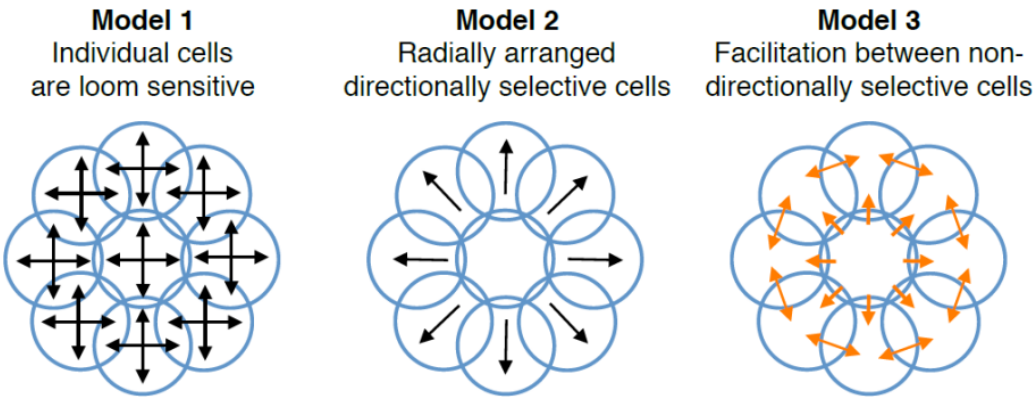

Fig.3.9 | Mechanism of loom sensitivity in LC neurons: hypothetical models

Receptive fields of 9 cells are shown as blue circles. The black arrows inside the circle denote the direction selectivity for these cells. The orange arrows denote facilitatory interactions between cells. The distances between cells are not to scale.

3.4.4 Single cell recordings are needed to understand underlying computations

It is likely that the selectivity for visual stimuli observed in LC neuron responses is both a property of the stimulus selectivity of their inputs—some selectivity was seen while imaging in the dendrites of the population of a few LC cell types (Aptekar et al. 2015)—and specific computations implemented by individual LC neuron types. However, I currently do not have a handle on single LC neuron selectivity due to my population GCaMP labeling strategy. Sparsely labeled GCaMP lines (Gruntman & Turner 2013) or single cell electrophysiology recordings are needed in order to obtain details of receptive field properties of single cells, and their selectivity (such as directional and orientation selectivity). These details are critical to understanding how looming preference arises in the population of these neurons. With imaging of the dendrite of single neurons, there is the opportunity to perhaps capture how inputs are computed along the dendrite, although this would require higher sampling rates, better spatial resolution (because of very thin arbors of LC neurons), and very bright GCaMP probes. Locating the source and extent of the inhibition (such as that seen with the quadrant loom stimuli), may provide additional insight, since there are many precedents where inhibition plays a key role in shaping spatiotemporal selectivity in

the visual system (Gabbiani et al. 2002; Fried et al. 2002; Mauss et al. 2015; Freifeld et al. 2013). To further characterize the inhibition would require electrophysiology, since with current Ca^{2+} indicators, inhibition cannot be measured robustly.

The locust LGMD system is a particularly well-studied model for understanding computations underlying loom sensitivity, allowing single cell electrophysiology. LGMD is a large widefield neuron having one dendritic field receiving excitatory inputs, and two dendritic fields receiving inhibitory inputs. Circuit mechanisms such as lateral inhibition between the excitatory inputs of LGMD has been shown to provide the null-preference for widefield motion (O'Shea & Rowell 1975). Since the excitatory inputs are retinotopically arranged, passive sublinear integration of these inputs provide the basis for the LGMD's orientation selectivity (Peron et al. 2009). Furthermore, the preference for looming motion over translational motion was shown to be conferred by spike frequency adaptation (Gabbiani & Krapp 2006; Peron & Gabbiani 2009). Concurrently, feedforward inhibition is known to provide an angular size threshold to the LGMD (Gabbiani et al. 2002). Interestingly, many of these stimulus preferences are found in the population response of LC6 and 16 as well. Therefore in future investigations, it would be interesting to find out how the circuit and biophysical level implementation of stimulus selectivity in *Drosophila* LC neurons compares to that of the locust LGMD.

Results in this chapter have contributed to the following publication:

Wu M*, Nern A*, Williamson R, **Morimoto MM**, Reiser MB, Card GM and Rubin GM Visual projection neurons in the *Drosophila* lobula link feature detection to distinct behavioral programs, eLife 2016; 5:e21022 *=equal contribution

CHAPTER 4

EXPLORATION OF LC6 DOWNSTREAM NEURONS

Data contributions:
All functional connectivity data collection and analysis were performed by Mai Morimoto with assistance from Allan Wong. Confocal images (Fig.4.2C, Fig4.3) were contributed by Aljoscha Nern.

4.1 Introduction

4.1.1 Identifying downstream circuits through functional connectivity

The optogenetic-activation induced behavior and response characterization of LC6 and LC16 showed that while we observed the induction of two distinct behaviors (jumping and backward walking), we did not find a large difference in the visual stimulus evoked response properties of these two cell types. Thus I considered the possibility that there is a bifurcation point downstream of the LC6 and LC16 neurons, where information from the two cell-types are somehow discriminated, and that those channels are connected to different descending pathways. To test this, we need to identify the downstream circuit components of LC6 and LC16 first. While this task of mapping the complete downstream circuits of a cell-type can seem daunting, in *Drosophila* it is feasible to conduct a step-wise whole brain search using genetics and imaging techniques. By combining two expression systems GAL4/UAS and LexA/LexAop, we are able to express a red-shifted variant of Channelrhodopsin (Chrimson) in the presynaptic neurons and activate them, while expressing GCaMP in the whole brain or candidate downstream neurons to image their activity (Fig.4.1). Following the work of others, we call this the "functional connectivity" method (Yao et al. 2012). While this method is less sensitive for confirming connected neurons (i.e. weakly connected neurons might be missed) compared to electrophysiological paired recordings or visualizing synaptic connections through EM reconstructions, it is particularly well suited for identifying downstream neurons that are completely unknown, in a time-efficient manner.

4.1.2 Measuring signal transformation between LC6 and downstream

As well as finding the circuit mechanism that may produce differential behavior downstream of LC6 and LC16, we saw this as an opportunity for asking, more generally, "How is visual information transformed across synapses at this stage of visual processing?" This question is hard to ask in mammalian systems, since finding connected neurons across the stages of early visual processing (such as retina to LGN, retina to superior colliculus, LGN to V1) and being able to map out this transformation, is a very challenging experiment. For this reason, the precise transformation between these stages of the visual pathway in the mammalian brain

remains an open debate (Carandini et al. 2005). We do not assume that the cellular mechanism in the *Drosophila* brain will echo that of the mammalian brain. However, at the level of visual information, I expect to find some similar transformations. Since there are shared ethological demands across the animal kingdom, such as escaping from danger and navigating to find mates or food, I may find extraction of visual information that is relevant to such behaviors that are common to all species.

With the above intensions, I focused on LC6 first, to identify downstream partners using the whole brain functional connectivity method. Once I had identified several downstream connected partners, I compared their response properties to see if I could find any information transformation between LC6 neurons and their downstream partners.

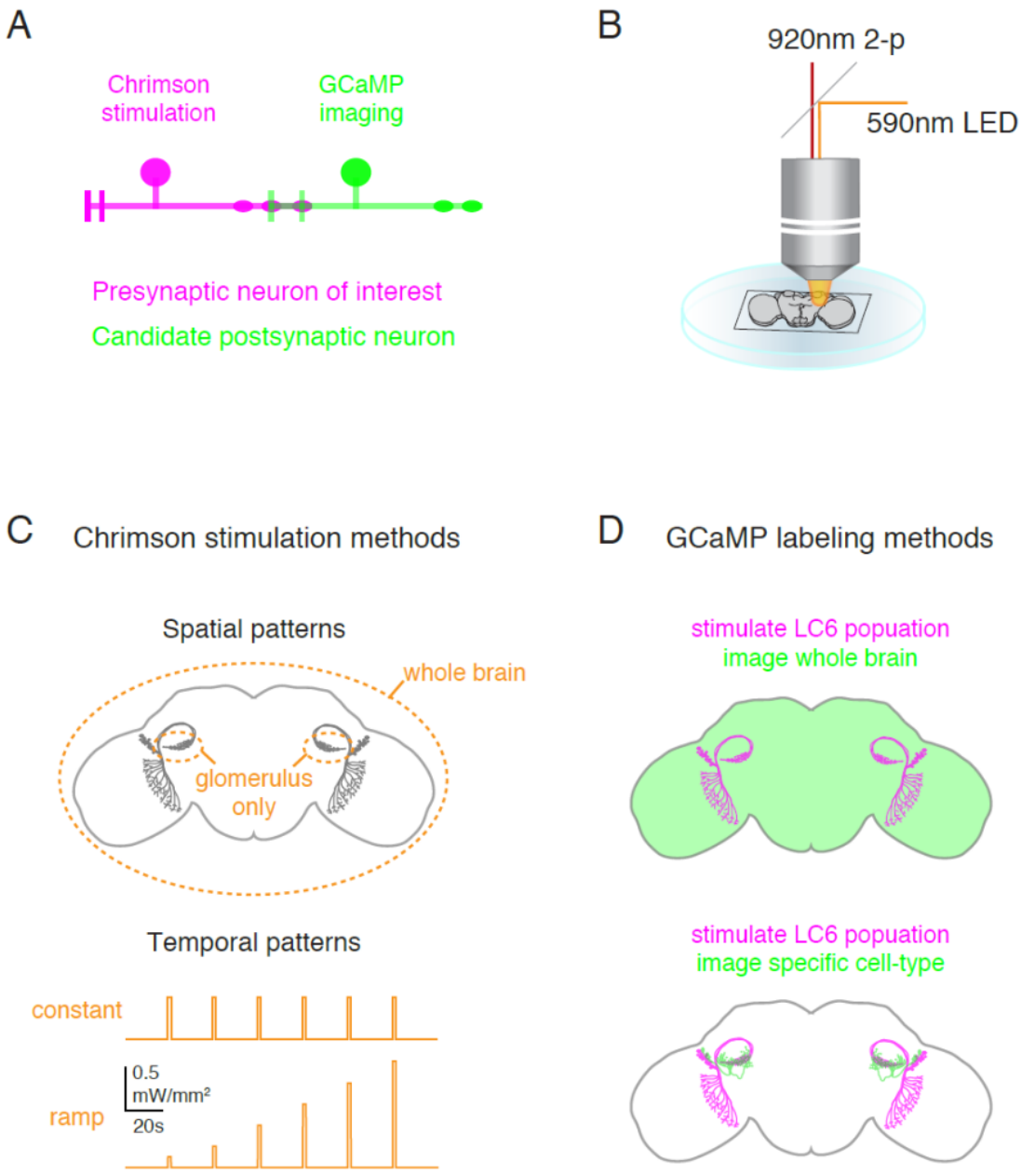

Fig.4.1 | Functional connectivity method for finding LC6 downstream neurons **(A)** Chrimson is expressed in the presynaptic neuron(s) of interest for optogenetic stimulation, and GCaMP is expressed in candidate postsynaptic neuron(s) to monitor its activity. **(B)** System for simultaneous Chrimson stimulation and GCaMP imaging in an ex-vivo brain. The brain was placed on a coverslip in a dish perfused with saline. GCaMP was imaged with 920nm 2-photon laser, while Chrimson was activated with 590nm LED via epi illumination pathway through the imaging objective. Modified from illustration by Allan Wong. **(C)** Chrimson stimulation was spatially and temporally modulated to stimulate different compartments of the presynaptic neuron, and to test for adaptation (constant protocol) or to obtain a presynapse activity dependent response curve (ramp protocol). **(D)** GCaMP was expressed either in the whole brain, or in selected candidate primary downstream neurons.

4.2 Methods

4.2.1 Fly lines

For the functional connectivity experiments, in order to express Chrimson and GCaMP in different target regions, LexA/LexAop and Split-GAL4/UAS systems were simultaneously used in the same animal. For exploring the whole brain, a Split-GAL4 driver line (OL0070B) was used to drive Chrimson in LC6, while a *nsyb*-LexA line was used to drive expression of opGCaMP6f in the majority of neurons in the fly brain. For exploring specific downstream candidate neurons, a LexA line containing the LC6 pattern (R42E06 in JK73A, Knapp et al. 2015) was used to drive Chrimson in LC6, while the Split-GAL4 lines (ss0825, ss2036, ss2099, ss3690, ss2409, ss3641) were used to drive expression of opGCaMP6f in candidate LC6 downstream neurons (images of lines in Fig4.3.). I received assistance from Allan Wong, Ed Rogers, and Aljoscha Nern, in the selection and implementation of these experimental genotypes.

Flies were reared under standard conditions (60% humidity, 25°C) on a cornmeal agar diet supplemented with retinal (0.2mM) in vials that were wrapped in foil to keep flies in the dark to prevent spurious activation of Chrimson by ambient light. Flies were collected following eclosion and held under the same rearing conditions until experiments were performed.

For the *in vivo* 2-photon Ca^{2+} imaging experiments, all flies were reared and crossed using the scheme described in Chapter 3 methods. Split-GAL4 driver lines (Bilaterally projecting downstream: ss0825, Ipsilaterally projecting downstream: ss2036) were crossed to pJFRC7-20×UAS-IVS-GCaMP6m in *VK00005* (DL background) effector line.

4.2.2 Functional connectivity experiments & data analysis

Functional connectivity experiments were conducted in collaboration with Allan Wong (functional connectivity project scientist at Janelia). Allan developed the pipeline for these methods, including optimization of GCaMP and Chrimson labeling strategies, microscopy methods, and image analysis methods.

Brains from adult flies 1-3 days post-eclosion, were isolated by dissecting the head in a saline bath (103mM NaCl, 3mM KCl, 2mM $CaCl_2$, 4mM $MgCl_2$, 26mM $NaHCO_3$, 1mM NaH_2PO_4, 8mM trehalose, 10mM glucose, 5mM TES, bubbled with 95% O_2 / 5% CO_2). The brain was then placed on a poly-lysine coated coverslip (neuVitro, Vancouver, WA, GG-12-PDL) posterior side up and perfused with saline (same composition as above, 21°C) (Fig4.1B). Images of the brain were acquired using a two-photon microscope (Custom made at Janelia by Dan Flickinger and colleagues, Nikon Apo LWD 25× NA1.1 water immersion #MRD77225, 2.5 fps, ~353 μm × ~353 μm field of view, ~0.68 × ~0.68 /pixel resolution for 512 × 512 image). The sample was imaged using a near-infrared laser (920nm, Spectra Physics, Insight DeepSee) that produced minimal collateral activation of Chrimson.

The light-gated ion channel Chrimson was activated by 590nm light (Thorlabs M590L3-C1) presented through the objective. Photoactivation light was delivered in a pulse train that consisted of six 1s pulses (square-wave modulation, 50 Hz, 10% duty cycle, 30s inter-pulse interval). Two stimulation protocols were used on the same brain subsequently, the first in which the light intensity increased for each of the six pulses (0.12, 0.24, 0.48, 0.72, 0.96, 1.21 mW; measured using Thorlabs S170C light power meter) and the second in which the light intensity was kept constant for each of the six pulses (0.48mW) (Fig.4.1C; “ramp” and “constant”). Stimulation light was spatially modulated using a DMD (Digital Micromirror Device, Texas Instruments, DLP LightCrafter v2.0), and was restricted to one hemisphere of the brain or the LC6 glomerulus depending on the experiment (Fig.4.1C). This spatial restriction limited the activation of other few non-specific cells labeled with the same driver line.

Image registration and regression analysis was conducted using code from the Thunder package (https://github.com/thunder-project/thunder, Freeman et al. 2014). The regression analysis highlights pixels that show high temporal correlation with the stimulus protocol by generating an image in which the r^2 values are assigned back to each pixel. Ideally this image would only contain structure responding to the optogenetic stimulation, which can be further examined to find candidate cell-types (Fig.4.2A, B).

The calcium responses of candidate LC6 downstream neurons to photoactivation were measured by calculating the ΔF/F for a manually drawn region of interest (ROI) in the imaging plane, which covered the largest section of its dendritic arborization. The ΔF/F was taken as $(F-F_0)/F_0$ where F is the instantaneous mean fluorescence of the ROI and F_0 is the baseline fluorescence of the ROI. The baseline fluorescence was taken as the 10^{th} percentile of the stimulation protocol period. Peak responses from each fly for the ramp protocol were taken and the mean ± SEM is shown as a stimulus-response curve for Fig.4.4C.

4.2.3 In vivo 2-photon Ca^{2+} imaging & data analysis

Select candidate LC6 downstream neurons were imaged using the same procedure as imaging of LC neurons in Chapter 3 (see Chapter 3 Methods). Most of the LC6 downstream neurons have low cell-count, with dendritic arbors that are sparsely distributed in the LC6 glomerulus region. These processes are a challenging target for measuring fluorescence changes, especially using my current single plane imaging method. Therefore one of the LC6 downstream neuron (ipsilaterally projecting, ss2036) was imaged at the soma.

The analysis method used in Chapter 3 was employed to analyse the *in vivo* 2-photon Ca^{2+} imaging data of the LC6 downstream neurons. Pearson's correlation coefficient (r) was used to assess the degree of correlation.

4.2.4 Visual stimuli

Visual stimuli were delivered using the procedure described in Chapter3 Methods. The same stimulus protocol was used for the candidate LC6 downstream neurons so that responses could be directly compared to LC6 neuron responses.

4.3 Results

4.3.1 Whole brain functional connectivity experiments reveal a single prominent downstream cell-type

To explore the downstream pathways of LC6, I first opted for a whole brain GCaMP imaging approach. This is particularly useful when one is completely naïve about the downstream pathways. Moreover, it has the potential to reveal the entire circuit in the whole brain, upon activation by a pre-synaptic neuron (secondary, tertiary connections, etc.). We expressed Chrimson in LC6 using a Split-GAL4 driver, and simultaneously expressed GCaMP in the whole brain using the *nsyb*-LexA driver line. By imaging the *ex vivo* brain on a dish and optogenetically activating LC6, we could image GCaMP activity throughout the whole brain (Fig.4.2A(i)). This image also contains activity of neurons that is not evoked by the optogenetic stimulation (i.e. spontaneous activity), thus it was processed further by extracting pixels that had high correlation to the timing of the light stimulation (raw correlation values shown, for details of the procedure, see methods). Upon examining the resulting image, it was clear that LC6 itself, and another neuron type that extends its axon bilaterally, were labeled (with occasional labeling in the mushroom body) (Fig.4.2A (ii)). This was rather surprising to us, since we expected many more neurons to be labeled, especially neurons that would connect the LC6 glomerulus to descending pathways that would lead to the jumping behavior observed with the activation screen (Chapter 3 Fig.3.2). We repeated this experiment, but never obtained images with neurons other than the bilaterally projecting neuron clearly labeled (Fig.4.2B top row, full field stimulation). Because the axon terminal of this neuron innervates the LC6 glomerulus on the contralateral brain hemisphere, we hypothesized that if this neuron type is inhibitory, it may be inhibiting the activity of other neurons innervating the LC6 glomerulus, thereby making other LC6 downstream neurons silent and undetectable. We tested this by activating the LC6 glomerulus only on one side of the brain by spatially restricting the stimulation light (Fig.4.2B, bottom row), but this did not reveal any additional downstream cell-types.

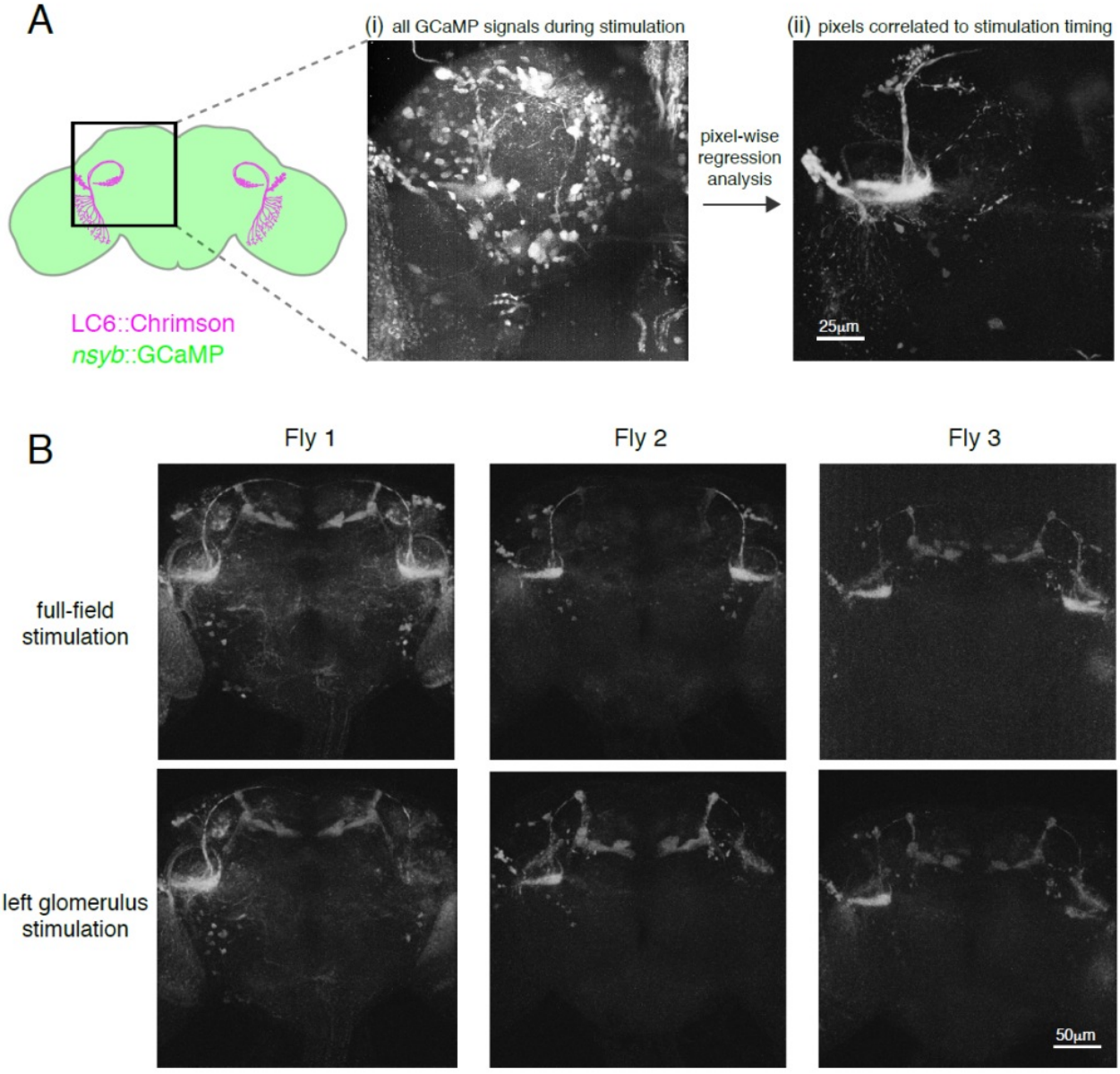
A
(i) all GCaMP signals during stimulation
(ii) pixels correlated to stimulation timing
pixel-wise regression analysis
LC6::Chrimson
nsyb::GCaMP
25μm
B
Fly 1
Fly 2
Fly 3
full-field stimulation
left glomerulus stimulation
50μm
C
LC6 split-GAL4 lines enhanced expression pattern
OL70B
OL77B
50μm

Fig.4.2 | Functional connectivity with whole-brain GCaMP labeling reveals a bilaterally projecting downstream cell-type
(A) GCaMP was imaged in the whole brain while Chrimson stimulation was delivered. GCaMP was expressed via *nsyb*-LexA, while Chrimson was expressed via split-GAL4 lines with targeted expression in LC6. (i) Maximum intensity projection image of the entire stimulation protocol period. This includes activity of neurons not evoked by Chrimson stimulation (i.e. spontaneous activity). (ii) Pixel-wise regression analysis extracts pixels that had correlated activity to the stimulation timing, revealing candidate downstream neurons. In this maximum intensity image, the intensity of the pixels represents the raw correlation value. **(B)** Result of regression analysis for 3 example flies. Top row used a full-field stimulation, and bottom row used stimulation spatially restricted to the left LC6 glomerulus region. **(C)** Expression pattern of split-GAL4 lines used to drive Chrimson in LC6. The images are intentionally saturated to show non-specific labeling. Some of the off-target labeling seen in (B), such as the occasional mushroom body labeling, is most likely due to direct activation of cells expressed within the OL77B pattern. Confocal images in (C) from Aljoscha Nern.

4.3.2 Targeted functional connectivity experiments reveal additional weaker connections

Since the whole brain GCaMP labeling approach did not yield additional candidate downstream neurons, we tried a more targeted approach, by searching for candidate downstream neuron types based on anatomical overlap and labeling them one by one, to conduct essentially an all-optical "paired recording" experiment. Split-GAL4 lines containing neurons that had neurites overlapping with the LC6 glomerulus were selected from the Rubin lab collection (Fig.4.3). Judging from the morphology, the ss825 split-GAL4 drove experession in the same bilaterally projecting cell-type found with the whole brain functional connectivity experiments. All other lines contain neurons that project ipsilaterally to a higher order multi-sensory area, the AVLP (Anterior Ventrolateral Protocerebrum). These candidate downstream split-GAL4 lines were then used to drive expression of GCaMP, while Chrimson (tagged with tdTomato) was expressed in LC6 using a LexA driver line (Fig.4.4A, magenta=LC6, green=candidate downstream neurons). In order to obtain a LC6 activity dependent stimulus-response curve for downstream responses, we conducted a "calibration" experiment to select light intensities that would evoke activity in the monotonically increasing part of the dynamic range of LC6 activity. We settled on a ramp stimulation protocol (light intensity increased over 6 pulses, 0.12~1.21mW/mm^2) with which we could observe a monotonically increasing LC6 GCaMP signal in response

to increasing levels of Chrimson activation (Fig.4.4B, LC6). Using this stimulation protocol, we measured responses from six candidate downstream neuron types while activating LC6 only at the glomerulus. The responses had different amplitude and temporal dynamics (Fig.4.4B), presumably reflecting their connection strengths to LC6, and also their intrinsic properties. The amplitude difference is most clear in the stimulus-response curves (Fig.4.4C): ss825 showed a strikingly large ΔF/F (~9.0) whereas the other cell-types showed an order of magnitude smaller increase in ΔF/F (~0.4), and ss3641 showed no obvious increase in response. The shape of these tuning curves could be related to the strength of the connection—saturating later in the curve indicating higher activation threshold and thus a weaker connection (Fig.4.4C, also see enlarged tuning curve). It is also possible that the weaker responses are reduced in part because of the challenges of sampling the diffuse processes of a small number of neurons of these downstream cells. The weakness of connection to LC6 may also suggest that these are neurons that integrate, requiring coincident input from other neurons to become sufficiently depolarized. Indeed, some of these downstream candidates innervate other optic glomeruli as well, strongly suggesting that they receive input from multiple LC neuron types (Fig.4.3, ss2036: LC6 and LC16, ss2099: LC6 and LC9, ss3690: LC6 and less overlap with LC16).

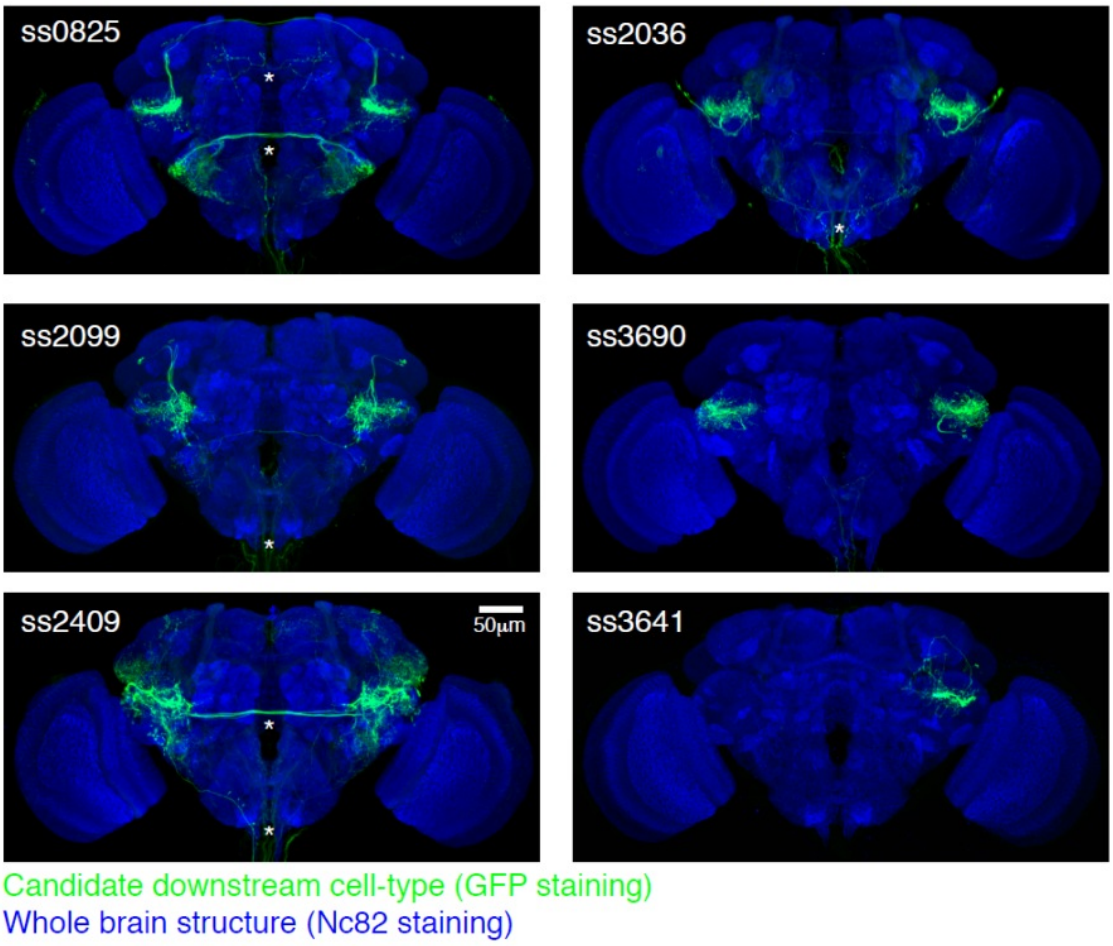

Fig.4.3 | LC6 downstream candidate cell-type split-GAL4 lines
Split GAL-4 lines were selected (with the help of Aljoscha Nern), based on their anatomical overlap with the LC6 glomerulus. These 6 lines were subsequently used for expressing GCaMP in functional connectivity experiments. All the images (except for ss3641) shows the full expression pattern, enhanced by GFP antibody staining. ss3641 image shows the downstream candidate cell-type labeled by the single cell flip-out strategy where a subset of the full expression pattern can be stochastically labelled. Asterisks denote expression outside of downstream candidate cell-type. Confocal images from Aljoscha Nern. Scale bar = ~50mm.

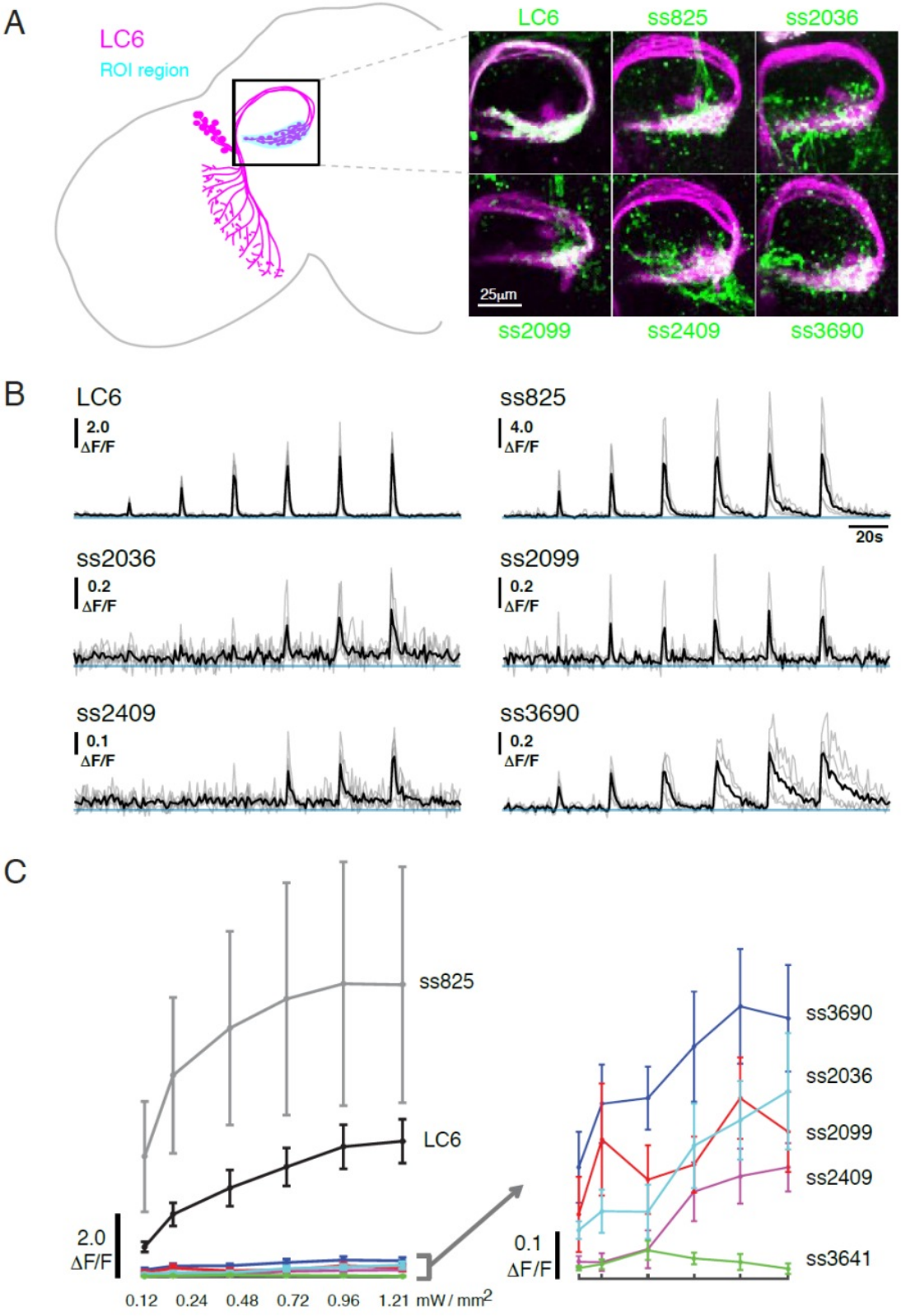
A
LC6
ROI region
LC6
ss825
ss2036
25μm
ss2099
ss2409
ss3690
B
LC6
2.0
ΔF/F
ss825
4.0
ΔF/F
20s
ss2036
0.2
ΔF/F
ss2099
0.2
ΔF/F
ss2409
0.1
ΔF/F
ss3690
0.2
ΔF/F
C
ss825
LC6
2.0
ΔF/F
0.12 0.24 0.48 0.72 0.96 1.21 mW / mm2
ss3690
ss2036
ss2099
ss2409
ss3641
0.1
ΔF/F

Fig.4.4 | Functional connectivity with sparse labeling reveals additional connected downstream cell-types
(A) Chrimson (tagged with tdTomato) was expressed in LC6 (magenta) using a LexA line while GCaMP was expressed in candidate downstream neurons (green) using split-GAL4 lines. Ca^{2+} responses were measured in the ROI region in cyan. **(B)** Ca^{2+} responses summed over an ROI drawn to include the glomerulus in candidate downstream neurons in response to LC6 Chrimson activation (N=4-5 for each genotype) with the ramp stimulus profile. A range of amplitudes and response timecourses were observed. Note **Δ**F/F are scaled differently. **(C)** Peak responses are shown for each candidate downstream cell-type for increasing light stimulation. The bilaterally projecting ss825 had the highest response, whereas other ipsilaterally projecting cell-types responded weakly in comparison. All cell-types (except ss3641) show response increase to increased light stimulation. Data shown for mean ± SEM.

4.3.3 Comparison of response properties: LC6 *vs.* LC6 downstream neurons

We took the same split-GAL4 lines that we used for the targeted functional connectivity experiments and expressed GCaMP6m in these cell-types for *in vivo* imaging, presenting the same visual stimulus set used for characterizing LC6 (Fig.4.5). The bilaterally projecting downstream (ss825) responded to the loom related stimuli and bar and small object motion stimuli in a very similar manner to LC6 (Fig.4.5, responses shown for slowest speed, see tuning curve for other speeds). In fact, for all the stimuli that we presented, the response of LC6 and the bilateral downstream neuron was consistently similar. This is well illustrated by the fact that the bilaterally projecting downstream neuron response plotted as a function of LC6 response clusters tightly around the unity line, with linear regression slope close to 1 (Fig.4.6A (i), slope=1.11, r^2=0.68). On the other hand, the ipsilaterally projecting downstream (ss2036), responded well to dark loom and edge-only loom, but did not show detectable responses to the other stimuli (Fig.4.5). The general dissimilarity of responses can also be observed from the broader clustering of data points around the unity line, and the linear regression showing weak correlation (Fig.4.6A (ii), slope=0.48, r^2=0.30). Since this ipsilaterally projecting cell-type (ss2036) seems to integrate from LC6 and LC16, we also assessed its correlation to LC16 responses. With this set of visual stimuli, we did not see a large difference in the correlation between LC6 and LC16 to this ipsilaterally projecting cell-type (compare Fig.4.6A(ii) and Fig.4.6B(ii)).

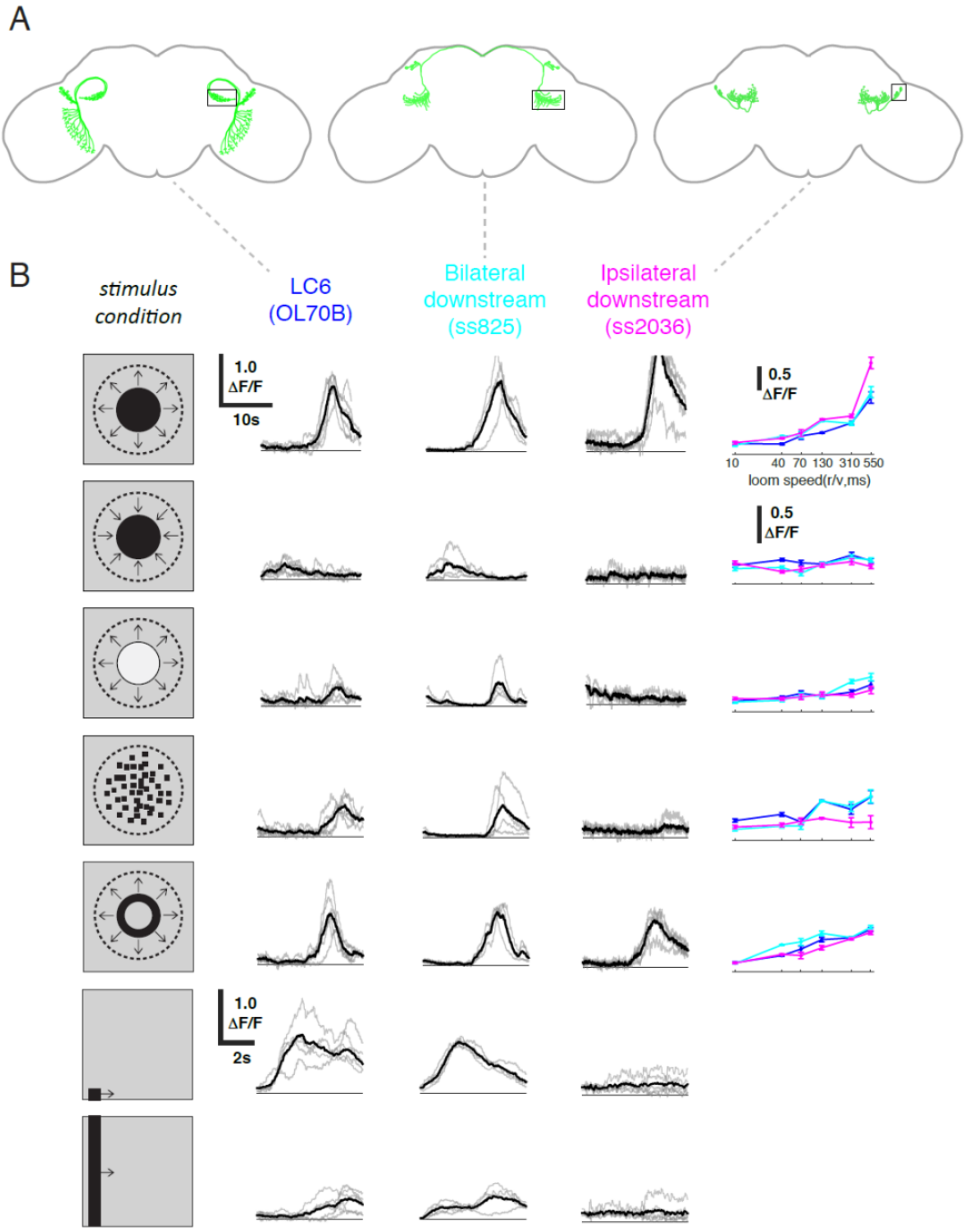

Fig.4.5 | *In vivo* Ca^{2+} imaging of one bilateral and ipsilateral LC6 downstream cell-types (A) Schematic of LC6, bilateral (ss825) and ipsilateral (ss2036) projecting downstream cell-types. Black rectangles indicate the ROI selected for GCaMP imaging. Note that LC6 ROI covers axons, bilateral ROI covers neurites, and ipsilateral ROI covers somata. **(B)** Evoked calcium responses in LC6 and downstream neurons by the visual stimuli indicated in the "stimulus condition" column. Timeseries traces are shown for the slowest speed in each stimulus category. Individual fly responses are in gray, and mean responses in black (LC6 N=6, ss825 N=4, ss2036 N=3, n=5 (N=number of flies, n=number of cells)). The tuning curves show peak responses for each speed of loom and loom related stimulus categories.

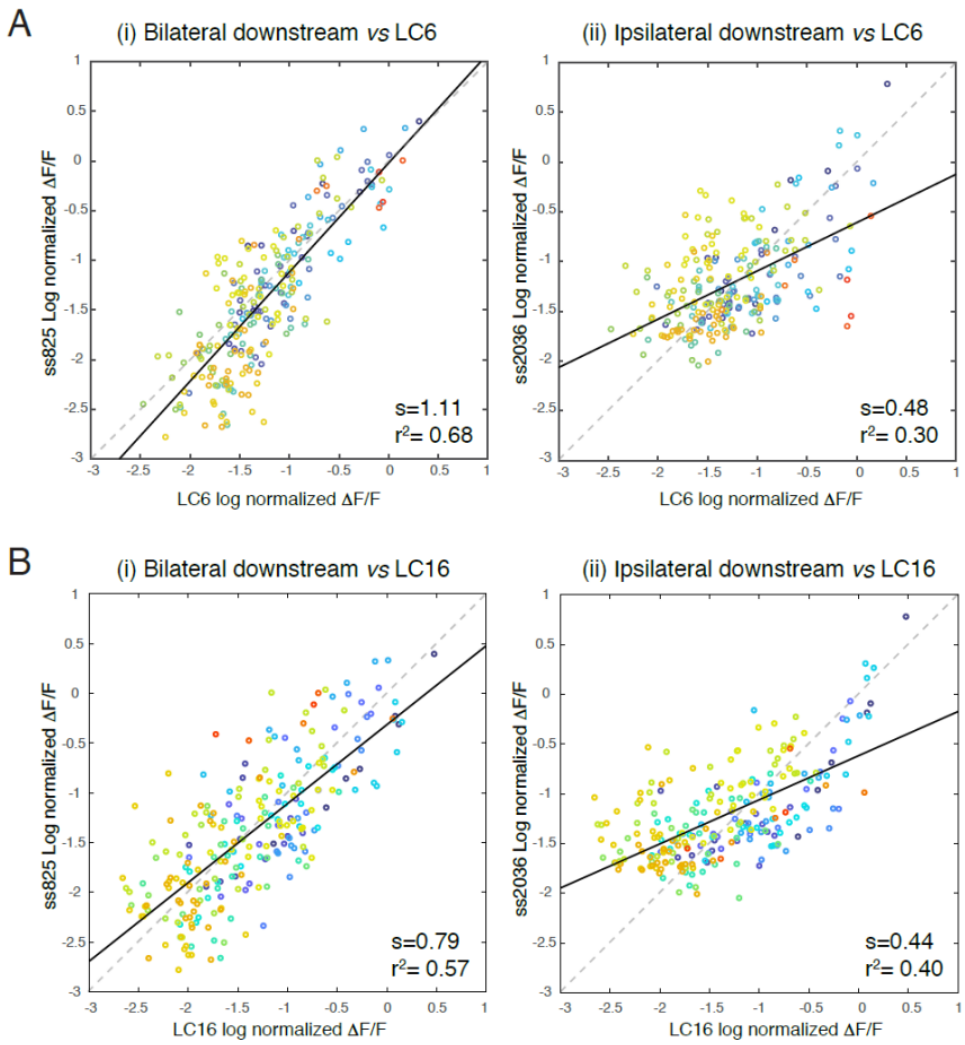

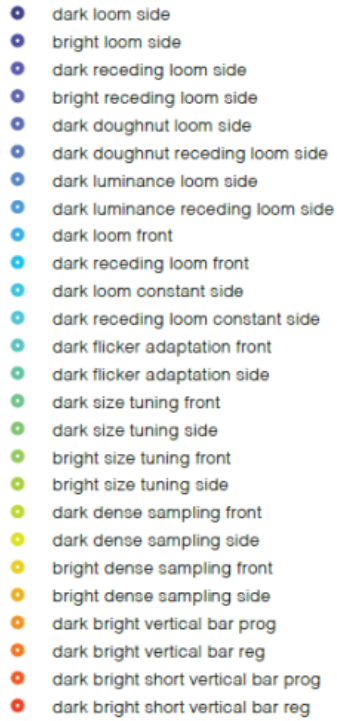

Fig.4.6 | Comparison between LC6 and downstream visual responses

(A) LC6 and LC6 downstream peak responses are log normalized and plotted against each other, where each data point represents a single stimulus condition Bilaterally projecting downstream (ss825) responses correlate well with that of LC6 (correlation coefficient $r^2 = 0.68$), while ipsilaterally projecting downstream (ss2036) correlates to a lesser extent ($r^2 = 0.30$). Linear fit is in black solid line, while the slope = 1 line representing identical responses is shown as a gray dashed line for comparison. The data points are color coded by visual stimulus category. **(B)** LC16 and LC6 downstream peak responses are log normalized and plotted against each other. ss825 (bilaterally projecting downstream) responses correlate well with that of LC16 (correlation coefficient $r^2 = 0.57$), but to a lesser extent than with LC6. ss2036 (ipsilaterally projecting downstream) correlates to a lesser extent than ss825, but slightly better than with LC6 ($r^2 = 0.40$).

4.4 Discussion

4.4.1 Technical considerations on the whole brain functional connectivity approach

While the whole brain labeled functional connectivity method provides many advantages, at least in my case, it did not reveal as many downstream cell-types as we expected. The limitations could be categorized as below:

1. Limits on the detection

There are a handful of factors that limit our ability to detect downstream neurons. The detection of activated neurons depends on the current labeling method (what promoter and Ca^{2+} indicator is used) and the post-hoc extraction method of relevant pixels. We used the *nsyb* promoter for whole brain labeling, but there are expression level differences amongst cells, and some cells are known not to be labeled with the driver line. For the Ca^{2+} indicator, we used GCaMP6s which has a high baseline fluorescence, so that weakly expressing cells could be detected. Nevertheless, different GCaMP versions have different reporting range of Ca^{2+} concentration (Chen et al. 2013), so that one GCaMP version could not fully cover the range that neurons in the whole brain may display. Additionally, the current method of extracting pixels responsive to photostimulation is by their temporal correlation, which is a robust measure, but not perfect (signal to noise, spurious correlation, etc.). These technical issues are currently being actively improved by labs working on whole brain imaging. The limitation that is more relevant for my experiments is the difficulty of separating signals from responsive cells that are spatially overlapping, especially if some signals are much weaker than others (which is the expected case, e.g. Figure 4.4.). In many areas of the *Drosophila* brain, neurites are densely packed, and if these thin neurites responded simultaneously, their responses are virtually impossible to separate with any currently available method. Therefore, the reason we could not detect the LC6 downstream cell-types found with anatomical overlap from the whole brain labeling experiments, could be partly owing to the fact that they were just inseparable from the LC6 glomerulus signals.

2. Unnatural stimulation pattern

Another reason we may not detect some LC6 downstreams could be the artificial way in which we are stimulating the brain. Stimulating only LC6 may not sufficiently depolarise LC6 downstream neurons that integrate from other LC types, or those that require disinhibition from other neurons. We could get closer to the natural condition by combinatorially activating LC neurons, or by switching to *in vivo* preparations where we can provide real visual stimulation, and therefore more naturalistic activation of presynaptic neurons.

3. State dependence

A perhaps less likely, but possible reason we may not uncover downstream pathways in the *ex vivo* brain is precisely because of its "out-of-body" state. It is known that without behavioral modulation, activity of some neurons may be hard to detect (Maimon 2011). Since whole brain imaging *in vivo* is not trivial, a reasonable compromise may be to add an octopamine agonist (Chlordimeform, CDM) to the *ex vivo* preparation to simulate the behaving state, which is known to have a similar effects on fly visual neurons (Rien et al. 2012; Suver et al. 2012; Longden & Krapp 2010).

4.4.2 Connectivity "strength" and response similarity

The amplitude of the Ca^{2+} signal from the functional connectivity experiments cannot be used quantitatively as a measure of connection strength for a number of reasons. For example, as mentioned above, the GCaMP expression level differs amongst cells, and the [Ca^{2+}] reporting range may not be suitable for some neurons. Additionally, with the difference in density of innervation to the LC6 glomerulus between cell-types, the fluorescence measurement made within an ROI of a cross section could not contain the same number of arbors, rendering the overall fluorescence from a sparsely innervating cell-type low. Nevertheless, the responses from bilateral and ipsilateral downstream cell-types are an order of magnitude different (Fig.4.4C), so that it seems safe to say that the bilateral downstream cell-type has a stronger connection to LC6 compared to all other downstream cell-types found.

From the two LC6 downstream neuron types I have been able to record from so far, it may be too premature to generalize that the connectivity "strength" (as measured by functional connectivity experiments) correlates to the similarity in their response

properties. However, this principle has previously been found in other systems such as the retinogeniculate connection of the cat (Usrey et al. 1999), and in local microcircuits of mouse V1(Cossell et al. 2015), so it would be interesting to see if it also holds true in the *Drosophila* visual system as well.

Connectivity "strength" between LC6 and its downstream neurons is likely to be implemented through synapse number as opposed to individual synaptic strengths. From the split-GAL4 expression pattern, it is clear that the density of innervation to the LC6 glomerulus is highest for ss825, while other downstream cell-types more diffusely innervate the glomerulus (Fig.4.4A, compare overlapped areas). This degree of innervation qualitatively correlates with the response amplitude in the functional connectivity experiments (Fig.4.4C). If we can assume that more innervation ≈ more synapse number, then we can infer that synapse number ≈ connectivity "strength". In the future, this relationship between the degree of innervation and synapse number could be established quantitatively by reconstructing these downstream cell-types from the EM data available at Janelia.

4.4.3 Possible mechanisms of information transformation across the synapse

The results from the whole brain and targeted LC6 functional connectivity experiments collectively revealed one strong connection (bilaterally projecting), and four weaker connections (all ipsilaterally projecting). We did not observe any direct decending neuron connections, but this may not be surprising, given that a previous anatomical study in *Calliphora* also found that decending neurons do not directly contact the optic glomeruli (Strausfeld & Okamura 2007).

The bilaterally projecting cell-type (ss825) consists of ~4-5cells, and seems to receive input from the LC6 population in one hemisphere, and extends its axon to the other side, providing output to the LC6 population in the contralateral hemisphere. This morphology suggests that it relays the LC6 population activity to the LC6 on the other side. This is supported by the fact that its response property is very similar to LC6. Because the recording was performed on the dendrites of these cells, it would be important to confirm in the future that the response property is corroborated at the axon terminal. We currently do not know the function of this bilateral downstream neuron, but we suspect that it is inhibitory. Further, if this is the case, we could speculate that it is involved in selective attention-like mechanisms such as that found in the dragonfly CSTMD (Wiederman & O'Carroll 2013).

The ipsilaterally projecting cell-type (ss2036) consists of ~3-4 cells that receive input from LC6 and LC16, and project to the AVLP. This type of ipsilateral neurons may be the ones that connect the optic glomeruli to descending neurons, which are known to also innervate the AVLP. In this case, these neurons may very well implement the "selection" of behaviors downstream of the LCs. The recordings I have so far from this particular ipsilateral neuron (ss2036) show that it seems to filter out stimuli that extend over a small field (small moving object and bar) and possibly amplifies the dark looming response. From the receptive field size of LC6, we can infer that the number of LC6s activated during the small moving object stimulus would be more or less constant over time, whereas with a dark looming stimulus, the number of activated LCs would build up to a peak, much like its temporal profile of ΔF/F. The spatiotemporal dynamics at the LC6 glomerulus that I observed with Ca^{2+} imaging are generally consistent with this expectation (data not shown).

We could speculate that perhaps the diffuse nature in which these downstream neurites innervate the LC6 glomerulus requires the coactivation of sufficient number of their arbours to reach the threshold (for us to observe Ca^{2+} signals). Alternatively, since this particular ipsilateral downstream (ss2036) innervates both LC6 and LC16, it could be performing a type of "coincidence detection" of the two cell-types, where it responds to the intersection of LC6 and LC16 response properties. This explanation may match my current observations if we assume that this downstream neuron requires the activity of both LC6 and LC16 to be above certain threshold (i.e. ΔF/F~1.0).

4.4.4 Systematic response characterization is needed to understand the transformation

The above mechanistic explanations are still in the realm of speculations, and I need to confirm these findings first with more recordings. Importantly, I have so far only obtained somatic Ca^{2+} signals from the ipsilaterally projecting neurons. Since somatic Ca^{2+} signals are usually thought to represent delayed and low-pass filtered versions of the response at the neurites, I need to obtain responses from the neurites to confirm that the response properties I observe at the soma is genuine. Another possibility is to record the voltage activity of these neurons through electrophysiology or imaging (Yang et al. 2016), since some transformation may occur at the temporal scale not resolvable with Ca^{2+} signals.

Moreover, it is necessary to assess the response properties of LC6 and its downstreams with more stimuli, since our speculation of mechanisms are deeply affected by how we define the response properties of these neurons. So far, I have probed these neurons with stimuli based on looming features and some linear edge motion and flicker stimuli, but in order to understand the transformation, we need a more thorough characterization of LC6 and its downstream response properties. The current set of stimuli is designed mainly around stimuli that LC6 prefers, but it is also important see whether the null-response is corroborated in the downstream responses, or alternatively, whether some response property emerges in downstream neurons. Therefore we need to sample the visual stimulus space more systematically, perhaps through the use of white noise stimuli (Sakai et al. 1988; Chichilnsky 2001), or a version containing higher order local motion apparently prevalent in nature (Nitzany & Victor 2014).

CHAPTER 5

GENERAL DISCUSSION

In this thesis, I aimed to contribute to the understanding of neural information processing by studying the filtering property of neurons at two levels, biophysical and circuit levels.

Below I discuss the broader implication of my findings, and suggestions for future investigations. It should be stressed that many of the results in the chapters are preliminary. All the discussions below assume no methodological issues for the results generated (for these discussions please refer to individual result chapters).

5.1 Biophysical level investigation

Active conductances such as voltage-gated potassium channels (Kvs) play an important role in shaping the response of neurons and sensory receptors. Kvs are in fact known to be the most diversified class of voltage-gated channels. I started by asking how variable the Kv conductances were amongst photoreceptor cells, with a focus on finding the molecular identity of I_{Kf}, a Kv current with intermediate kinetics. The results showed that the three classes of Kv currents (Shaker, Shab and I_{Kf}) expressed in photoreceptor cells are similarly variable, and showed that the molecular identity of I_{Kf} is not Shal (Kv4), but is likely to be the slow component of Shaker (Kv1) or a combination of its splice variants. The role of this intermediate Kv current in shaping the final voltage response of the photoreceptor cell is currently unclear, and needs to be assessed through computational models (Niven et al. 2003; Vähäsöyrinki et al. 2006; Song et al. 2012). Nevertheless, our proposed mechanism of generating variability of Kv kinetics presents an interesting possibility for single neuron non-linear transformations. In some cases, single neurons are even known to "compute", using active conductances (London & Häusser 2005; Koch & Segev 2000). For example, the locust LGMD firing rate is well captured by a model that assumes multiplication of size and velocity signals, a computation that is thought to take place at the dendrites (Gabbiani et al. 2002). Similarly, the mouse starburst amacrine cells are thought to compute direction of motion, using dendrite-autonomous active conductances and inhibitory interactions between cells (Vaney et al. 2012). The detailed biophysical implementation of these computations is still a topic of debate, and is being deduced through extensive computational modeling (Peron et al. 2009; Peron & Gabbiani 2009; Poznanski 1992; Tukker et al. 2004). It would be interesting to incorporate the rich diversity of kinetics in active conductances, such as that generated by mechanisms proposed here for Kvs in

Drosophila photoreceptors, into such models, to see how they affect single neuron computations.

One of our original questions however, about whether there is some kind of pattern in the spatial distribution of responses across the retina remains unanswered. We could perhaps have tried *in-situ* hybridization methods, but usually such methods are only semi-quantitative. Ideally one would want to record the potassium conductances from an intact retina, and observe their spatial distribution. For this, we need a method with high temporal and spatial resolution. With methods we have at hand, such as single cell electrophysiology recordings or Ca^{2+} imaging, we are always trading temporal resolution for spatial resolution, and vice versa. So perhaps this question should be left for the future, when methods that fulfill these requirements such as voltage imaging become more developed, and the signal to noise is improved.

5.2 Circuit level investigation

We chose the lobula columnar (LC) cells to study the filtering properties, because these neurons are expected to serve as the information bottleneck between the optic lobe and central brain, from the anatomical evidence that the number of cell-types dramatically decrease at this stage. It had been postulated further that this compression of information would result in the extraction of behaviorally relevant information by these neurons. We found that LC6 and LC16 indeed respond to behaviorally relevant visual stimuli, such as dark slow looming stimuli and its variants, a stimulus that evokes avoidance behaviors in *Drosophila*. This is in agreement with the fact that optogenetic activation of LC6 and LC16 induces avoidance-like jumping and backward walking behaviors respectively. We then went on to identify the downstream circuit components of LC6, and found two classes of direct downstream neurons: one bilaterally projecting cell-type, and four ipsilaterally projecting cell-types. The response properties of the bilateral downstream cell-type and one of the ipsilateral downstream cell-type were assessed and compared to LC6. This revealed that the former had a very similar response property to LC6, which suggests that they presumably relay the LC6 information to the other hemisphere. In contrast, the latter seemed to filter out some information (i.e. non-loom related motion). This result still needs to be confirmed with more recordings, but if true, would be consistent with our initial expectation of information compression. We have yet to demonstrate, whether other transformations exist for the other downstream

neurons, and what the cellular mechanism of the transformation is. Given these results, I speculated on some possible mechanisms for the generation of loom selectivity in the LC neuron and the information transformation downstream. The most flexible way to generate loom sensitivity using a population of non-directional LC neurons might be through lateral facilitatory mechanisms, one that could be implemented by gap junctions among cells. I have so far not found evidence for directional selectivity in individual neurons, but this should be characterized in detail in the future by single neuron recording methods. For the downstream mechanisms, because the ipsilateral cell-types innervate the LC6 glomerulus diffusely ("weak" connection), we can assume that many of these arbors need to be activated sufficiently over the integration time window for the cell to reach its threshold to respond. The spatiotemporal response profile of the LC6 non-loom related responses could be filtered out through such mechanisms. Similarly, because of the weak connection, the coincident activation of LC6 and LC16 may be necessary for the cell to reach its threshold. In this case, the cell would respond to the intersection of LC6 and LC16 responses.

Do any of these results generalize to other visual systems? The analogy of the lobula to stages of the vertebrate visual system is an open debate. The anatomical similarity between the *Drosophila* optic lobe and vertebrate retina had been recognized by Cajal, who famously stated that *" If from the visual organ of the insect, we discount the crucial fact of the dislocation of the soma, then the analogy between the visual apparatus [of the vertebrates and insects] converts almost in identity."* (Cajal and Sanchez 1915). In a more recent account inspired by this anatomical comparison, visual projection neurons (LC neurons included) are proposed to be analogous to LGN neurons projecting to the cortex (Sanes & Zipursky 2010). However, the small number of visual projection neuron axons projecting across the optic lobe to the central brain, is structurally reminiscent of the optic fibres of retinal ganglion cells (RGCs) leaving the eye to LGN. This is supported by a physiological argument that is based on the emergence of spiking cells in the visual system. In the vertebrate visual system, the RGCs layer is the first stage where a substantial number of spiking cells are observed (Demb & Singer 2015)(but see (Baden et al. 2011)). The neurons preceding the lobula-complex (lobula and lobula plate) communicate via graded potentials, making lobula-complex the first stage in the optic lobe where spiking neurons emerge (but see (Jansonius & Van Hateren 1993)) (some LC neurons are also

experimentally confirmed to spike; personal communication from Eyal Gruntman). The spiking nature of neurons imply conversion from analog to digital encoding which is thought to be an important step in the processing of visual information. The emergence of spiking cells also suggests their role in distributing information across a wide distance with fidelity.

Another argument is a functional one, which compares the selectivity of neurons between vertebrates and invertebrates. The dragonfly STMDs in the lobula are highly selective for small targets and have been compared to hypercomplex cells, neurons that are found in mammalian visual cortex (Hubel & Wiesel 1965). These neurons have an "end-stopping" nature, in which they respond to small targets optimally while extended bars attenuate the response. Looming sensitive neurons are found in the lobula, such as the LGMD in locusts, and LC neurons described here. In vertebrates, looming sensitivity can be found as early as RGCs, for example, in mouse PV-5 ganglion cells (Münch et al. 2009), and also in a subset of zebrafish RGCs (Temizer et al. 2015), but also in mouse and cat superior colliculus (Liu et al. 2011; Zhao et al. 2014), and pigeon thalamic nucleus rotundus (Frost & Sun 1998). From what we know about the anatomy, physiology and selectivity of neurons in the lobula, it seems that the vertebrate analog of lobula could fall anywhere between retinal ganglion cells to visual cortex. However, important organizational differences exist between invertebrate and vertebrate visual systems, which make this comparison difficult. In vertebrate visual systems, because of the sequential pooling and integration across layers, generally, the receptive field (RF) size becomes larger and the selectivity of neurons become higher as we progress deeper into the brain. In contrast, in many invertebrate visual systems, wide-field and small-field neurons co-exist in each layer, so that RF size and selectivity does not necessarily scale sequentially through the layers. This organization may confer the lobula neurons to have a range of RF sizes and selectivity that are comparable to a wide range of visual processing stages in the vertebrate visual system.

5.3 Concluding Remarks

To understand the filtering property of a neuron, one would need to study its intrinsic properties, but also in the context of the circuit it is embedded in. In this thesis (and in many current research settings) these biophysical and circuit levels are studied in isolation. In the future, fine manipulations such as changing the kinetics of the active

conductances via genetics and recording from a neuron in an intact circuit, may provide means to bridge this gap. This type of fine perturbation could provide insight into how the biophysics of the neuron affects the filtering property of the cell and consequently, the computation performed at the circuit level.

The genetically tractable and small *Drosophila* brain is an attractive system to ask such biophysical and circuit level questions. However, the organizational difference between arthropod and vertebrate brains presents a difficult challenge when one tries to make literal comparisons between the two systems. Rather, the interesting comparison to make may be at the implementation level. In the visual system, because of shared ethological demands such as escaping from danger and finding food and mates, we can expect to find representations of such behaviorally relevant visual features across the animal kingdom. By investigating and comparing the implementation of these representations across species, we not only accumulate knowledge about how these computations can be implemented, but also may uncover common underlying principles.

REFERENCES

Agrawal, S., Safarik, S. & Dickinson, M., 2014. The relative roles of vision and chemosensation in mate recognition of *Drosophila melanogaster*. *Journal of Experimental Biology*, 217(15), pp.2796–2805.

Ammer, G. et al., 2015. Functional specialization of neural input elements to the *Drosophila* ON motion detector. *Current Biology*, 25(17), pp.2247–2253.

Anderson, J. & Hardie, R.C., 1996. Different photoreceptors within the same retina express unique combinations of potassium channels. *Journal of Comparative Physiology A*, 178(4), pp.513–522.

Aptekar, J.W. et al., 2015. Neurons forming optic glomeruli compute figure-ground discriminations in *Drosophila*. *The Journal of Neuroscience,* 35(19), pp.7587–7599.

Autrum, H., Zettler, F. & J rvilehto, M., 1970. Postsynaptic potentials from a single monopolar neuron of the ganglion opticum I of the blowfly *Calliphora*. *Journal of Comparative Physiology A*, 70(4), pp.414–424.

Baden, T. et al., 2011. Spikes in retinal bipolar cells phase-lock to visual stimuli with millisecond precision. *Current Biology*, 21(22), pp.1859–1869.

Bahl, A. et al., 2013. Object tracking in motion-blind flies. *Nature Neuroscience*, 16(6), pp.730–738.

Behnia, R. et al., 2014. Processing properties of ON and OFF pathways for *Drosophila* motion detection. *Nature*, 512(7515), pp.427–430.

Bergquist, S., Dickman, D.K. & Davis, G.W., 2010. A hierarchy of cell intrinsic and target-derived homeostatic signaling. *Neuron*, 66(2), pp.220–234.

Borst, A., Haag, J. & Reiff, D.F., 2010. Fly motion vision. *Annual Review of Neuroscience*, 33, pp.49–70.

Briggman, K.L., Helmstaedter, M. & Denk, W., 2011. Wiring specificity in the direction-selectivity circuit of the retina. *Nature*, 471(7337), pp.183–188.

Burton, B.G. & Laughlin, S.B., 2003. Neural images of pursuit targets in the photoreceptor arrays of male and female houseflies *Musca domestica*. *The Journal of Experimental Biology*, 206(Pt 22), pp.3963–3977.

Burton, B.G., Tatler, B.W. & Laughlin, S.B., 2001. Variations in photoreceptor response dynamics across the fly retina. *Journal of Neurophysiology*, 86(2), pp.950–960.

Cajal, S.R., and Sanchez, D. (1915). Contribucion al conocimiento de los centros nerviosos del los insectos. Trab. Lab. Invest. Biol 13, 1–167.

Carandini, M. et al., 2005. Do we know what the early visual system does? *The Journal of Neuroscience*, 25(46), pp.10577–10597.

Card, G. & Dickinson, M.H., 2008. Visually mediated motor planning in the escape

response of *Drosophila*. *Current Biology*, 18(17), pp.1300–1307.

Card, G.M., 2012. Escape behaviors in insects. *Current Opinion in Neurobiology*, 22(2), pp.180–186.

Chen, T.-W. et al., 2013. Ultrasensitive fluorescent proteins for imaging neuronal activity. *Nature*, 499(7458), pp.295–300.

Chiappe, M.E. et al., 2010. Walking modulates speed sensitivity in *Drosophila* motion vision. *Current Biology*, 20(16), pp.1470–1475.

Chichilnsky, E.J., 2001. A simple white noise analysis of neuronal light responses. *Network: Computation in Neural Systems*, 12, pp.199–213.

Clark, D.A. et al., 2011. Defining the computational structure of the motion detector in *Drosophila*. *Neuron*, 70(6), pp.1165–1177.

Coen, P. et al., 2016. Sensorimotor transformations underlying variability in song intensity during *Drosophila* courtship. *Neuron*, 89(3), pp.629–644.

Cook, R., 1979. The courtship tracking of *Drosophila melanogaster*. *Biological Cybernetics*, 34(2), pp.91–106.

Cossell, L. et al., 2015. Functional organization of excitatory synaptic strength in primary visual cortex. *Nature*, 518(7539), pp.399–403.

Cuttle, M.F. et al., 1995. Diurnal modulation of photoreceptor potassium conductance in the locust. *Journal of Comparative Physiology A*, 176(3).

de Vries, S.E.J. & Clandinin, T.R., 2012. Loom-sensitive neurons link computation to action in the *Drosophila* visual system. *Current Biology*, 22(5), pp.353–362.

Demb, J.B. & Singer, J.H., 2015. Functional circuitry of the retina. *Annual Review of Vision Science*, 1(1), pp.263–289.

Demerec, M. et al., 1965. Biology of *Drosophila*, *Wiley*

Diao, F. et al., 2010. SIDL interacts with the dendritic targeting motif of Shal (Kv4) K+ channels in *Drosophila*. *Molecular and Cellular Neuroscience,* 45(1), pp.75-83.

Diao, F., Waro, G. & Tsunoda, S., 2009. Fast inactivation of Shal (Kv4) K+ channels is regulated by the novel interactor SKIP3 in *Drosophila* neurons. *Molecular and Cellular Neuroscience*, 42(1), pp.33-44.

Dyakova, O. et al., 2015. A higher order visual neuron tuned to the spatial amplitude spectra of natural scenes. *Nature Communications*, 6, p.8522.

Emiliani, V. et al., 2015. All-optical interrogation of neural circuits. *The Journal of Neuroscience,* 35(41), pp.13917–13926.

Fettiplace, R. & Fuchs, P.A., 1999. Mechanisms of hair cell tuning. *Annual review of*

physiology, 61, pp. 809-34

Field, D.J., 1987. Relations between the statistics of natural images and the response properties of cortical cells. *Journal of the Optical Society of America. A*, 4(12), pp.2379–2394.

Fischbach, K.F. & Dittrich, A., 1989. The optic lobe of *Drosophila melanogaster*. I. A Golgi analysis of wild-type structure. *Cell and Tissue Research*, 96(2), pp.445-66.

Fotowat, H. & Gabbiani, F., 2011. Collision detection as a model for sensory-motor integration. *Annual Review of Neuroscience*, 34(1), pp.1–19.

Fotowat, H., Harrison, R.R. & Gabbiani, F., 2011. Multiplexing of motor information in the discharge of a collision detecting neuron during escape behaviors. *Neuron*, 69(1), pp.147–158.

Freeman, J. et al., 2014. Mapping brain activity at scale with cluster computing. *Nature Methods*, 11(9), pp.941–950.

Freifeld, L. et al., 2013. GABAergic lateral interactions tune the early stages of visual processing in *Drosophila*. *Neuron*, 78(6), pp.1075–1089.

Fried, S.I., Münch, T.A. & Werblin, F.S., 2002. Mechanisms and circuitry underlying directional selectivity in the retina. *Nature*, 420(6914), pp.411–414.

Frost, B.J. & Sun, H., 1998. Computation of different optical variables of looming objects in pigeon nucleus rotundus neurons. *Nature Neuroscience*, 1(4), pp.296–303.

Gabbiani, F. et al., 2002. Multiplicative computation in a visual neuron sensitive to looming. *Nature*, 420(6913), pp.320–324.

Gabbiani, F., Krapp, H.G. & Laurent, G., 1999. Computation of object approach by a wide-field, motion-sensitive neuron. *The Journal of Neuroscience*, 19(3), pp.1122–1141.

Gabbiani, F., Mo, C. & Laurent, G., 2001. Invariance of angular threshold computation in a wide-field looming-sensitive neuron. *The Journal of Neuroscience*, 21(1), pp.314-29

Gao, S. et al., 2008. The neural substrate of spectral preference in *Drosophila*. *Neuron*, 60(2), pp.328–342.

Gruntman, E. & Turner, G.C., 2013. Integration of the olfactory code across dendritic claws of single mushroom body neurons. *Nature Neuroscience*, 16(12), pp.1821–1829.

Gu, Y. et al., 2005. Mechanisms of light adaptation in *Drosophila* photoreceptors. *Current Biology*, 15(13), pp.1228–1234.

Hardie, R.C., 2011. Phototransduction mechanisms in *Drosophila* microvillar

photoreceptors. *Wiley Interdisciplinary Reviews: Membrane Transport and Signaling*, 1(2), pp.162–187.

Hardie, R.C., 1991. Voltage-sensitive potassium channels in *Drosophila* photoreceptors. *The Journal of Neuroscience*, 11(10), pp.3079–3095.

Hardie, R.C. & Franze, K., 2012. Photomechanical responses in *Drosophila* photoreceptors. *Science*, 338(6104), pp.260–263.

Hardie, R.C. et al., 1991. Novel potassium channels encoded by the Shaker locus in *Drosophila* photoreceptors. *Neuron*, 6(3), pp.477–486.

Hatsopoulos, N., Gabbiani, F. & Laurent, G., 1995. Elementary computation of object approach by a wide-field visual neuron. *Science*, 270(5238), pp.1000–1003.

Hausen, K., 1984. The lobula-complex of the fly: structure, function and significance in visual behaviour. *Photoreception and Vision in Invertebrates*, 74, pp. 523–559.

Hegde, P. et al., 1999. Mutational analysis of the Shab-encoded delayed rectifier K(+) channels in *Drosophila*. *The Journal of Biological Chemistry*, 274(31), pp.22109–22113.

Henderson, S.R., Reuss, H. & Hardie, R.C., 2000. Single photon responses in *Drosophila* photoreceptors and their regulation by Ca2+. *The Journal of Physiology*, 524 Pt 1, pp.179–194.

Hevers, W. & Hardie, R.C., 1995. Serotonin modulates the voltage dependence of delayed rectifier and Shaker potassium channels in *Drosophila* photoreceptors. *Neuron*, 14(4), pp.845–856.

Hofbauer, A. & Campos-Ortega, J.A., 1990. Proliferation pattern and early differentiation of the optic lobes in *Drosophila melanogaster*. *Roux's Archives of Developmental Biology*, 198(5), pp.264–274.

Holmqvist, M. & Srinivasan, M., 1991. A visually evoked escape response of the housefly. *Journal of Comparative Physiology A*, 169(4), pp.451-9.

Hoshi, T., Zagotta, W.N. & Aldrich, R.W., 1991. Two types of inactivation in Shaker K+ channels: effects of alterations in the carboxy-terminal region. *Neuron*, 7(4), pp.547–556.

Hubel, D.H. & Wiesel, T.N., 1965. Receptive fields and functional architecture in two nonstriate visual areas (18 and 19) of the cat. *Journal of Neurophysiology*, 28, pp.229-89.

Ito, M. et al., 2013. Systematic analysis of neural projections reveals clonal composition of the *Drosophila* brain. *Current Biology*, 23(8), pp.644–655.

Jan, L.Y. & Jan, Y.N., 2012. Voltage-gated potassium channels and the diversity of electrical signalling. *The Journal of Physiology*, 590(11), pp.2591–2599.

Jansonius, N.M. & Van Hateren, J.H., 1993. On spiking units in the first optic chiasm

of the blowfly. *Journal of Comparative Physiology A*., 168(6), pp.631-7.

Jaramillo, A.M. et al., 2004. Pattern of distribution and cycling of SLOB, Slowpoke channel binding protein, in *Drosophila*. *BMC Neuroscience*, 5, p.3.

Jenett, A. et al., 2012. A GAL4-driver line resource for *Drosophila* neurobiology. *Cell Reports*, 2(4), pp.991–1001.

Jensen, C.S., Rasmussen, H.B. & Misonou, H., 2011. Neuronal trafficking of voltage-gated potassium channels. *Molecular and Cellular Neuroscience*, 48(4), pp.288–297.

Joesch, M. et al., 2008. Response properties of motion-sensitive visual interneurons in the lobula plate of *Drosophila melanogaster*. *Current Biology*, 18(5), pp.368–374.

Jones, P.W. & Gabbiani, F., 2010. Synchronized neural input shapes stimulus selectivity in a collision-detecting neuron. *Current Biology*, 20(22), pp.2052–2057.

Klapoetke, N.C. et al., 2014. Independent optical excitation of distinct neural populations. *Nature Methods*, 11(3), pp.338–346.

Knapp, J.-M., Chung, P. & Simpson, J.H., 2015. Generating Customized Transgene Landing Sites and Multi-Transgene Arrays in *Drosophila* Using phiC31 Integrase. *Genetics*, 199(4), pp.919–934.

Koch, C. & Segev, I., 2000. The role of single neurons in information processing. *Nature Neuroscience*, 3(Suppl), pp.1171–1177.

Krapp, H.G. & Hengstenberg, R., 1996. Estimation of self-motion by optic flow processing in single visual interneurons. *Nature*, 384(6608), pp.463–466.

Krapp, H.G., Hengstenberg, B. & Hengstenberg, R., 1998. Dendritic structure and receptive-field organization of optic flow processing interneurons in the fly. *Journal of Neurophysiology*, 79(4), pp.1902–1917.

Kvon, E.Z. et al., 2014. Genome-scale functional characterization of *Drosophila* developmental enhancers *in vivo*. *Nature*, 512(7512), pp.91–95.

Laughlin, S., 1981. A simple coding procedure enhances a neuron's information capacity. *Zeitschrift für Naturforschung C*., 36(9-10), pp.910-2.

Laughlin, S.B., Howard, J. & Blakeslee, B., 1987. Synaptic limitations to contrast coding in the retina of the blowfly *Calliphora*. *Proceedings of the Royal Society B: Biological Sciences*, 231(1265), pp.437–467.

Lichtinghagen, R. et al., 1990. Molecular basis of altered excitability in Shaker mutants of *Drosophila melanogaster*. *The EMBO Journal*, 9(13), pp.4399–4407.

Liu, L. et al., 1999. Context generalization in *Drosophila* visual learning requires the mushroom bodies. *Nature*, 400(6746), pp.753–756.

Liu, Y.-J., Wang, Q. & Li, B., 2011. Neuronal responses to looming objects in the superior colliculus of the cat. *Brain, Behavior and Evolution*, 77(3), pp.193–205.

London, M. & Häusser, M., 2005. Dendritic computation. *Annual Review of Neuroscience*, 28, pp.503–532.

Longden, K.D. & Krapp, H.G., 2010. Octopaminergic modulation of temporal frequency coding in an identified optic flow-processing interneuron. *Frontiers in Systems Neuroscience*, 4, p.153.

Luan, H. et al., 2006. Refined spatial manipulation of neuronal function by combinatorial restriction of transgene expression. *Neuron*, 52(3), pp.425–436.

Maddess, T. & Yang, E.C., 1997. Orientation-sensitive neurons in the brain of the honey bee (*Apis mellifera*). *Journal of Insect Physiology*, 43(4), pp.329–336.

Maimon, G., 2011. Modulation of visual physiology by behavioral state in monkeys, mice, and flies. *Current Opinion in Neurobiology*, 21(4), pp.559–564.

Maimon, G., Straw, A.D. & Dickinson, M.H., 2008. A simple vision-based algorithm for decision making in flying *Drosophila*. *Current Biology*, 18(6), pp.464–470.

Mauss, A.S. et al., 2015. Neural circuit to integrate opposing motions in the visual field. *Cell*, 162(2), pp.351–362.

Medan, V. et al., 2015. A network of visual motion-sensitive neurons for computing object position in an arthropod. *The Journal of Neuroscience*, 35(17), pp.6654–6666.

Medan, V., Oliva, D. & Tomsic, D., 2007. Characterization of lobula giant neurons responsive to visual stimuli that elicit escape behaviors in the crab *Chasmagnathus*. *Journal of neurophysiology*, 98(4), pp.2414–2428.

Mu, L. et al., 2012. Optic glomeruli and their inputs in *Drosophila* share an organizational ground pattern with the antennal lobes. *The Journal of Neuroscience*, 32(18), pp.6061–6071.

Muijres, F.T. et al., 2014. Flies Evade looming targets by executing rapid visually directed banked turns. *Science*, 344(6180), pp.172–177.

Münch, T.A. et al., 2009. Approach sensitivity in the retina processed by a multifunctional neural circuit. *Nature Neuroscience*, 12(10), pp.1308–1316.

Nitzany, E.I. & Victor, J.D., 2014. The statistics of local motion signals in naturalistic movies. *Journal of Vision*, 14(4), pp.10.

Niven, J.E. et al., 2003. The contribution of Shaker K+ channels to the information capacity of *Drosophila* photoreceptors. *Nature*, 421(6923), pp.630–634.

Nordström, K. & O'Carroll, D.C., 2006. Small object detection neurons in female hoverflies. *Proceedings of the Royal Society B: Biological Sciences*, 273(1591), pp.1211–1216.

Nordström, K., Barnett, P.D. & O'Carroll, D.C., 2006. Insect detection of small targets moving in visual clutter. *PLOS Biology*, 4(3), e54.

O'Carroll, D., 1993. Feature-detecting neurons in dragonflies. *Nature*, 362(6420), pp.541–543.

Okamura, J.-Y. & Strausfeld, N.J., 2007. Visual system of calliphorid flies: motion- and orientation-sensitive visual interneurons supplying dorsal optic glomeruli. *The Journal of Comparative Neurology*, 500(1), pp.189–208.

Otsuna, H. & Ito, K., 2006. Systematic analysis of the visual projection neurons of *Drosophila melanogaster*. I. Lobula-specific pathways. *The Journal of Comparative Neurology*, 497(6), pp.928–958.

Parigi, A. et al., 2014. How predator hunting-modes affect prey behaviour: Capture deterrence in *Drosophila melanogaster*. *bioRxiv*

Paulk, A.C. et al., 2008. The processing of color, motion, and stimulus timing are anatomically segregated in the bumblebee brain. *The Journal of Neuroscience*, 28(25), pp.6319–6332.

Peron, S. & Gabbiani, F., 2009. Spike frequency adaptation mediates looming stimulus selectivity in a collision-detecting neuron. *Nature Neuroscience*, 12(3), pp.318–326.

Peron, S.P., Jones, P.W. & Gabbiani, F., 2009. Precise subcellular input retinotopy and its computational consequences in an identified visual interneuron. *Neuron*, 63(6), pp.830–842.

Pfeiffer, B.D. et al., 2010. Refinement of tools for targeted gene expression in *Drosophila*. *Genetics*, 186(2), pp.735–755.

Pfeiffer, B.D. et al., 2008. Tools for neuroanatomy and neurogenetics in *Drosophila*. *Proceedings of the National Academy of Sciences*, 105(28), pp.9715–9720.

Poznanski, R.R., 1992. Modelling the electrotonic structure of starburst amacrine cells in the rabbit retina: a functional interpretation of dendritic morphology. *Bulletin of Mathematical Biology*, 54(6), pp.905-28.

Randall, A.S. et al., 2015. Speed and sensitivity of phototransduction in *Drosophila* depend on degree of saturation of membrane phospholipids. *The Journal of Neuroscience,* 35(6), pp.2731–2746.

Reiff, D.F. et al., 2010. Visualizing retinotopic half-wave rectified input to the motion detection circuitry of *Drosophila*. *Nature Neuroscience*, 13(8), pp.973–978.

Reiser, M.B. & Dickinson, M.H., 2008. A modular display system for insect behavioral neuroscience. *Journal of Neuroscience Methods*, 167(2), pp.127–139.

Rien, D., Kern, R. & Kurtz, R., 2012. Octopaminergic modulation of contrast gain adaptation in fly visual motion-sensitive neurons. *The European Journal of Neuroscience*, 36(8), pp.3030–3039.

Rind, F.C. & Simmons, P.J., 1992. Orthopteran DCMD neuron: a reevaluation of responses to moving objects. I. Selective responses to approaching objects. *Journal of Neurophysiology*, 68(5), pp.1654–1666.

Robie, A.A., Straw, A.D. & Dickinson, M.H., 2010. Object preference by walking fruit flies, *Drosophila melanogaster*, is mediated by vision and graviperception. *Journal of Experimental Biology*, 213(Pt 14), pp.2494–2506.

Rogero, O. & Tejedor, F.J., 1995. Immunochemical characterization and developmental expression of Shaker potassium channels from the nervous system of *Drosophila*. *The Journal of Biological Chemistry*, 270(43), pp.25746–25751.

Rogero, O., Hämmerle, B. & Tejedor, F.J., 1997. Diverse expression and distribution of Shaker potassium channels during the development of the *Drosophila* nervous system. *The Journal of Neuroscience*, 17(13), pp.5108–5118.

Rowell, C.H.F., M, O. & Williams, J.L.D., 1977. The neuronal basis of a sensory analyser, the acridid movement detector system. IV. The preference for small field stimuli. *Journal of Experimental Biology*, 68, pp.157–185.

Sakai, H.M., Ken-Ichi, N. & Korenberg, M.J., 1988. White-noise analysis in visual neuroscience. *Visual Neuroscience*, 1(03), pp.287–296.

Sanes, J.R. & Zipursky, S.L., 2010. Design principles of insect and vertebrate visual systems. *Neuron*, 66(1), pp.15–36.

Schnaitmann, C. et al., 2013. Color discrimination with broadband photoreceptors. *Current Biology*, 23(23), pp.2375–2382.

Serbe, E. et al., 2016. Comprehensive characterization of the major presynaptic elements to the *drosophila* off motion detector. *Neuron*, 89(4), pp.829–841.

Simmons, P.J. & Rind, F.C., 1992. Orthopteran DCMD neuron: a reevaluation of responses to moving objects. II. Critical cues for detecting approaching objects. *Journal of Neurophysiology*, 68(5), pp.1667–1682.

Song, Z. et al., 2012. Stochastic, adaptive sampling of information by microvilli in fly photoreceptors. *Current Biology*, 22(15), pp.1371–1380.

Srinivasan, M.V., Zhang, S.W. & Rolfe, B., 1993. Is pattern vision in insects mediated by "cortical" processing? *Nature*, 362(6420), pp.539–540.

Strausfeld, N.J. & Okamura, J.-Y., 2007. Visual system of calliphorid flies: organization of optic glomeruli and their lobula complex efferents. *The Journal of Comparative Neurology*, 500(1), pp.166–188.

Strother, J.A., Nern, A. & Reiser, M.B., 2014. Direct observation of ON and OFF pathways in the *Drosophila* visual system. *Current Biology*, 24(9), pp.976–983.

Suver, M.P., Mamiya, A. & Dickinson, M.H., 2012. Octopamine neurons mediate flight-induced modulation of visual processing in *Drosophila*. *Current Biology*, 22(24), pp.2294-302

Takemura, S.-Y. et al., 2013. A visual motion detection circuit suggested by *Drosophila* connectomics. *Nature*, 500(7461), pp.175–181.

Tammero, L.F. & Dickinson, M.H., 2002. Collision-avoidance and landing responses are mediated by separate pathways in the fruit fly, *Drosophila melanogaster*. *The Journal of Experimental Biology*, 205(Pt 18), pp.2785–2798.

Temizer, I. et al., 2015. A visual pathway for looming-evoked escape in larval zebrafish. *Current Biology*, 25(14), pp.1823–1834.

Tukker, J.J., Taylor, W.R. & Smith, R.G., 2004. Direction selectivity in a model of the starburst amacrine cell. *Visual Neuroscience*, 21(4), pp.611–625.

Usrey, W.M., Reppas, J.B. & Reid, R.C., 1999. Specificity and strength of retinogeniculate connections. *Journal of Neurophysiology*, 82(6), pp.3527–3540.

van Breugel, F. & Dickinson, M.H., 2012. The visual control of landing and obstacle avoidance in the fruit fly *Drosophila melanogaster*. *Journal of Experimental Biology*, 215(Pt 11), pp.1783–1798.

Vaney, D.I., Sivyer, B. & Taylor, W.R., 2012. Direction selectivity in the retina: symmetry and asymmetry in structure and function. *Nature Reviews Neuroscience*, 13(3), pp.194–208.

Vähäsöyrinki, M. et al., 2006. Robustness of neural coding in *drosophila* photoreceptors in the absence of slow delayed rectifier K+ channels. *The Journal of Neuroscience,* 26(10), pp.2652-60.

von Reyn, C.R. et al., 2014. A spike-timing mechanism for action selection. *Nature Neuroscience*, 17(7), pp.962–970.

von Reyn, C.R. et al., 2017. Feature integration drives probabilistic behavior in the *Drosophila* escape response. *Neuron*, 94(6), pp.1190–1204.

Weckström, M. & Laughlin, S.B., 1995. Visual ecology and voltage-gated ion channels in insect photoreceptors. *Trends in Neurosciences*, 18(1), pp.17–21.

Wei, A. et al., 1990. K+ current diversity is produced by an extended gene family conserved in *Drosophila* and mouse. *Science*, 248(4955), pp.599–603.

Wicklein, M. & Strausfeld, N.J., 2000. Organization and significance of neurons that detect change of visual depth in the hawk moth *Manduca sexta*. *The Journal of Comparative Neurology*, 424(2), pp.356–376.

Wiederman, S.D. & O'Carroll, D.C., 2011. Discrimination of features in natural scenes by a dragonfly neuron. *The Journal of Neuroscience*, 31(19), pp.7141–7144.

Wiederman, S.D. & O'Carroll, D.C., 2013. Selective attention in an insect visual neuron. *Current Biology*, 23(2), pp.156–161.

Wilson, R.I. & Laurent, G., 2005. Role of GABAergic inhibition in shaping odor-

evoked spatiotemporal patterns in the *Drosophila* antennal lobe. *The Journal of Neuroscience*, 25(40), pp.9069–9079.

Wu, M et al., 2016. Visual projection neurons in the *Drosophila* lobula link feature detection to distinct behavioral programs. *eLife*, 2016; 5:e21022

Yang, E.-C., Lin, H.-C. & Hung, Y.-S., 2004. Patterns of chromatic information processing in the lobula of the honeybee, *Apis mellifera L*. *Journal of Insect Physiology*, 50(10), pp.913–925.

Yang, H.H. et al., 2016. Subcellular imaging of voltage and calcium signals reveals neural processing in vivo. *Cell*, 166(1), pp.245–257.

Yao, Z. et al., 2012. Analysis of functional neuronal connectivity in the *Drosophila* brain. *Journal of Neurophysiology*, 108(2), pp.684–696.

Yu, H.-H. et al., 2013. Clonal development and organization of the adult *Drosophila* central brain. *Current Biology*, 23(8), pp.633–643.

Zeng, H. et al., 2005. The amino terminus of Slob, Slowpoke channel binding protein, critically influences its modulation of the channel. *The Journal of General Physiology*, 125(6), pp.631–640.

Zhang, X. et al., 2013. Lobula-specific visual projection neurons are involved in perception of motion-defined second-order motion in *Drosophila*. *Journal of Experimental Biology*, 216(Pt 3), pp.524–534.

Zhao, X., Liu, M. & Cang, J., 2014. Visual cortex modulates the magnitude but not the selectivity of looming-evoked responses in the superior colliculus of awake mice. *Neuron*, 84(1), pp.202–13